

UNIVERSITY OF OKLAHOMA

GRADUATE COLLEGE

THE OXIDATIVE COUPLING OF METHANE USING AN AC ELECTRIC GAS DISCHARGE

A THESIS APPROVED FOR THE  
THE OXIDATIVE COUPLING OF METHANE USING AN AC ELECTRIC GAS  
AND MATERIALS SCIENCE  
DISCHARGE

A THESIS

SUBMITTED TO THE GRADUATE FACULTY

in partial fulfillment of the requirements for the

degree of

MASTER OF SCIENCE

(CHEMICAL ENGINEERING)

By

BOBBY JOE HILL

Norman, Oklahoma

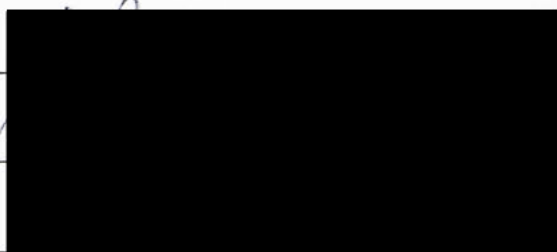
1997

U  
HESIS  
IL  
op. 2

THE OXIDATIVE COUPLING OF METHANE USING AN AC ELECTRIC GAS  
DISCHARGE

A THESIS APPROVED FOR THE  
SCHOOL OF CHEMICAL ENGINEERING  
AND MATERIALS SCIENCE

BY



## ACKNOWLEDGMENTS

I would like to thank the faculty and staff of the University of Oklahoma for all their assistance. I would especially like to thank my research advisors Dr. Larry Latham and Dr. Richard [unclear] for their special assistance and guidance throughout my graduate research. I am grateful for the financial support and encouragement they provided me. I would also like to thank Dr. David [unclear] for serving as my master's thesis committee.

Many thanks to all the people of CUIC: Abdul Mustafa, Dr. Changin Liu, Brian Sharkey, Phil Howard, Terry Caldwell, Dave Latta, Chris [unclear], and Sim [unclear]. Thanks guys for helping me learn many ways. I would like to especially thank Dr. Changin Liu and Abdul Mustafa for their suggestions and advice. I would like to thank Larry Lacey and Jim Young for helping me build the remote system.

I would like to thank my family and friends for all their encouragement and support.

## ACKNOWLEDGMENTS

I would like to thank the faculty and staff of the University of Oklahoma for all their assistance. I would especially like to thank my research advisors Dr. Lance Lobban and Dr. Richard Mallinson for all their special assistance and guidance throughout my graduate coursework and research. I am grateful for the financial support and opportunities that they provided me. I would also like to thank Dr. Daniel Resasco for serving on my masters thesis committee.

Many thanks to all the people of C110; Abdul Marafee, Dr. Changin Liu, Bhanu Murthy, Phil Howard, Terry Caldwell, Dave Larkin, Chris Gordon, and Srinivas. Thanks guys for helping me in so many ways. I would like to especially thank Dr. Changin Liu and Abdul Marafee for their suggestions and advice. I would like to thank Larry Isley and Jim Yeager for helping me build the reactor system.

I would like to thank my family and friends for all their encouragement and support.

# TABLE OF CONTENTS

ACKNOWLEDGMENTS.....	iv
APPENDICES.....	vi
LIST OF FIGURES.....	vii
CHAPTER	
1. Introduction and Literature Review	
1.1 Introduction.....	1
1.2 Background.....	2
1.3 Plasma Literature Review.....	4
1.4 Electrical Discharges.....	6
1.5 Plasma Industrial Applications.....	9
1.6 Methane Conversions.....	10
1.7 Research Objectives.....	13
1.8 Present Work.....	13
Works Cited.....	15
CHAPTER	
2. AC Electric Gas Discharge Reactor and Experimental Procedure	
2.1 AC Electric Gas Discharge Reactor .....	17
2.2 Calibration.....	22
2.3 Calculations.....	24
2.4 Experimental Procedure.....	24
CHAPTER	
3. An Experimental Study on the Oxidative Coupling of Methane Using an AC Electric Gas Discharge	
3.1 Results and Discussion.....	28
3.1.1 Effect of Oxygen Partial Pressure.....	28
3.1.2 Effect of Helium.....	33
3.1.3 Effect of Flowrate.....	35
3.1.4 Effect of Gap Width.....	38
3.1.5 Effect of Voltage.....	43
3.1.6 Effect of Frequency.....	47
3.1.7 Conclusions.....	57
3.1.8 Energy Analysis.....	54
Works Cited.....	56
CHAPTER	
4. Experiments with Helium (Nonadiabatic & Adiabatic)	
4.1 Nonadiabatic Experiments.....	58
4.1.1 Nonadiabatic vs. Adiabatic.....	58
4.1.2 Adiabatic Temperature Measurements.....	63

CHAPTER		
5. Rate Expressions		
5.1 Differential Method.....		67
Works Cited.....		71
CHAPTER		
6. Conclusions and Recommendations		
6.1 Conclusions.....		72
6.2 Recommendations.....		74
Appendix A. Electron Molecule Reactions.....		75
Appendix B. Calibration Factors		
Computer Program.....		76
Appendix C. Experimental Data from		
Chapter Three.....		80
Appendix D. Experimental Data from		
Chapter Four.....		88
Appendix E. Rate Expression Charts.....		94

## List of Figures

Figure 2.1 AC Electric Gas Discharge Reactor.....	17
Figure 2.2 AC Electric Gas Discharge System.....	18
Figure 3.1 Effect of Oxygen Partial Pressure.....	34
Figure 3.2 Effect of Helium Diluent.....	37
Figure 3.3 Effect of Helium on Power.....	39
Figure 3.4 Effect of Flowrate.....	41
Figure 3.5 Effect of Gap Width on OCM.....	43
Figure 3.6 Effect of Gap Width on Power.....	45
Figure 3.7 Effect of Voltage on OCM.....	48
Figure 3.8 Effect of Voltage on Power.....	50
Figure 3.9 Effect of Voltage on Temperature.....	51
Figure 3.10 Effect of Frequency on OCM.....	53
Figure 3.11 Effect of Frequency on Power.....	55
Figure 3.12 Effect of Frequency on Temperature.....	56
Figure 4.1 Adiabatic 60 Hz: Yield vs. Voltage.....	60
Figure 4.2 Adiabatic 100 Hz: C <sub>2</sub> Yield vs. Voltage.....	61
Figure 4.3 Nonadiabatic 60 Hz: C <sub>2</sub> Yield vs. Voltage.....	62
Figure 4.4 Adiabatic Temperature vs. Frequency.....	65
Figure 4.5 Adiabatic Temperature vs. Voltage.....	66

# THE OXIDATIVE COUPLING OF METHANE USING AN AC ELECTRIC GAS DISCHARGE

## CHAPTER ONE

### INTRODUCTION AND LITERATURE REVIEW

#### 1.1 Introduction

The world is very dependent upon petrochemicals such as vehicle fuels and chemical feedstocks produced from oil. The depletion of the world's oil reserves is expected to occur in the latter half of the next century with the current rate of oil consumption. Therefore, it becomes necessary to utilize alternative sources of hydrocarbons to produce petrochemicals. Methane, the primary component of natural gas, could provide the next abundant hydrocarbon source. Despite recent investigations into methane conversion, the challenge still remains to develop an economical methane conversion process competitive with the production of petrochemicals from oil.

Alternative and innovative methane conversion methods must be investigated to develop improved methane conversions to higher hydrocarbons. The stability of the methane molecule has usually limited its use as a chemical feedstock. The unique characteristics of the nonequilibrium plasma (cold plasma) promote reactions with very stable gas molecules at low temperatures. The oxidative coupling of methane using an AC electric gas discharge or nonequilibrium plasma is an alternative and innovative methane conversion method for the production of higher hydrocarbons.



## 1.2 Background

Proven methane conversion technologies involve indirect methane conversions to higher valued hydrocarbons. Indirect methane conversion first requires steam reforming of methane to synthesis gas (CO and H<sub>2</sub>). The indirect methane conversion technologies include Fischer-Tropsch synthesis to methanol or light hydrocarbons (in the gasoline range) and Mobil's MTG (methanol to gasoline) process. Both technologies consist of high temperature, multistep, large scale processes. Due to the initial steam reforming of methane, they require a very high energy input. Extremely high utility and capital costs prevent their industrial application in most situations. Industrial applications exist in New Zealand (MTG) and South Africa (Fischer-Tropsch) due to favorable economics from their special situations.

The ultimate goal for methane conversion is to develop a methane conversion method that would provide a direct conversion to liquids in the gasoline range. Since natural gas occurs in remote locations and the size of natural gas basins vary, the method should be adaptable to large and small scale processes. Conversion of methane to liquids would allow the utilization of natural gas even at remote locations which is now usually flared or reinjected into a well. However, advancements in direct methane conversion technologies have not produced a direct methane conversion to liquids in the gasoline range. The recent developments in methane conversion technologies for the production of higher valued hydrocarbons produce intermediates, such as ethylene, ethane, and methanol.

The oxidative coupling of methane (OCM) provides a direct conversion to ethylene and ethane ( $C_2$  products). Ethylene and ethane can be further processed to hydrocarbons in the liquid range or used as feedstocks for chemical reactions. Since OCM converts methane to the gases ethylene and ethane, an improved OCM methane conversion process is most adaptable near large natural gas basins or in natural gas processing plants where infrastructure exist for gas transportation.

Recently, OCM has been an active area for catalysis research. Research on the heterogeneous catalytic OCM began in the early 1980s. In 1982, Keller and Bhasin presented one of the first reports on OCM over metal oxide catalysts. Since then many other investigations over OCM have been reported as reviewed by Lee and Oyama (1988) and Amenomiya (1990). High temperatures ( $>700^\circ$ ) are required to initiate the OCM reactions and oxidation of methane decreases the  $C_2$  yield. Improvements in  $C_2$  selectivity and  $C_2$  yield have been achieved, although the  $C_2$  yields are still too low for the heterogeneous catalytic OCM to be economically feasible. Limiting  $C_2$  yields are reported to be around 26%, and most catalysts yielded much smaller  $C_2$  yields. (Krylov, 1992)

An important development in the catalytic OCM was the development of mechanisms over the catalysts. Researchers demonstrated that the activation of methane occurs by negatively charged lattice oxygen ions abstracting hydrogen from methane (Capitan et al., 1993; Deboy and Hicks, 1988; Otsuka et al., 1987). In addition, researchers have also demonstrated that negative oxygen ions are produced in nonequilibrium plasmas (Grill, 1994; Chang et al., 1991). Therefore, the activation of

methane probably results from excited oxygen species abstracting hydrogen from methane in the AC electric gas discharge, and the reactivity should be similar to catalytic OCM.

### 1.3 Plasma Literature Review

#### Plasmas

A plasma is a quasineutral gas consisting of charged and neutral gas particles with a collective behavior in which the charged particles follow the path of the electric field.

Due to the high particle energy of plasmas, they can be considered a fourth state of matter when compared to the particle energy of solids, liquids, and gases. Characterization of plasmas uses the gas temperature ( $T_g$ ), and the electron temperature ( $T_e$ ). Plasmas that exist under controlled conditions consist of two types:

- **local thermodynamic equilibrium plasmas (LTE)** - LTE plasmas exist when the temperature of the gas equals the temperature of the electrons ( $T_g=T_e$ ). LTE plasmas are also called thermal plasmas. LTE plasmas exist when gas temperatures are greater than 6000 K at atmospheric pressure.
- **non-LTE plasmas** - Non-LTE plasmas exist when the temperature of the gas is much less than the temperature of the electrons ( $T_g \ll T_e$ ). Electron temperatures may reach temperatures of  $10^4$ - $10^5$  K. Non-LTE plasmas are also called cold plasmas or nonequilibrium plasmas and their non-equilibrium properties provide the capability for chemical reactions at low temperature. Non-LTE plasmas are utilized in a wide application of processes. (Grill, 1994)

## **Generation of Non-Equilibrium Plasmas**

Non-equilibrium plasmas are generated and excited by alternating current (AC), direct current (DC), radio frequency (RF), or microwave (MW) electric power applied to the gas. When an electric potential is applied across the electrodes, electrons are accelerated between the electrodes gaining kinetic energy. At low voltages, only elastic collisions occur between electrons and gas molecules, and the electrons lose only a very small amount of their kinetic energy in elastic collisions. When the voltage reaches the breakdown voltage, the electrons eventually gain enough kinetic energy to promote inelastic collisions. Ionization of gas molecules occurs due to the inelastic collisions transferring their energy to the gas molecules. Secondary electrons are produced from the inelastic collisions. The electric field accelerates the secondary electrons which continue to promote further ionization by impact with gas molecules. Therefore, an electron multiplication process or electron avalanche occurs, sustaining the discharge. (Grill, 1994)

## **Plasma Chemical Reactions**

A main advantage of the nonequilibrium or cold plasmas is that reactions occur at much lower gas temperatures than is required for corresponding thermal reactions. Reactions in the nonequilibrium discharges depend only on the electron energy of the discharge. Energetic electrons accelerated by the electric field transfer their energy to the gas through inelastic collisions or electron/molecule reactions. The collisions produce excited species which include free radicals, ions, and excited neutral species. Appendix A lists the major types of inelastic collisions. Collisions between atoms, free radicals, ions,

and gas molecules lead to chemical reactions. These reactions are typically called radical-molecule and ion-molecule reactions. (Grill, 1994)

#### 1.4 Electrical Gas Discharges

The nonequilibrium plasmas or discharges are generally distinguished by their electrode geometry, pressure range, and the type of applied electric power. The nonequilibrium plasmas are referred to as electric gas discharges. Differences in the discharges produce different characteristics for each discharge, such as different electron energies, electron temperatures, electron densities, and electric field strengths. The five main types of nonequilibrium discharges include microwave, glow, radio frequency, and corona discharges.

##### DC Glow Discharge

The DC glow discharge is established in a tube between two electrodes with a parallel plate geometry. The DC discharge is commonly called a glow discharge because of the glow established at the breakdown voltage, and produces discharges with positive and negative charge concentrations. The pressure is typically smaller than 10 mbar resulting in low mass flowrates. The DC glow discharges produce low average electron energies (0.5 - 2 eV) and densities ( $10^8$ - $10^{11}$   $\text{cm}^{-3}$ ), as a result of low electric field strengths. Due to low mass flowrates, low pressure, and low power the DC discharge has not been used for chemical production. (Eliasson and Kogelschatz, 1991)

## Radio Frequency

The radio frequency (RF) discharge operates either inductively or capacitively in the radio frequency region of 2 to 60 MHz. The RF discharge avoids electrode contamination since electrodes exist on the outside of the reactor. Unlike the DC glow discharge, the radio frequency discharge produces neutral charge concentrations due to the reversing polarity of the electric field. If an electron makes an elastic collision with an atom, reversing its motion at the time the electric field changes direction, it will continue to gain energy and speed. Due to this behavior the RF discharge is more efficient than the DC discharge for promoting ionization. (Grill, 1994) The RF discharge operates best at low pressure, but it may also operate up to atmospheric pressure. A transition to thermal equilibrium occurs if the frequency of the discharge reaches the collision frequency. (Eliasson and Kogelschatz, 1991)

## Microwave Discharge

The microwave discharge is an electrodeless discharge and operates in a frequency range of 2.45 to 10 GHz. A waveguide or resonant cavity transfers the microwave power to the plasma. The pressure range of the discharge may vary from 1 mbar up to about atmospheric pressure. The power of the microwave discharge is low with a typical electric field strength being only about 30 V/cm. The discharge volume decreases with increasing microwave frequency. Therefore, at a particular high microwave frequency the discharge volume is very small promoting almost no reaction. (Grill, 1994)

## Corona Discharge

The corona discharge uses point to point, point to plane, packed bed, and coaxial or wire duct electrode geometries. The inhomogeneous point to plane electrode geometry is used to stabilize high current discharges in order to prevent the discharge from becoming an arc discharge. The packed bed reactors usually contain electrodes in a parallel plate geometry with a high dielectric ceramic pellet layer ( $\text{BaTiO}_3$ ,  $\text{SrTiO}_3$ , or  $\text{PbTiO}_3$ ) for chemical destruction. A micro breakdown occurs around the pellets enhancing the contact region of the electric field with the gas.

Generation of the discharge may occur with either DC or AC voltage. Depending upon the polarity of the DC voltage, the corona discharges may exist in the positive or negative corona form in the point to plane geometry. The negative corona first exhibits trichel pulses, however with increasing voltage the discharge transforms to a pulseless discharge. A burst pulse corona followed by a streamer, and eventually a glow corona are observed with a positive corona as the applied voltage increases. Both the positive and negative coronas eventually reach spark discharges when the voltage and current continue to increase. AC corona discharges exhibit no polarity effects due to the alternating electric field creating a continuous discharge.

The corona discharge operates under conditions that are adaptable to industrial application. Operation occurs at atmospheric pressure which allows high mass flowrates. High electric field strengths vary from 0.5 kV/cm to 50 kV/cm and produce average electron energies ( $>5$  eV) sufficient for chemical synthesis. The plasma zone of the corona

discharge is small, but high mass flow rates and atmospheric conditions are well suited for chemical synthesis. (Chang, et al., 1991)

### **Silent Discharge**

The silent discharge consists of electrodes in a parallel plate or concentric geometry with one electrode covered with a dielectric material. The dielectric material promotes microdischarges over its surface, therefore creating a large discharge volume. The electric field strength may vary from 0.1-100 kV/cm and produces average electron energies up to 10 eV. The silent discharge is an attractive method for chemical synthesis, since it operates at atmospheric pressure and has a large discharge volume. (Eliasson and Kogelschatz, 1991)

### **1.5 Plasma Industrial Applications**

The use of nonequilibrium plasmas occurs in a variety of areas which include chemical synthesis, electrostatic precipitators, electrophotography, and semiconductors. Utilization of silent discharge reactors for ozone chemical synthesis has occurred since the early 1900s. Ozone is used in water purification processes around the world. As a result, production of ozone by the silent discharge reactors has become one of the most important plasma chemical processes. (Eliasson and Kogelschatz, 1991)

The most important industrial applications of the corona discharge include electrostatic precipitators (ESP) and electrophotography. The utility, iron/steel, paper manufacturing, cement, and ore-processing industries utilize ESP for the collection of particulate emissions. The electronics industry utilizes electrophotography for creating



images using corona charging of particles in printers and copy machines. (Chang, et al., 1991)

The semiconductor industry uses a low pressure radio frequency discharge for plasma etching in the manufacturing of semiconductors. Plasma etching techniques produce semiconductors with higher density microelectronics than wet etching techniques. (Kenward, 1995)

### 1.6 Methane Conversion

Several studies of methane conversion using microwave plasmas have been reported. In 1993, Huang and Suib reported the methane dimerization to ethane and ethylene via microwave plasma. Conversions of methane varied from 0 to 11 % under low pressures ranging from 10 to 100 mmHg. The selectivities to ethylene and ethane are high, but excessive microwave power promotes carbon formation. They concluded that the efficiency of driving the methane dimerization reaction is only 2 - 8 %.

A study by Suib and Zerger (1993) included the use of catalysts to enhance the dimerization of methane in the microwave discharge. Product selectivities reached levels as high as 77 % ethylene, 25 % ethane, and 25 % acetylene. Nickel and platinum catalysts were placed below the plasma zone providing reaction sites for radical combination. Reaction rates increased with the use of catalyst. The maximum conversion observed without a catalyst was 31 %. Conversion became as high as 52 % with catalyst. Once again, the operating pressures were very low ranging from 10 to 50 Torr.

Another microwave plasma study activated methane in the presence of air. The objectives involved converting methane into  $C_2$  hydrocarbons or synthesis gas. The microwave power varied from 350 to 650 watts with a microwave frequency of 2.45 GHz. Pressure varied from 10 to 60 mbar. About 90 to 95 % of the oxygen was consumed in the discharge reactions. A  $C_2$  hydrocarbon yield of 22 % was achieved with 80 % methane conversion and synthesis gas was also produced. (Oumghar et al., 1995)

In 1985, a study by Fraser and coworkers investigated the decomposition of methane in an AC electric discharge at atmospheric pressure and 60 Hz. The AC electric discharge operated capacitively using a pyrex condenser with silver coating electrodes. A high voltage AC power supply and transformer generated the AC discharge. Methane destruction efficiencies reached 67 % with an input methane concentration of 120 ppm. Higher input oxygen concentrations in the nitrogen stream were shown to increase the production of  $CO_2$ .

In 1986, Mallinson and Sliepcevich reported the first preliminary work with nonequilibrium discharges at the University of Oklahoma. They studied the partial oxidation of methane using an ozonolysis type reactor with applied AC voltage. Several experiments were conducted to develop an understanding of how the operating variables affected the discharge reactions. Experiments showed that methane conversion increases with frequency and that gas temperature and different types of waveforms have no major effect on the discharge reactions.

Bhatnagar also studied the partial oxidation of methane using the ozonolysis discharge reactor. It was found that increases in the methane/oxygen ratio decrease the methane conversion, but the selectivity of methanol slightly increases. Residence time experiments showed a series pathway to carbon oxides. Alcohols and ethane were intermediates in the reactions. The formation of ethanol was found to be independent of the formation of ethane or methanol.

Recently at the University of Oklahoma, Lobban and coworkers (1996) investigated the oxidative coupling of methane using DC and AC corona discharges. Temperature programmed corona reaction experiments for DC positive and negative corona discharges showed that the rate of  $C_2$  formation below  $450^\circ C$  is very slow and that the complete consumption of oxygen occurred at  $875^\circ C$ . The positive corona produced higher  $C_2$  yields than the negative corona, therefore the streamers of the positive corona are more favorable for OCM than the trichel pulses of the negative corona. However, with no applied external heating the AC corona produced a maximum  $C_2$  yield of 21 %. Experiments were conducted with the AC corona to determine the effects of frequency, voltage, residence time, and oxygen partial pressure. An OCM discharge mechanism was also suggested by Lobban and coworkers.

A similar study demonstrated the effects of OCM over a  $Sr/La_2O_3$  catalyst in a DC corona discharge reactor. They showed that the operating temperature of the corona discharge with  $Sr/La_2O_3$  catalyst was much lower ( $<200^\circ C$ ) than the required temperature without the presence of a discharge. They found that increases in the oxygen partial

pressure increased the methane conversion and the yield of C<sub>2</sub> products. The highest C<sub>2</sub> yield achieved was 11 %. (Lobban, et. al, 1997)

## 1.7 Research Objectives

The corona and silent nonequilibrium discharges appear to be better suited for chemical synthesis than microwave, DC glow, and radio frequency discharges due to their operating conditions. The AC electric gas discharge reactor operates under corona discharge conditions with homogeneous OCM reactions. This research continues the previous work conducted by Lobban and coworkers at the University of Oklahoma.

Research objectives include:

1. To investigate the OCM using an AC electric gas discharge for the development of an improved methane conversion to higher hydrocarbons.
2. To determine the effects of operating variables on the AC electric gas discharge reactor.

## 1.8 Present Work

The following chapters report research investigations on the oxidative coupling of methane using an AC electric gas discharge reactor. Chapter two explains the AC electric gas discharge reactor setup, gas and liquid analysis, mass flow controller and GC calibrations, calculations, and general experimental procedures. Chapter three reports a study on the oxidative coupling of methane using and AC electric gas discharge. In this study the effects of operating variables on the AC electric gas discharge reactions were investigated. Chapter four describes preliminary experiments with helium, adiabatic experiments, and temperature measurement experiments. Chapter five explains attempts

to develop rate expressions for the AC electric gas discharge reactor. Finally, chapter six presents the conclusions and further recommendations for the oxidative coupling of methane using an AC electric gas discharge.

*Methane Under the Influence of an AC Electric Discharge. A Thesis for Master of Science, University of Oklahoma, 1991.*

Caplan, M.J.; Miles, P.; Caputo, M.A.; Mingo-Perez, A.; Carlsone, T.; O'Brien, J.A. *Sr<sub>2</sub>O<sub>2</sub>/Al<sub>2</sub>O<sub>3</sub> Catalyst for Methane Coupling: Influence of the Structure of Surface Sr-OH Phases on the Reactivity.* *J. Phys. Chem.* 1990, 94, 5233.

Chakrabarti, A. *Gas Cleaning with Semi-Wet Type Plasma Reactor.* *IEEE TRANS ON IND. APPL.* 1995, 23, 582.

Cheng, J.; Levine, P.A.; Yamamoto, Y. *Corona Discharge Processes.* *IEEE Trans Plasma Sci.* 1991, 19, 1132.

DeBoy, J.M.; Eick, R.F. *Kinetics of the Oxidative Coupling of Methane over a Sr<sub>2</sub>O<sub>2</sub>/Al<sub>2</sub>O<sub>3</sub>.* *J. Catal.* 1990, 123, 547.

Elango, B.; Engelmann, B. *Transportation Volume/Plasma Chemical Processing.* *IEEE Trans Plasma Sci.* 1991, 19, 1089.

Frost, M.R.; Fox, D.A.; Harrison, R.B. *Decomposition of Silanes in an AC Discharge Plasma.* *Chem. and Plasma Proc.* 1985, 3, 143.

Gilb, A. *Cold Plasma in Microvial Fabrication: From Academic to Commercial.* *IEEE Proc.* New York, 1994.

Huang, J.H.; Solt, S.L. *Methane Dissociation Via Microwave Plasma.* *Acc Chem Journal.* 1994, 20, 133.

Kowarski, M. *Why Plasma Science Matters Now.* *Pipe World* 1995, 5, 41.

Krylov, O.V. *Methods for Improving the Efficiency of Catalysts for the Oxidative Combustion of Methane.* *Russian Chemical Review.* 1992, 61, 851.

LeBlond, S.; Liu, C.; Mirovits, A.; Hill, B.J.; Xu, B.; Mallinson, B. *Oxidative Coupling of Methane with 50 and 60 Corona Discharges.* *AIChE* 1996, 35, 3295.

## WORKS CITED

- Bhatnagar, R. A Study of Partial Oxidation of Methane Under the Influence of an AC Electric Discharge. A Thesis for Master of Science, University of Oklahoma, 1993.
- Capitan, M.J.; Malet, P.; Centeno, M.A.; Munoz-Paez, A.; Carrizosa, I.; Odriozola, J.A.  $\text{Sm}_2\text{O}_3/\text{Al}_2\text{O}_3$  Catalysts for Methane Coupling. Influence of the Structure of Surface Sm-Al-O Phases on the Reactivity. *J. Physics. Chem.* **1993**, 97, 9233.
- Chakrabarti, A. Gas Cleaning with Semi-Wet Type Plasma Reactor. *IEEE TRANS. on IND. APPL.*, **1995**, 31, 500.
- Chang, J.; Lawless, P.A.; Yamamoto, T. Corona Discharge Processes. *IEEE Trans. Plasma Sci.* **1991**, 19, 1152.
- DeBoy, J.M.; Hicks, R.F. Kinetics of the Oxidative Coupling of Methane over 1 wt % Sr/La<sub>2</sub>O<sub>3</sub>. *J. Catal.* **1988**, 113, 517.
- Eliasson, B.; Kogelschatz, U. Nonequilibrium Volume Plasma Chemical Processing. *IEEE Trans. Plasma Sci.* **1991**, 19, 1063.
- Fraser, M.E.; Fee, D.A.; Sheinson, R.S. Decomposition of Methane in an AC Discharge. *Plasma Chem. and Plasma Proc.*, **1985**, 5, 163.
- Grill, A. *Cold Plasma in Materials Fabrication: From fundamentals to applications*; IEEE Press: New York, 1994.
- Huang, J.H.; Suib, S.L. Methane Dimerization Via Microwave Plasmas. *Res. Chem. Intermed.* **1994**, 20, 133.
- Kenward, M. Why Plasma Science Means Business. *Phys. World*, **1995**, 6, 31.
- Krylov, O.V. Methods for Increasing the Efficiency of Catalysts for the Oxidative Condensation of Methane. *Russian Chemical Reviews*, **1992**, 8, 851.
- Lobban, L.; Liu, C.; Marafee, A.; Hill, B.J.; Xu, G.; Mallinson, R. Oxidative Coupling of Methane with ac and dc Corona Discharges. *I&EC*, **1996**, 35, 3295.

- Lobban, L.; Marafee, A.; Liu, C.; Xu, G.; Mallinson, R. An Experimental Study on the Oxidative Coupling of Methane in a Direct Current Corona Discharge Reactor over Sr/La<sub>2</sub>O<sub>3</sub> Catalyst. *I&EC*, **1997**, 36, 632.
- Maezono, I.; Chang, J. Reduction of CO<sub>2</sub> from Combustion Gases by DC Corona Torches. *IEEE TRANS on IND. APPL.*, **1990**, 26, 651.
- Mallinson, R.G., Sliepcevich, C.M. Field Effect Catalysis Program Final Report. *University Technologist, Inc.*, 1986.
- Mizuno, A.; Yamazaki, Y.; Ito, H.; Yoshida, H. ac Energized Ferroelectric Pellet Bed Gas Cleaner. *IEEE TRANS. on IND. APPL.*, **1992**, 28, 535.
- Otsuka, K.; Shimizu, Y.; Komatsu, T. Ba Doped Cerium Oxides Active for Oxidative Coupling of Methane. *Chem. Lett.* **1987**, 1835.
- Oumghar, A.; Legrand, J.C.; Diamy, A.M.; Turillon, N. Methane Conversion by an Air Microwave Plasma. *Plasma Chem. and Plasma Proc.* **1995**, 15, 87.
- Phelps, A.V. Basic Parameters for Electrical Discharges in Gases. in *Proc. of Symp. on Chemical Reactions in Electrical discharges, 153 rd ACS National Meeting, Miami Beach Florida, April 11-13, 1967*, pp 18-28.
- Ruihong, Z.; Yamamoto, T.; Bundy, D.S. Control of Ammonia and Odors in Animal Houses by a Ferroelectric Plasma Reactor. *IEEE TRANS. on IND. APPL.*, **1996**, 32, 113.
- Suib, S.L.; Zenger, R.P. A Direct, Continuous, Low-Power Catalytic Conversion of Methane to Higher Hydrocarbons via Microwave Plasmas. *J. of Catalysis*, **1993**, 139, 383.

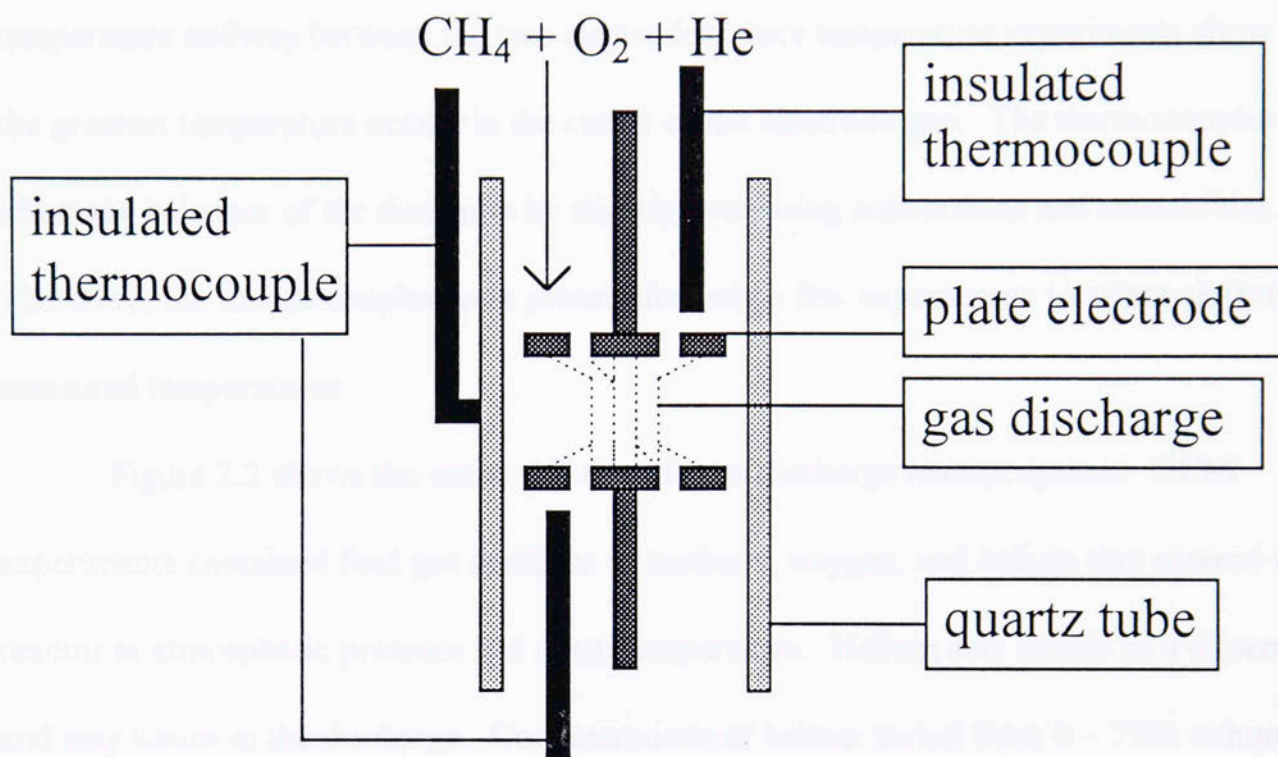
## The AC Electric Gas Discharge Reactor System and Experimental Procedure

### 2.1 AC Electric Gas Discharge Reactor

Figure 2.1 is a schematic of the AC electric gas discharge reactor. The discharge occurs in a quartz tube between the two electrodes. The inside and outside diameters of the quartz tube are 7 and 9 millimeters, respectively. The quartz tube length is approximately 46.7 centimeters. In addition, the electrodes are constructed of stainless steel and positioned in a parallel plate geometry. The electrode gap width varies from 0.635 cm to 2.54 cm. Stainless steel rods (1.6 mm diameter) connect the electrodes to the AC power source. Each electrode contains four small holes to allow even gas distribution through the electrode gap. The diameter of each electrode is approximately 0.152 millimeters less than the inside quartz tube diameter. This allows for thermal expansion of the electrodes caused by heating effects from the electric gas discharge and exothermic reactions.



Figure 2.1: AC Electric Gas Discharge Reactor



Rxn. Products:  $\text{C}_2\text{H}_6$ ,  $\text{C}_2\text{H}_4$ ,  $\text{CO}$ ,  $\text{CO}_2$ , water,  
& trace formaldehyde

Two insulated thermocouples positioned inside the reactor measure the gas temperatures as shown in Figure 2.1. An external thermocouple measures the outside wall temperature midway between the two electrodes, since temperature experiments show that the greatest temperature occurs in the center of the electrode gap. The thermocouples affect the behavior of the discharge by slightly decreasing conversions and selectivities. Therefore, the thermocouples were present for only a few experiments to relate all three measured temperatures.

Figure 2.2 shows the entire AC electric gas discharge reactor system. OCM experiments contained feed gas mixtures of methane, oxygen, and helium that entered the reactor at atmospheric pressure and room temperature. Helium acts mainly as a diluent and may ionize in the discharge. Concentrations of helium varied from 0 – 75% volume. All experiments were performed well above the upper explosive limit (1.45 methane/oxygen % volume) for methane in oxygen at atmospheric conditions. The methane/oxygen ratios varied from 3/1 to 8/1 % volume.

Operation of the reactor was usually under non-adiabatic conditions and with no external heating. However, operation of a few experiments occurred under near adiabatic conditions. Glass wool insulation was wrapped around the quartz tube reactor to achieve the near adiabatic conditions.

Porter Instrument Co. Model 201 mass flow controllers were calibrated as discussed in Section 2.2 and regulated all feed gases. The feed gases were combined and flowed downward through the reactor. Total flow rates varied from 50 - 200 cm<sup>3</sup>/min.

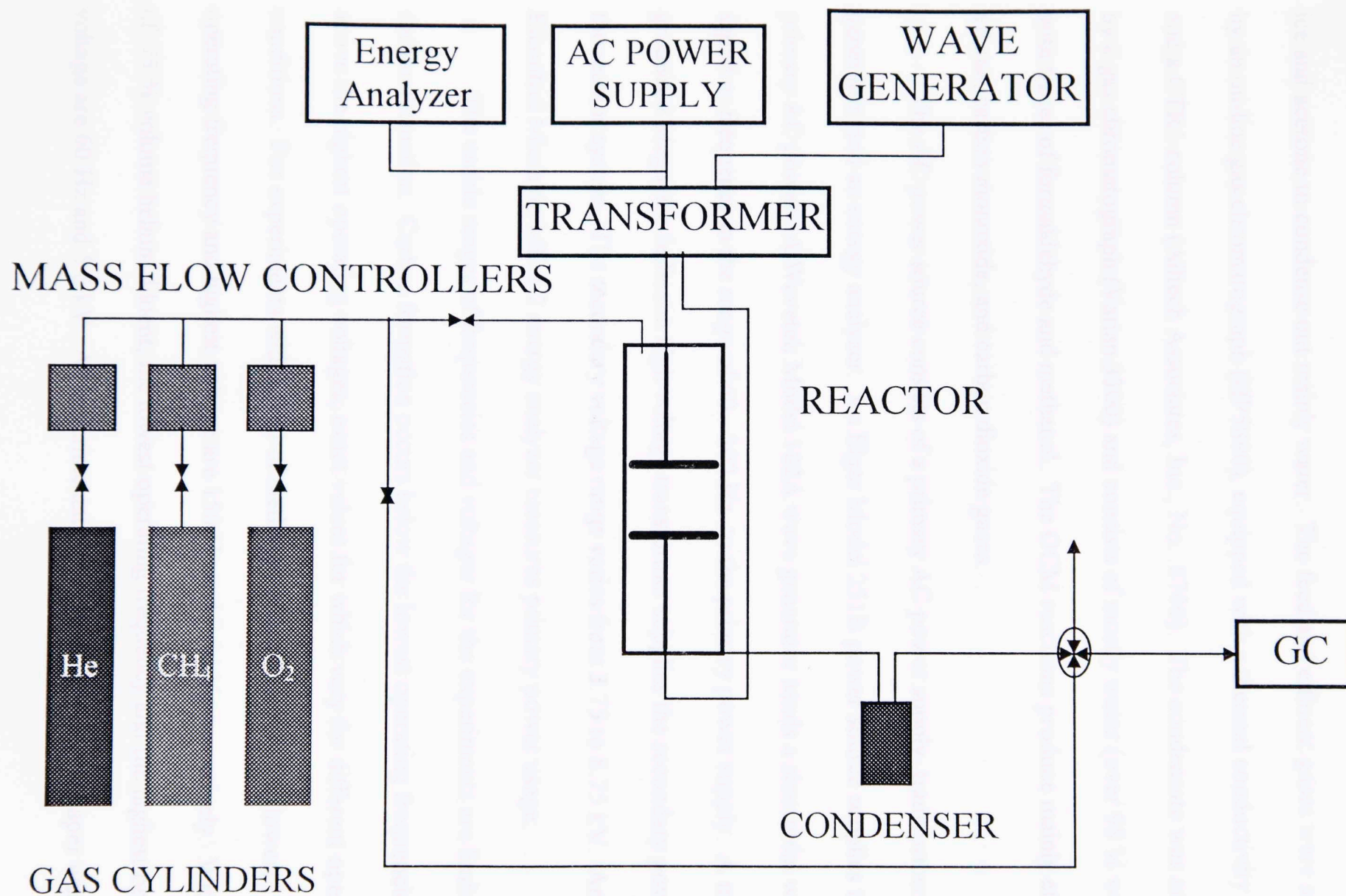


Figure 2.2: AC Electric Gas Discharge Reactor System

Exhaust gases from the reactor flowed through a condenser containing a mixture of dry ice and acetone to condense out mainly water. The feed and effluent gases were analyzed by an on-line gas chromatograph (HP5890), equipped with a thermal conductivity detector and a CTR1 column (Alltech Associates, Inc., No. 8700). The condensate was analyzed by a gas chromatograph (Varian 3300) and consists of mostly water (over 98 % weight) with traces of formaldehyde and methanol. The OCM reactions produce mainly ethylene, ethane, carbon monoxide, and carbon dioxide gases.

The AC power source consists of a primary AC power supply, transformer, wave generator, and an energy analyzer. An Elgar Model 251B power source supplies the primary AC power. A Wavetek Model 182A wave generator sends a sinusoidal wave signal or frequency in the range of 60 - 300 Hz to the primary power supply. A midpoint grounded Magnetec Jefferson high voltage transformer supplies the secondary power to the reactor system. The secondary voltage range varies from 3.75 to 8.75 kV. An Elcontrol Microvip MK 1.2 energy analyzer measures primary power usage.

The usable ranges of frequencies and voltages for the experiments are limited by carbon formation. Carbon formation occurs below the lowest operating frequencies and above the highest operating voltages, exact values for which vary for different operating conditions. For experiments with a feed of methane and oxygen only, the lowest operating frequency and highest voltage are 150 Hz and 7.5 kV, respectively. With a feed of 75 % volume helium diluent, the lowest operating frequency and the highest operating voltage are 60 Hz and 5.6 kV. All experimental results presented in this paper were

obtained under operating conditions where carbon formation is not significant. However, the carbon balance error in some of the experiments is significant, typically at high methane conversions (above 20 %). Unknown products are assumed to account for the carbon balance error and will be referred to as “unknowns” in the results and discussions of Chapter Three. The unknowns vary in a consistent rather than random fashion with operating conditions. The unknown products are believed to correspond to liquid and/or gas products that are not quantified by the analysis. We are currently developing analytical techniques to identify and quantify the unknown products.

## 2.2 GC Calibration

The GC calibration requires flowing known amounts of gases through the GC. Therefore, the first step involved in the GC calibration consists of calibrating the Porter mass flow controllers. The flowrate calibrations were performed at room temperature and atmospheric pressure. A bubble meter was used to measure the flowrate. The Porter mass flow controllers each contain an electronic control valve and the flowrate depends on the opening of the valve. A Porter flow controller interface regulates the opening of the valve by displaying a reading (%R) from 0 to 100 %. If the mass flow controller operates correctly, a linear relationship exists between %R and the flowrate. Next, linear regression of calibration data (%R vs. flowrate) from each mass flow controller yields the calibration factors. For example, the calibration factor for the methane mass flow controller (500 SCCM) is 0.1889. The desired flowrate of methane results from the equation:

$$\%R = 0.1889 * (\text{methane flowrate})$$

Similar equations exist for all other Porter mass flow controllers used in the AC electric gas discharge experiments. Appendix B lists the calibration factors for the Porter mass flow controllers.

The relative calibration factor method was used to quantify the feed and effluent gases from the AC electric gas discharge reactor system. This method utilizes relative calibration factors to quantify the amount of a gas relative to a reference gas (which itself has a calibration factor of one). Methane is the best choice for the reference gas, since methane is always present in both feed and effluent gases. The relative calibration factor corresponds to a proportionality coefficient between the amount of a gas and the GC peak area. This allows the gas sample size to vary, an advantage of the method. Calculation of the amount of a gas  $M_I$  results from the equation:

$$M_I = f_I A_I$$

Here,  $f_I$  and  $A_I$  correspond to the relative calibration factor and GC peak area of a gas, respectively. The relative calibration factors are obtained for the gases (ethane, ethylene, CO, CO<sub>2</sub>, O<sub>2</sub>) using the following equation:

$$f_I = M_I A_R / M_R A_I \quad (\text{Guiochon and Guillemin, 1988})$$

Here, the R represents the reference gas methane and the I represents one of the other gases. The mass flow controller and GC calibration factors were checked periodically with time to determine their accuracy. In short, the relative calibration factors aid in determining

the effluent gas compositions, the starting point of calculations. Appendix B lists the relative calibration factors for the gases ( $C_2H_6$ ,  $C_2H_4$ , CO,  $CO_2$ ,  $O_2$ ).

### 2.3 Calculations

The calculations usually necessary to evaluate the experimental data include both methane and oxygen conversions,  $C_2$  yield, and selectivities. The calculations of methane and oxygen conversions resulted from the differences in their feed and effluent gas GC peak areas. The GC relative calibration factors along with GC peak areas allowed the calculation of effluent gas compositions and the carbon balance error. Next, the effluent gas compositions allowed the calculation of the  $C_2$  yield and individual selectivities. A BASIC computer program was used to calculate the experimental results. Carbon balance closure errors greater than 5% were treated as unknown products in the calculations.

The calculations assumed ideal gas behavior. If changes in the effluent gas flowrate due to reactions occurred, the effluent gas flowrate was entered into the BASIC computer program. Appendix B contains a copy of the computer program.

### 2.4 General Experimental Procedure

The AC electric gas discharge reactor experiments investigated the effects of operating variables on the oxidative coupling of methane in the AC electric gas discharge. The operating variables include oxygen partial pressure, flowrate, gap width, voltage, and frequency. In a typical experiment, an operating variable was varied, while all other operating variables were held constant. For example, the frequency range in an

experiment may vary from 150 to 300 Hz to determine the effects of frequency on conversions and selectivities.

### **Startup**

Startup of an experiment first involves establishing the desired flowrate through the AC electric gas discharge reactor system. Starting the flow first requires opening the valves about 3/4 of a turn on the helium, methane, and oxygen gas cylinders. Then the mass flow controller interface is turned on and the % readings are set for each gas. If a problem exists with the reactor system, the feed gases are switched to the bypass in order to fix the problem. The mass flow controllers are given ten minutes to warm up and reach stabilization. Dry ice and acetone are added to the condenser, and feed gas samples are taken. Explosive concentrations of methane and oxygen are avoided by operating above the upper explosive limit for methane in oxygen at atmospheric pressure (1.45 methane/oxygen % volume).

Initiating the discharge requires turning on the wave generator and the AC power supply. A high frequency (400 Hz) initiates the discharge easier than frequencies in the normal operating range (60 - 300 Hz). This may prevent carbon formation from occurring on the electrodes due to a high breakdown voltage. Next, the voltage is slowly increased from zero to the breakdown voltage. The breakdown voltage will vary as a result of different gas compositions. After establishing the initial discharge, the voltage and frequency are simultaneously reduced until reaching the desired settings. The GC and



power measurement data collection are now begun at the desired settings. Three GC readings are taken for each setting.

### **Shutdown**

After data collection, the experiment is shutdown by reducing the voltage meter on the AC power supply to zero. This extinguishes the discharge. Next, the AC power supply is turned off, as is the wave generator. The gas flowrate are turned off by turning off the Porter flow controller interface. Finally, the valves on the helium, methane, and oxygen cylinders are closed.

## Literature Cited

Guiochon, G., and C.L. Guillemin. *Quantitative Gas Chromatography for Laboratory Analysis and On-Line Process Control*. Elsevier, 1988, 587.

### 3.1 Results and Discussion

The following sections discuss the effects of operating variables on catalyst and oxygen conversion, the  $C_2$  yield, selectivity, power, and current. The operating variables include oxygen partial pressure, catalyst diameter, flowrate, gap width, voltage, and frequency.

#### 3.1.1 Effect of Oxygen Partial Pressure

As mentioned earlier, researchers generally agree that in homogeneous (CH<sub>3</sub>)<sub>2</sub>CO oxidation of the surface is inhibited when by negatively charged oxygen species ( $O_2^{\cdot-}$ ). The oxygen atoms adsorbed on the surface form the oxygen ( $O_2$ ) molecule. This molecule is then desorbed in the gas phase to form oxygen. In contrast, the mechanism proposed by Leibel et al. (1975) to explain plasma induced oxidation of methane suggests oxidative attachment, an electron-molecule reaction (reaction 1 below), forms the negatively charged oxygen species  $O_2^{\cdot-}$ . Next, O

## CHAPTER THREE

### An Experimental Study on the Oxidative Coupling of Methane Using an AC Electric Gas Discharge

#### 3.1 Results and Discussion

The following sections discuss the effects of operating variables on methane and oxygen conversions, the C<sub>2</sub> yield, selectivities, power, and current. The operating variables include oxygen partial pressure, helium dilution, flowrate, gap width, voltage, and frequency.

##### 3.1.1 Effect of Oxygen Partial Pressure

As mentioned earlier, researchers generally agree that in heterogeneous OCM activation of the methane molecule occurs by negatively charged lattice oxygen ions (O<sup>-</sup> and O<sup>2-</sup>). The oxygen ions abstract hydrogen from methane to form the methyl (CH<sub>3</sub>) radicals. The methyl radicals then dimerize in the gas phase to form ethane. In comparison, the mechanism proposed by Lobban et al. (1996) to explain plasma induced oxidative coupling of methane suggests dissociative attachment, an electron-molecule reaction (reaction 1 below), forms the negatively charged oxygen specie O<sup>-</sup>. Next, O<sup>-</sup>

abstracts hydrogen from the methane molecule to form the methyl radicals in the corona discharges (reaction 2). Other ionization reactions, such as dissociative ionization and attachment may also produce negatively charged oxygen species. However, dissociative attachment is probably responsible for most of the  $O^-$  formation because it requires the least amount of energy (Grill, 1994; Eliasson and Kogelschatz, 1991).

Furthermore, the electron energy of the AC electric gas discharge is certainly sufficient to promote the dissociative attachment of oxygen. The proposed mechanism for the dissociative attachment of oxygen and the formation of the methyl radical:



Subsequently, methyl radicals combine to form ethane which may react further to produce ethylene, CO, CO<sub>2</sub>, and unknown products. Alternately, the methyl radicals may react with oxygen to form CO and CO<sub>2</sub>. Experimental results investigating the effect of oxygen partial pressure suggest that ethylene forms from ethane, but not directly from methane.

Other possible oxygen species that activate methane to form the methyl radical include metastable oxygen species. Researchers have shown that the metastable oxygen specie ( $O^1D$ ) activates methane to form the methyl radical (Oumghar et al. 1995; Marston

1996). Metastable species are characterized by long lives because of excitation to higher quantum levels. In addition, they cannot easily release energy to reach the ground state. However, the metastable oxygen species may release energy through inelastic collisions with methane producing the methyl radical. We have not determined the predominant oxygen species in the methane activation.

The oxygen partial pressure experiments investigated the effects of increased oxygen partial pressure on the OCM discharge reactions. Experimental conditions consisted of a flowrate of 100 cm<sup>3</sup>/min, 2.54 cm electrode gap width, and a constant methane partial pressure of 0.5 atm with a varying helium/oxygen ratio. Figure 3.1 illustrates how increases in oxygen partial pressure effect both conversions and selectivities.

The methane and oxygen conversions increase almost linearly as the oxygen partial pressure increases while the C<sub>2</sub> selectivity decreases. The C<sub>2</sub> yield increases, but much slower than the methane and oxygen conversions due to a tradeoff between C<sub>2</sub> selectivity (SC<sub>2</sub>H<sub>6</sub> + SC<sub>2</sub>H<sub>4</sub>) and methane conversion. The C<sub>2</sub> yield reached a maximum (16 %) at the highest oxygen partial pressure (0.17 atm). Conversely, the highest C<sub>2</sub> selectivity (66 %) occurred at the lowest oxygen partial pressure (0.05 atm).

Increased oxygen partial pressures probably increase the rate of complete oxidation of the C<sub>2</sub> products as suggested by increasing CO selectivity and decreasing C<sub>2</sub> selectivity. Based upon chemical stability, ethane and ethylene should oxidize more easily than methane. Hence, the complete oxidation of the methyl radical and C<sub>2</sub>

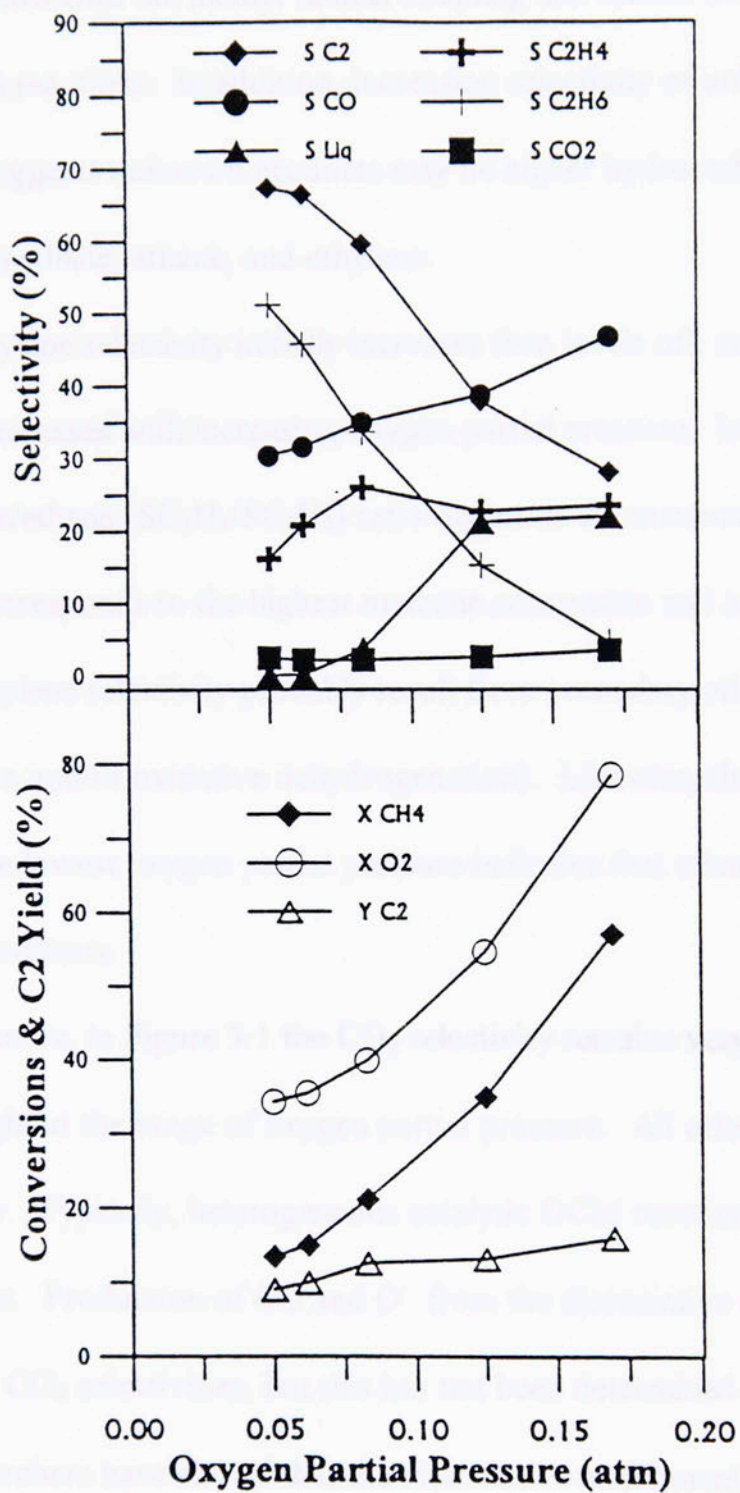


**Figure 3.1:** Effect of oxygen partial pressure on selectivities and conversions. Flowrate: 100 cm<sup>3</sup>/min. CH<sub>4</sub>/O<sub>2</sub>: 3-10. Applied voltage: 7.5 kV. Frequency: 200 Hz. Gap width: 2.54 cm. Methane Partial Pressure: 0.5 atm, balance helium.

products competes with the methyl radical coupling and ethane dehydrogenation in the OCM discharge reactions. In addition, increasing selectivity of unknowns with decreasing  $C_2$  selectivity suggests unknown products may be higher hydrocarbons from secondary reactions with methane, ethane, and ethylene.

The ethylene selectivity initially increases then levels off, and the ethane selectivity continuously decreases with increasing oxygen partial pressure. In this experiment, the highest ethylene/ethane ( $SC_2H_4/SC_2H_6$ ) ratio occurs at the maximum oxygen partial pressure and corresponds to the highest methane conversion and lowest  $C_2$  selectivity. Increases in ethylene selectivity probably result from secondary ethane reactions (i.e., dehydrogenation and/or oxidative dehydrogenation). Likewise, the extremely high ethane selectivity at the lowest oxygen partial pressure indicates that ethane is indeed one of the first synthesis products.

Furthermore, in Figure 3.1 the  $CO_2$  selectivity remains very low and almost constant throughout the range of oxygen partial pressure. All other experiments reveal a similar behavior. Typically, heterogeneous catalytic OCM reactions produce significant  $CO_2$  selectivities. Production of CO and  $O^-$  from the dissociative attachment of  $CO_2$  may explain the low  $CO_2$  selectivities, but this has not been determined in our system. However, researchers have shown that the dissociative attachment of  $CO_2$  occurs within the electron energies of corona discharges (Chantry, 1972; Orient and Srivastava, 1983). In addition, the AC electric gas discharge reactor produces CO and  $C_2$  products with a feed containing methane and  $CO_2$ .

### 3.1.2 Effect of Helium

The purpose of the helium experiment is to investigate the effect of a diluent on AC OCM discharge reactions. Helium was used as a diluent instead of nitrogen to avoid possible HCN and NO<sub>x</sub> formation that may occur from nitrogen in the discharge reactions. The helium partial pressures varied from 0 - 0.87 atm helium with the methane/oxygen ratio held constant at 3/1. The flowrate was constant at 100 cm<sup>3</sup>/min. Figure 3.2 shows the effects of increased helium diluent on conversions and selectivities.

Both methane and oxygen conversions decrease with increasing helium partial pressure until reaching 0.6 atm helium. The conversions both increase with further increases in helium partial pressure. The same conversion and selectivity results were observed with repeat experiments. Similarly, the C<sub>2</sub> selectivity increases with helium partial pressure (until reaching 0.6 atm helium), but decreases with further increases in helium partial pressure. Therefore, the C<sub>2</sub> yield very slightly increases (until reaching 0.6 atm helium), and then subsequently decreases with increasing in helium partial pressure.

Unlike the C<sub>2</sub> selectivity, the selectivity of unknowns initially decreases with increasing helium partial pressure suggesting unknown products result from secondary reactions with C<sub>2</sub> products. The increase in ethane selectivity may result from the decrease in secondary reactions producing unknowns from C<sub>2</sub> products. Beyond 0.6 atm helium, the decrease in ethylene selectivity and the increase in the selectivity of unknowns suggest the unknown formation mainly occurs from a secondary reaction with ethylene.

Figure 3.2: Effect of helium diluent on selectivities and conversions, flowrate: 100 cm<sup>3</sup>/min, CH<sub>4</sub>/O<sub>2</sub> = 3, Applied Voltage: 6.25 kV, Frequency: 100 Hz, Discharge: 100 s.



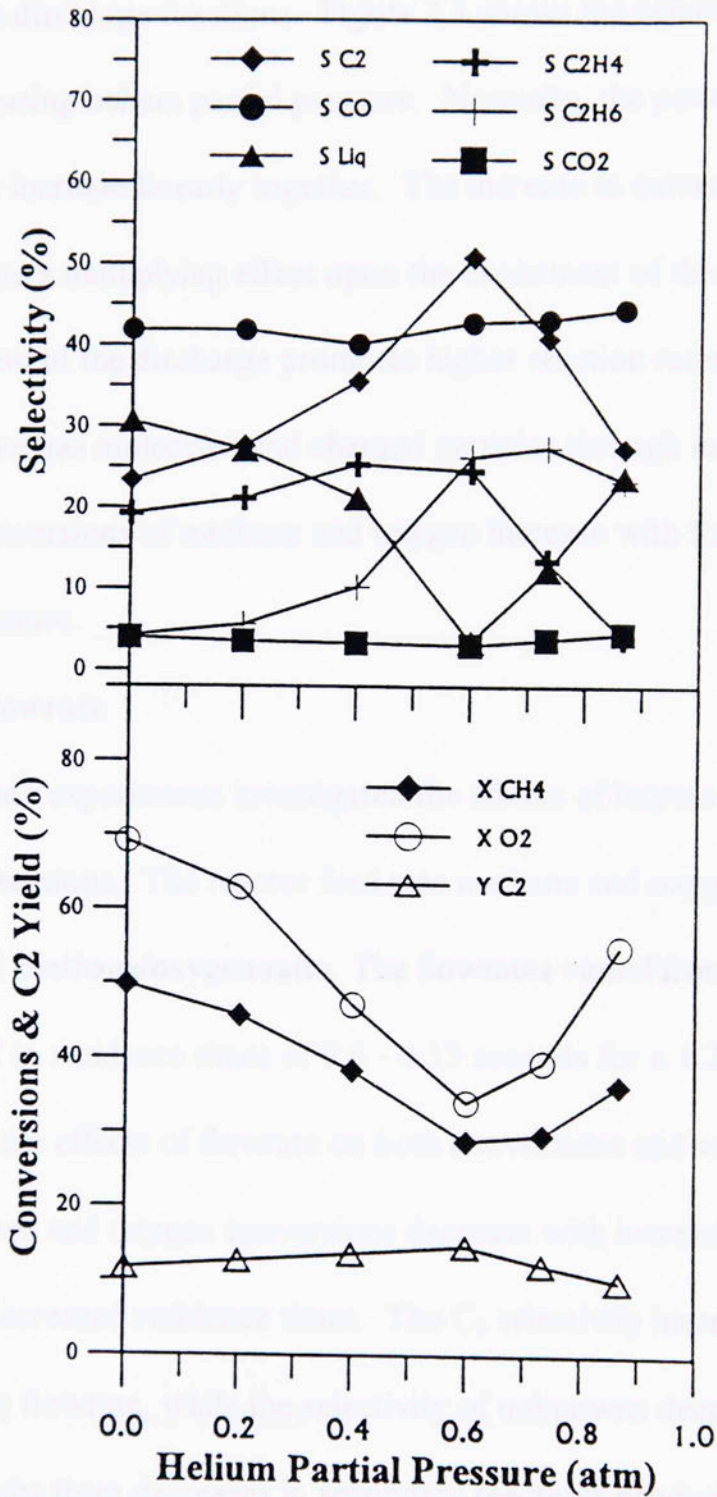


**Figure 3.2:** Effect of helium diluent on selectivities and conversions. Flowrate: 100 cm<sup>3</sup>/min. CH<sub>4</sub>/O<sub>2</sub>: 3. Applied voltage: 6.25 kV. Frequency: 150 Hz. Gap width: 1.27 cm.

The main effects of helium include the helium acting as a diluent and eventually as a “catalyst” to the discharge reactions. Figure 3.3 shows the behavior of the power and current with increasing helium partial pressure. Normally, the power and current would either decrease or increase linearly together. The increase in current beyond 0.6 atm helium must initiate a multiplying effect upon the excitement of the discharge. The increased excitation of the discharge promotes higher reaction rates due to increased interaction between gas molecules and charged particles through inelastic collisions. Therefore, the conversions of methane and oxygen increase with further increases in helium partial pressure.

### 3.1.3 Effect of Flowrate

The flowrate experiments investigated the effects of increased flowrate on the OCM discharge reactions. The reactor feed was methane and oxygen only (i.e. no helium diluent) with a 4/1 methane/oxygen ratio. The flowrates varied from 50 - 200 cm<sup>3</sup>/min which correspond to residence times of 0.6 - 0.15 seconds for a 1.27 cm gap width. Figure 3.4 shows the effects of flowrate on both conversions and selectivities.

The methane and oxygen conversions decrease with increasing flowrates as expected due to decreased residence times. The C<sub>2</sub> selectivity increases (from 24 % to 37 %) with increasing flowrate, while the selectivity of unknowns decreases. The increase in C<sub>2</sub> selectivity results from decreases in secondary reactions producing unknown products with increasing flowrates. Condensation on the quartz tube wall below the plasma zone decreases with increasing flowrates. The rapid increase in ethane selectivity and the

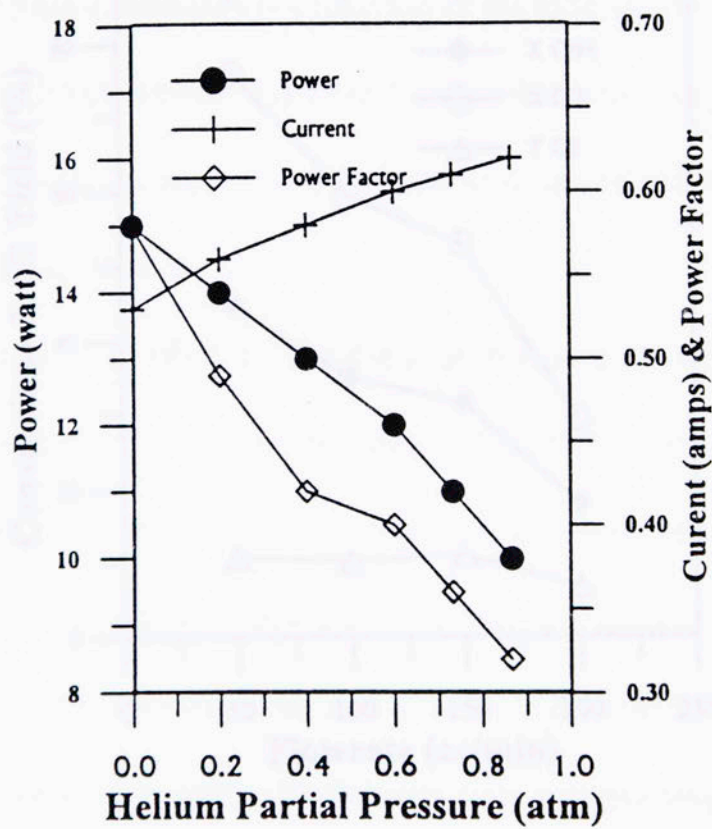


Figure 3.3: Effect of helium diluent on power. Flowrate: 100 cm<sup>3</sup>/min. CH<sub>4</sub>/O<sub>2</sub>: 3. Applied voltage: 6.25 kV. Frequency: 150 Hz. Gap width: 1.27 cm.

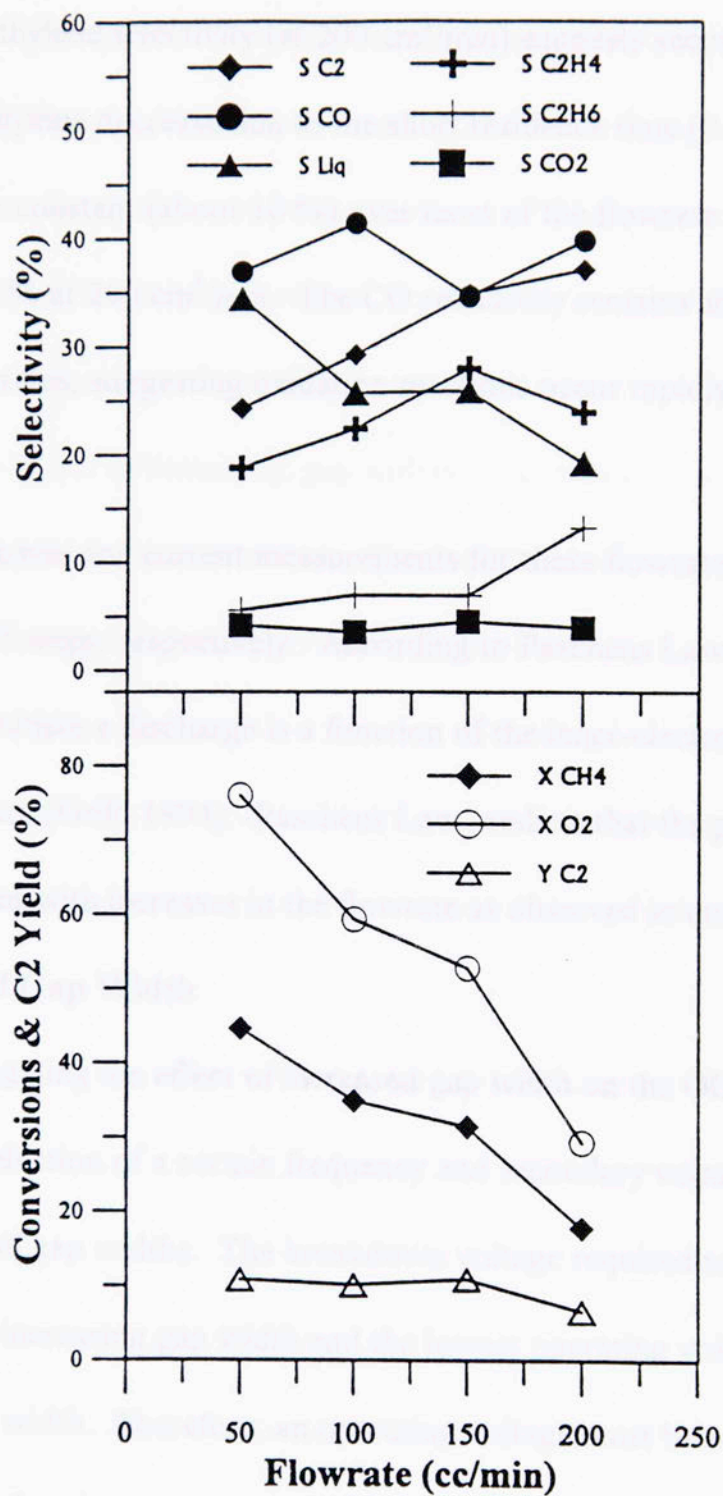


Figure 3.4: Effect of flowrate on selectivities and conversions. Flowrates: 50 -200  $\text{cm}^3/\text{min}$ .  $\text{CH}_4/\text{O}_2$ : 4. Applied voltage: 6.25 kV. Frequency: 150 Hz. Gap width: 1.27 cm. Methane Partial Pressure: 0.8 atm. Oxygen Partial Pressure: 0.2 atm.

decrease in ethylene selectivity (at 200 cm<sup>3</sup>/min) suggests secondary ethane reactions producing ethylene decrease due to the short residence time (0.6 seconds). The C<sub>2</sub> yield remains fairly constant (about 10 %) over most of the flowrate range, but finally decreases to less than 7 % at 200 cm<sup>3</sup>/min. The CO selectivity remains above 34 % over the entire range of flowrates, suggesting oxidation reactions occur rapidly in the AC OCM discharge.

The power and current measurements for these flowrates were constant at 12 watts and 0.45 amps, respectively. According to Paschens Law the breakdown voltage necessary to initiate a discharge is a function of the inner-electrode distance or gap width and the pressure (Grill, 1994). Paschens Law predicts that the power and current will remain constant with increases in the flowrate as observed in our experiments.

### 3.1.4 Effect of Gap Width

Investigating the effect of increased gap width on the OCM discharge reactions required the selection of a certain frequency and secondary voltage, thus allowing normal operation for all gap widths. The breakdown voltage required to initiate the discharge increases with increasing gap width and the lowest operating voltage also increases with increasing gap width. Therefore, an operating voltage must be selected that is within the voltage range of each gap width. Sufficiently high voltages may cause carbon filament formation on the electrodes for smaller gap widths (0.635 cm and 1.27 cm). In addition, increases in the gap width require higher frequency operation because lower frequencies raise the current and power to excessive levels, which may also cause carbon filament

formation. An acceptable frequency of 300 Hz and a secondary voltage of 8.75 kV was selected for all the gap width experiments. The electrode gap widths varied from 0.635 cm to 2.54 cm. Breakdown of the discharge was difficult to achieve beyond the 2.54 cm gap due to power limitations of the AC power supply. The 0.64 cm gap was selected as the lower gap limit due to decreasing conversions and very small residence times. Figure 3.5 shows the effect of increasing gap widths on conversions and selectivities.

The  $C_2$  yield and conversions of both methane and oxygen increase with increasing gap width. Once again a tradeoff exists between the  $C_2$  selectivity and methane conversion, therefore limiting the increase in  $C_2$  yield. As a result, the maximum  $C_2$  yield (12 %) occurs at the largest gap width (2.54 cm) with a methane conversion of 45 %. Both the methane and oxygen conversions appear to level off at the largest gap width (2.54 cm). Here, the oxygen conversion becomes greater than 70 %. Possibly, methane and oxygen conversions both behave asymptotically due to the depletion of oxygen in the discharge. Furthermore, the electric field strength ( $E/\text{gap width}$ ) decreases with increasing gap width. Therefore, the charge characteristics of the discharge may change causing the conversions to level off for the largest gap width.

As the gap width is increased, the methane conversion increases, but the  $C_2$  selectivity decreases from 42 % to 24 %. The CO and  $CO_2$  selectivities remain relatively constant. Therefore, the large increase in the selectivity of unknowns (from the 1.27 cm gap to the 1.91 cm gap) suggests other products form by secondary reactions with  $C_2$

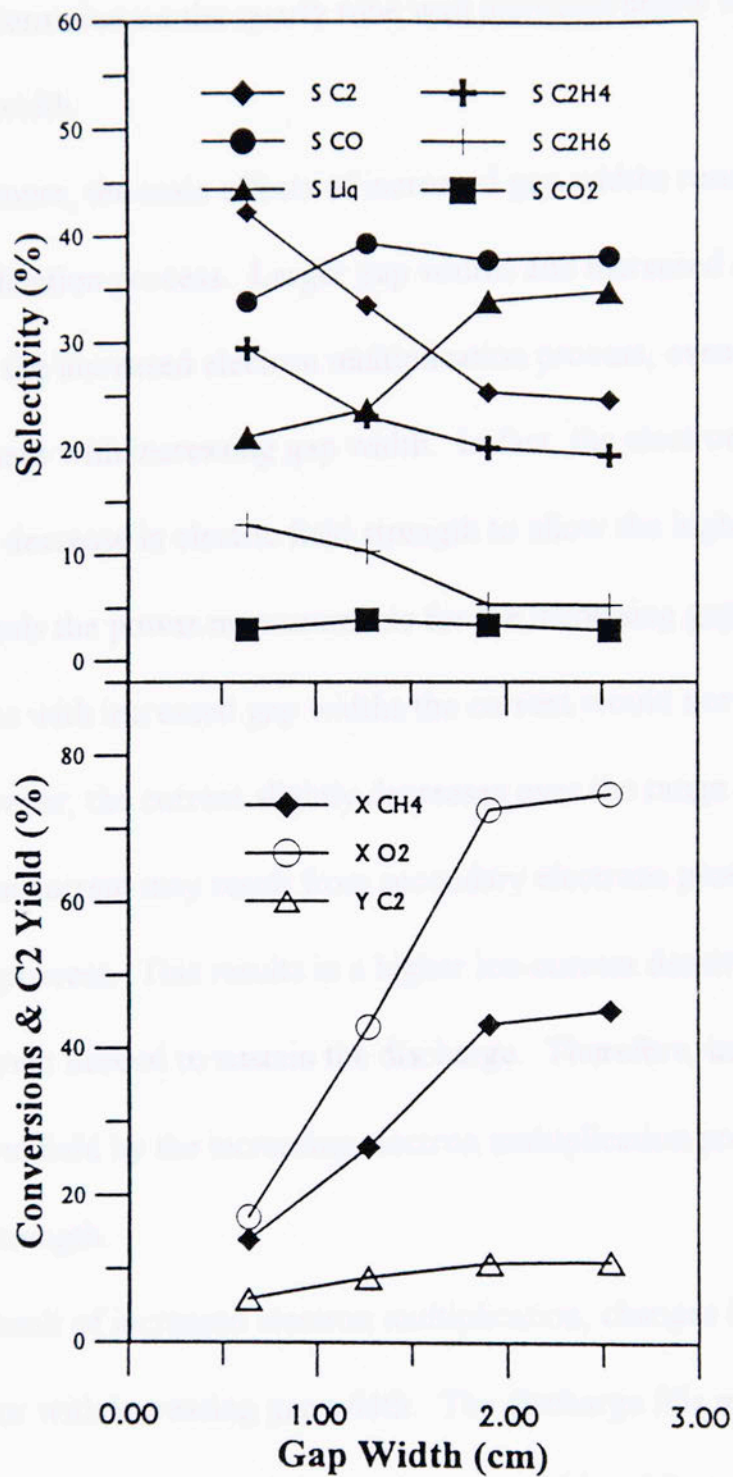


**Figure 3.5:** Effect of gap width on selectivities and conversions. Flowrate: 100 cm<sup>3</sup>/min. CH<sub>4</sub>/O<sub>2</sub>: 4. Applied voltage: 8.75 kV. Frequency: 300 Hz. Gap width: 0.635-2.54 cm. Methane Partial Pressure: 0.8 atm. Oxygen Partial Pressure: 0.2 atm.

products. Condensation on the quartz tube wall increases below the plasma zone with increasing gap width.

Furthermore, the main effects of increased gap widths result from an increased electron multiplication process. Larger gap widths and increased residence times are responsible for the increased electron multiplication process, even though the electric field strength decreases with increasing gap width. In fact, the electron multiplication process overcomes the decrease in electric field strength to allow the higher conversions. Next, Figure 3.6 reveals the power measurements for the increasing gap widths. Since the power increases with increased gap widths the current would normally be expected to increase. However, the current slightly decreases over the range of gap widths. Likewise, decreases in the current may result from secondary electrons produced by the electron multiplication process. This results in a higher ion-current density and decreases the amount of current needed to sustain the discharge. Therefore, increases in the gap width alter the electric field by the increasing electron multiplication process and decreasing the electric field strength.

As a result of increased electron multiplication, changes in the appearance of the discharge occur with increasing gap width. The discharge fills more of the reactor volume and becomes more luminous with increasing gap width, while emitting a bluish-white light. The luminosity of the discharge or emission of visible radiation probably results from excited gas particles returning to the ground state. Increases in methane and oxygen conversions correspond to more excited gas particles. Therefore, the greater



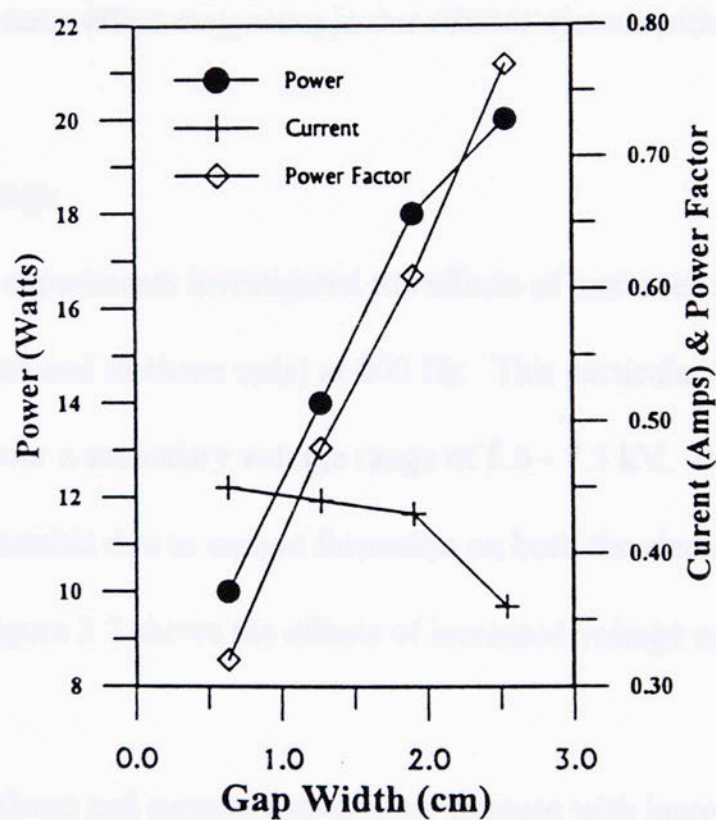


**Figure 3.6:** Effect of gap width power. Flowrate: 100 cm<sup>3</sup>/min. CH<sub>4</sub>/O<sub>2</sub>: 4. Applied voltage: 8.75 kV. Frequency: 300 Hz. Gap width: 0.635-2.54 cm. Methane Partial Pressure: 0.8 atm. Oxygen Partial Pressure: 0.2 atm.

luminosity of the discharge may occur because of the electron multiplication process increasing conversions.

Larger gap widths also allow electrons to travel further distances between the electrodes, increasing the chance for inelastic collisions and subsequent reactions. In addition, in radio frequency plasma reactors, increases in gap widths increase ionization at low pressures due to increases in the volume/surface ratio (Bell, 1972). The increase in volume/surface ratio decreases recombination reactions that occur due to collisions with reactor walls. This same effect may occur in our reactor system with increasing gap width.

### **3.1.5 Effect of Voltage**

The voltage experiments investigated the effects of increased voltage (for a feedstream of oxygen and methane only) at 200 Hz. This particular frequency allowed normal operations over a secondary voltage range of 5.6 - 7.5 kV. Beyond 7.5 kV the discharge became unstable due to carbon formation on both the electrodes as well as the quartz tube wall. Figure 3.7 shows the effects of increased voltage on both conversion and selectivities.

Both the methane and oxygen conversions increase with increasing voltage. The C<sub>2</sub> yield increases only slightly due to decreases in the C<sub>2</sub> selectivity from 33.6 % to 26.5 %. The highest ratio of ethylene/ethane occurs at 7.5 kV, the maximum operating voltage. Increases in the ethylene/ethane ratio along with increases in the selectivity of unknowns, suggest that secondary reactions increase with increasing voltage. Likewise,

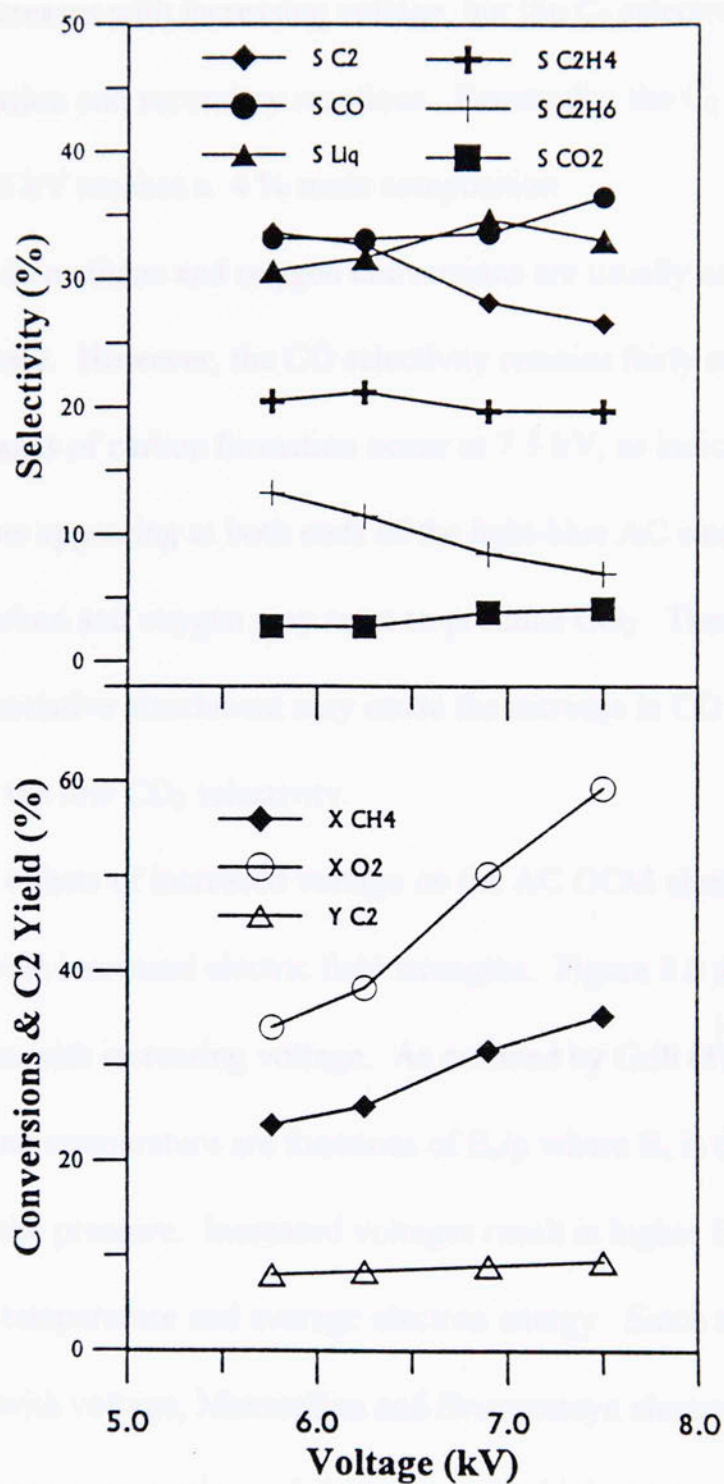


**Figure 3.7:** Effect of voltage on selectivities and conversions. Flowrate: 100 cm<sup>3</sup>/min. CH<sub>4</sub>/O<sub>2</sub>: 4. Applied voltage: 5.6-7.5 kV. Frequency: 200 Hz. Gap width: 1.27 cm. Methane Partial Pressure: 0.8 atm. Oxygen Partial Pressure: 0.2 atm.

C<sub>2</sub> production increases with increasing voltage, but the C<sub>2</sub> selectivity decreases due to increases in oxidation and secondary reactions. Eventually, the C<sub>2</sub> composition of the effluent gas at 7.5 kV reaches a 4 % mole composition.

Increases in methane and oxygen conversions are usually accompanied by increases in the CO selectivity. However, the CO selectivity remains fairly constant until 7.5 kV. The beginning stages of carbon formation occur at 7.5 kV, as indicated by an extremely small, orange glow appearing at both ends of the light-blue AC electric discharge. Consequently, carbon and oxygen may react to produce CO<sub>2</sub>. Therefore, CO produced from CO<sub>2</sub> by dissociative attachment may cause the increase in CO selectivity at 7.5 kV and still maintain the low CO<sub>2</sub> selectivity.

The main effects of increased voltage on the AC OCM electric gas discharge reactions result from increased electric field strengths. Figure 3.8 shows the increases in power and current with increasing voltage. As outlined by Grill (1994), the average electron energy and temperature are functions of  $E_0/p$  where  $E_0$  is the electric field strength and  $p$  is the pressure. Increased voltages result in higher  $E_0$ , therefore promoting a higher electron temperature and average electron energy. Since the average electron energy increases with voltage, Maxwellian and Druyvesteyn electron energy distributions both predict greater concentrations of electrons in the high energy tails of the electron distributions. Consequently, the number of inelastic collisions should increase in the AC electric gas discharge due to increased concentrations of high energy electrons, therefore promoting higher reaction rates. In our studies, the methane and oxygen conversions

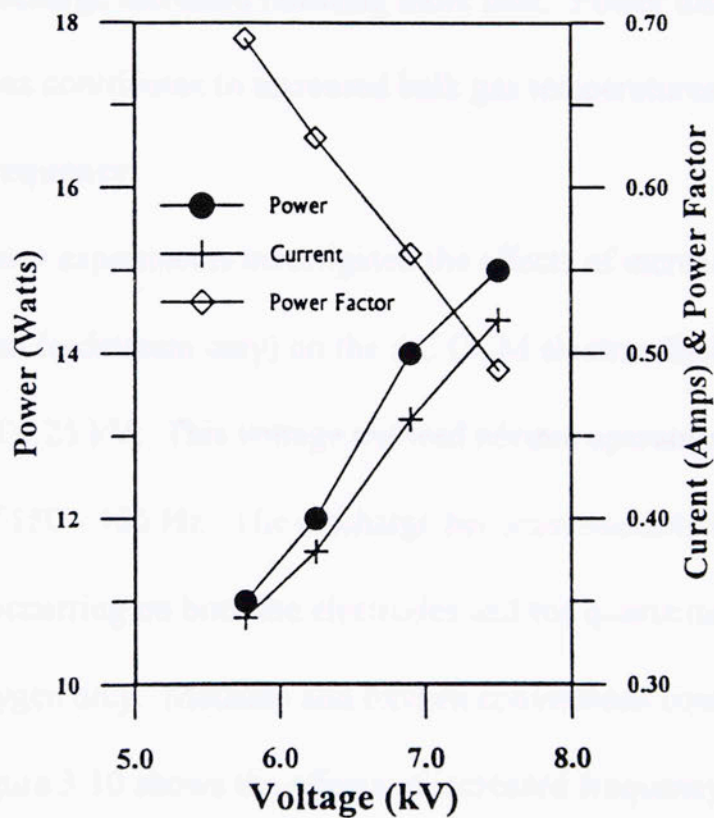


**Figure 3.8:** Effect of voltage on power. Flowrate: 100 cm<sup>3</sup>/min. CH<sub>4</sub>/O<sub>2</sub>: 4. Applied voltage: 5.6-7.5 kV. Frequency: 200 Hz. Gap width: 1.27 cm. Methane Partial Pressure: 0.8 atm. Oxygen Partial Pressure: 0.2 atm.

both increase with increasing voltage or greater electric field strength.

Similarly, gas temperature increases with greater electric field strength. Figure 3.9 shows increases in temperature with increasing voltage (with a feedstream that contained 75% helium). The gas temperature increases because of increased electric field strength providing higher energy electrons, the same reason methane and oxygen conversions increase with increasing voltage. As the electric field strength increases, the amount of electric power dissipated as heat increases. Furthermore, the rate of exothermic reactions in the AC OCM discharge increases releasing more heat. Power dissipation along with exothermic reactions contributes to increased bulk gas temperatures.

### 3.1.6 Effect of Frequency

The frequency experiments investigated the effects of increased frequency (for a methane and oxygen feedstream only) on the AC OCM electric discharge reactions with a constant voltage of 6.25 kV. This voltage allowed normal operation throughout a frequency range of 150 - 300 Hz. The discharge becomes unstable below 150 Hz with carbon formation occurring on both the electrodes and the quartz tube wall for a flowrate of methane and oxygen only. Methane and oxygen conversions continue to decrease above 300 Hz. Figure 3.10 shows the effects of increased frequency on the AC OCM discharge reactions.

Both the methane and oxygen conversions decrease with increasing frequency, while the  $C_2$  selectivity increases. As a result, the  $C_2$  yield remains almost constant. The

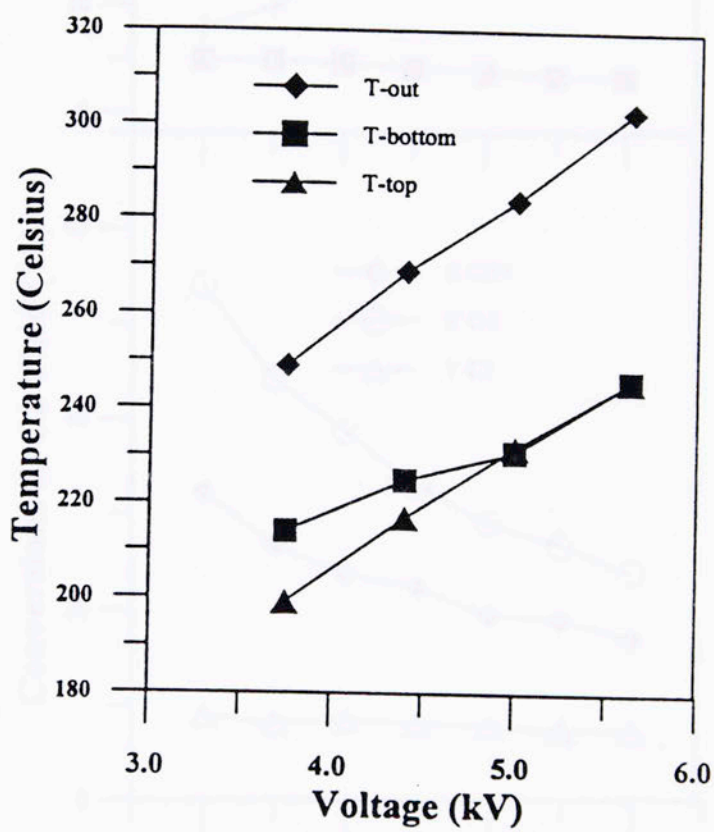


**Figure 3.9:** Effect of voltage on temperature. Flowrate: 100 cm<sup>3</sup>/min. CH<sub>4</sub>/O<sub>2</sub>: 4. Applied voltage: 3.75-5.63 kV. Frequency: 60 Hz. Gap width: 1.27 cm. Methane Partial Pressure: 0.2 atm. Oxygen Partial Pressure: 0.05 atm. Helium Partial Pressure: 0.75

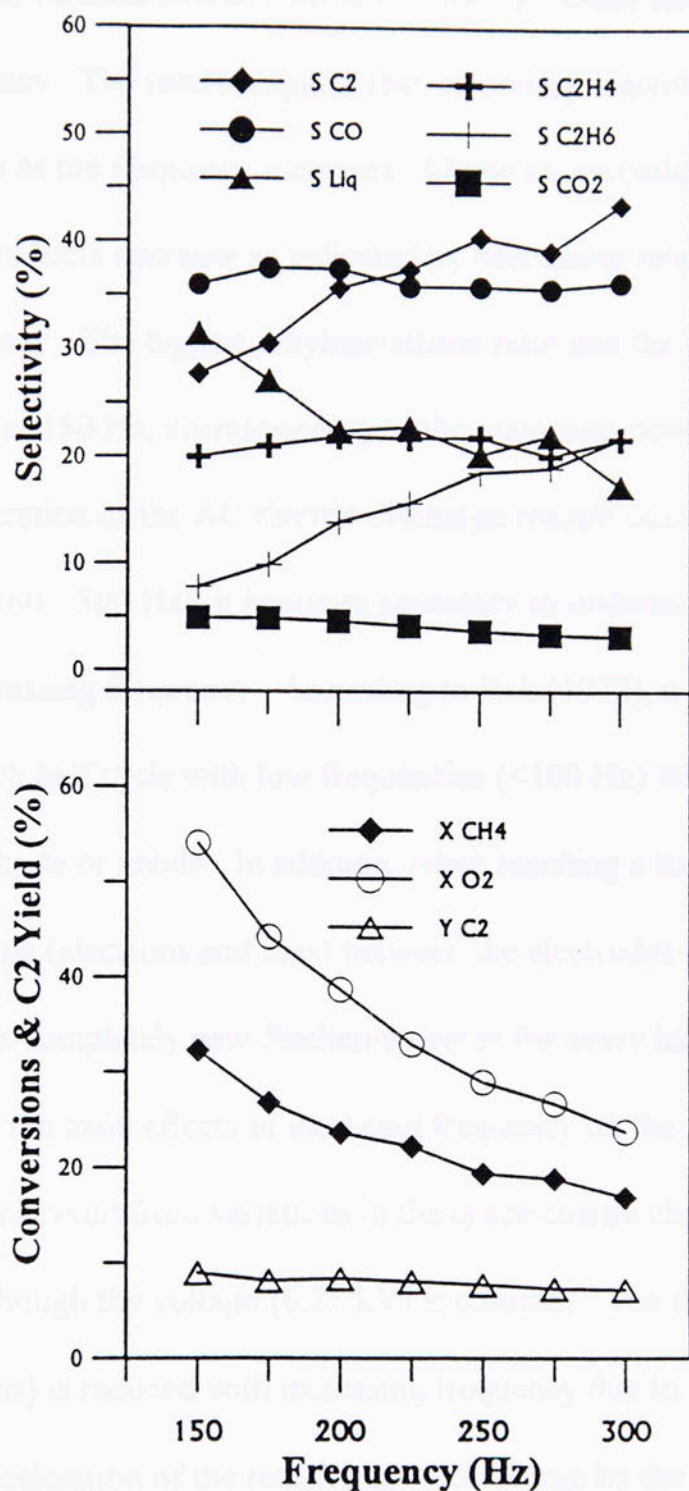


**Figure 3.10:** Effect of frequency on selectivities and conversions. Flowrate: 100 cm<sup>3</sup>/min. CH<sub>4</sub>/O<sub>2</sub>: 4. Applied voltage: 6.25 kV. Frequency: 150-300 Hz. Gap width: 1.27 cm. Methane Partial Pressure: 0.8 atm. Oxygen Partial Pressure: 0.2 atm.



ethylene selectivity remains almost constant, while the ethane selectivity increases with increasing frequency. The results suggest that secondary reactions with ethane to form ethylene decrease as the frequency increases. Likewise, secondary ethane reactions that form unknown products decrease as indicated by decreasing selectivity of unknowns with increasing frequency. The highest ethylene/ethane ratio and the highest selectivity of unknowns occur at 150 Hz, corresponding to the maximum power input.

Since operation of the AC electric discharge reactor occurs in a relatively low frequency range (60 - 300 Hz), it becomes necessary to understand how the discharge changes with increasing frequency. According to Bell (1972), a temporary DC discharge occurs during each half cycle with low frequencies (<100 Hz) where each electrode acts alternately as cathode or anode. In addition, when reaching a sufficiently low frequency, all the space charge (electrons and ions) between the electrodes is eliminated and the establishment of a completely new discharge occurs for every half cycle.

Similarly, the main effects of increased frequency on the AC OCM electric gas discharge reactions result from variations in the space charge characteristics of the discharge, even though the voltage (6.25 kV) is constant. The decay of the space charge (electrons and ions) is reduced with increasing frequency due to a faster reversal of the electric field. Acceleration of the remaining space charge by the reversing electric field decreases the amount of current needed to sustain the discharge. Figure 3.11 shows decreases in current and power with increasing frequency. The number of inelastic collisions decreases with decreasing current, therefore promoting lower reaction rates.

The gas temperature decreases with increasing frequency as a result of decreasing current. Figure 3.12 shows decrease in temperature with increasing frequency (with a feed containing 75 % helium). Since the power decreases with increasing frequency, the amount of power dissipated as heat decreases. In addition, decreasing electrode resistance releases less heat with increasing frequency. Both of these effects contribute to decreasing temperature.

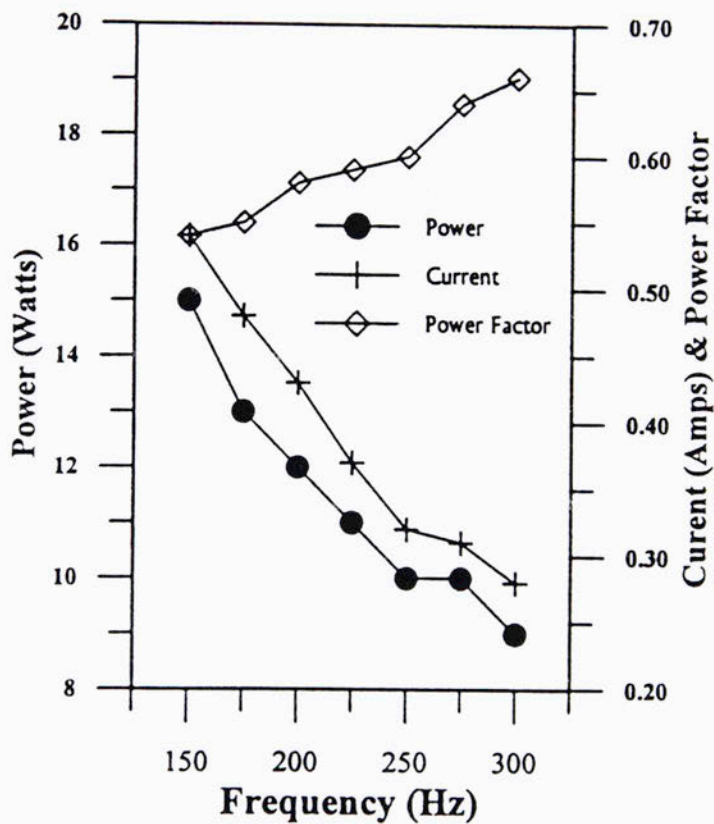


**Figure 3.11:** Effect of frequency on power. Flowrate: 100 cm<sup>3</sup>/min. CH<sub>4</sub>/O<sub>2</sub>: 4. Applied voltage: 6.25 kV. Frequency: 150-300 Hz. Gap width: 1.27 cm. Methane Partial Pressure: 0.8 atm. Oxygen Partial Pressure: 0.2 atm.

The gas temperatures decrease with increasing frequency as a result of decreasing power or current. Figure 3.12 shows decreases in temperature with increasing frequency (with a feed containing 75 % helium). Since the power decreases with increasing frequency, the amount of power dissipated as heat decreases. In addition, decreasing exothermic reactions release less heat with increasing frequency. Both of these effects contribute to decreasing temperatures.

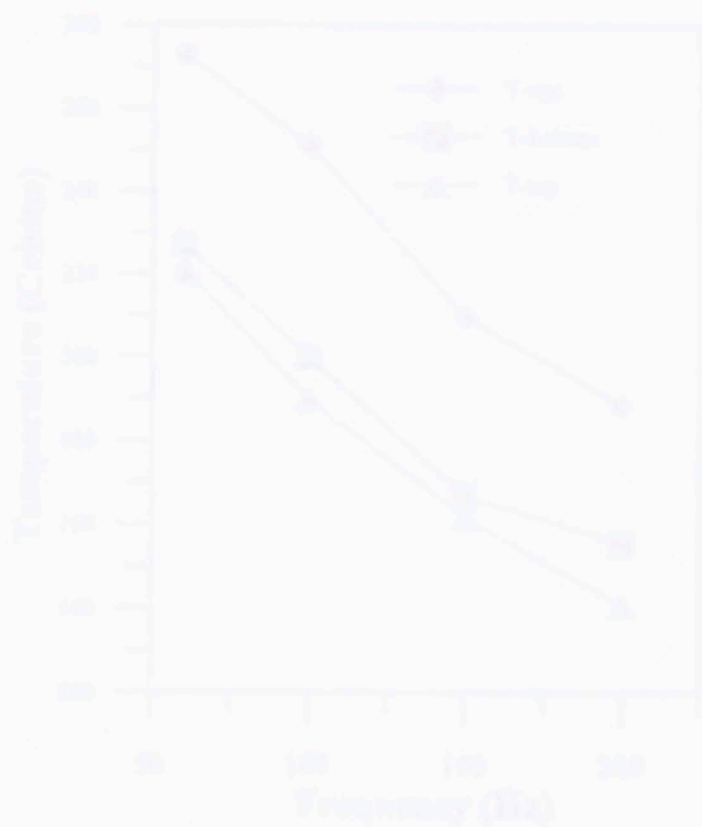
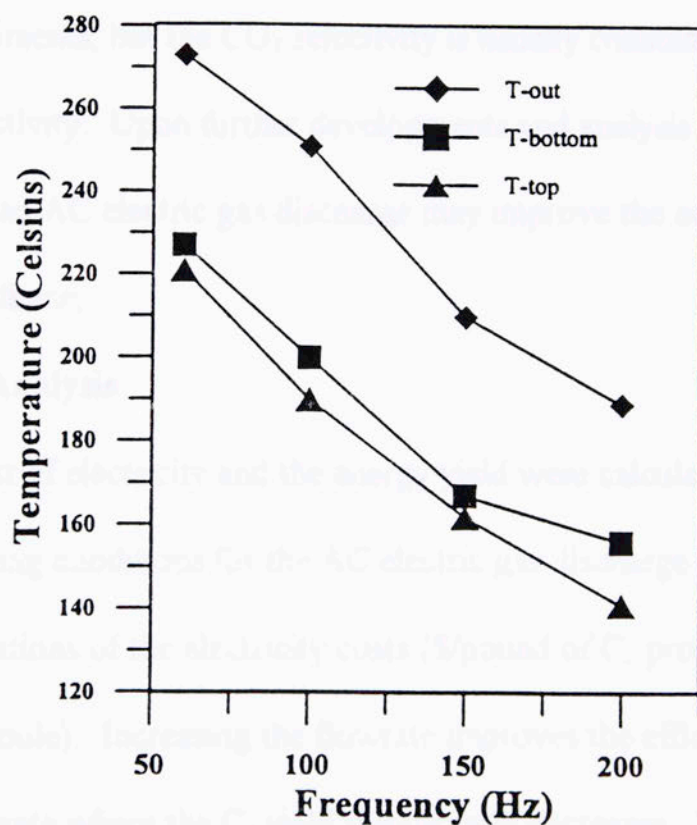


Figure 3.12: Effect of frequency on temperature. Flowrate: 100 cm<sup>3</sup>/min CH<sub>4</sub>/O<sub>2</sub>; Applied voltage: 4.4 kV; Frequency: 50-200 Hz; Gap width: 1.25 cm; Methane Partial Pressure: 0.1 atm; Oxygen Partial Pressure: 0.01 atm; Helium Partial Pressure: 0.21 atm.



**Figure 3.12:** Effect of frequency on temperature. Flowrate: 100 cm<sup>3</sup>/min. CH<sub>4</sub>/O<sub>2</sub>: 4. Applied voltage: 4.4 kV. Frequency: 60-200 Hz. Gap width: 1.27 cm. Methane Partial Pressure: 0.2 atm. Oxygen Partial Pressure: 0.05 atm. Helium Partial Pressure: 0.75

### 3.1.7 Conclusions

Under corona discharge conditions, the energy of the AC electric gas discharge sufficiently promotes the conversion of methane at moderately low temperatures. Methane conversion increases with increasing oxygen partial pressure, voltage, and gap width, but decreases with increasing flowrate and frequency. Conditions where the methane conversion increases cause the  $C_2$  selectivity to decrease, so the  $C_2$  yield remains nearly constant except at low methane conversions. Secondary reactions and CO formation increase with increasing methane conversion. The CO selectivity remains high in all the experiments, but the  $CO_2$  selectivity is usually constant and very low compared to the CO selectivity. Upon further developments and analysis the oxidative coupling of methane using an AC electric gas discharge may improve the economics for the oxidative coupling of methane.

### 3.1.8 Energy Analysis

The cost of electricity and the energy yield were calculated in order to determine efficient operating conditions for the AC electric gas discharge reactor. Appendix C contains calculations of the electricity costs (\$/pound of  $C_2$  products) and the energy yield (grams of  $C_2$ /Joule). Increasing the flowrate improves the efficiency of operation until reaching a flowrate where the  $C_2$  yield significantly decreases. Likewise, larger gap widths improve the efficiency of operation due to increasing  $C_2$  yields even though the power increases. With increasing voltage the efficiency of operation remains about the same as the  $C_2$  yield and power increase. The efficiency of operation increases with increasing

frequency due to the increasing C<sub>2</sub> selectivity and decreases in power. The efficiency of operation continuously improves as the amount of helium diluent is reduced.

In the experiments the primary power is the only power measured for the AC electric gas discharge reactor system. If the secondary power was also measured the actual power efficiency could be calculated. The cost of electricity and the energy yield may be further reduced by a more efficient AC power source. Therefore, further research should investigate more efficient AC power sources.

## Works Cited

- Bell, A.T. A Model for the Dissociation of Hydrogen in an Electric Discharge. *Ind. Eng. Chem. Fundamentals*. **1972**, 11, 209.
- Capitan, M.J.; Malet, P.; Centeno, M.A.; Munoz-Paez, A.; Carrizosa, I.; Odriozola, J.A.  $\text{Sm}_2\text{O}_3/\text{Al}_2\text{O}_3$  Catalysts for Methane Coupling. Influence of the Structure of Surface Sm-Al-O Phases on the Reactivity. *J. Physics. Chem.* **1993**, 97, 9233.
- Chang, J.; Lawless, P.A.; Yamamoto, T. Corona Discharge Processes. *IEEE Trans. Plasma Sci.* **1991**, 19, 1152.
- Chantry, P.J. Dissociative Attachment in Carbon Dioxide. *J. Chem. Phys.* **1972**, 57, 3180.
- DeBoy, J.M.; Hicks, R.F. Kinetics of the Oxidative Coupling of Methane over 1 wt % Sr/La<sub>2</sub>O<sub>3</sub>. *J. Catal.* **1988**, 113, 517.
- Eliasson, B.; Kogelschatz, U. Nonequilibrium Volume Plasma Chemical Processing. *IEEE Trans. Plasma Sci.* **1991**, 19, 1063.
- Eng, D.; Stoukides, M. Catalytic and electrocatalytic Methane Oxidation with Solid Oxide Membranes. *Catal. Rev., Sci. Eng.*, **1991a**, 33, 375.
- Gaffney, A.M.; Jones, C.A.; Leonard, J.J.; Sofranko, J.A. Oxidative Coupling of Methane over Sodium Promoted Praseodymium Oxide. *J. Catal.* **1988**, 114, 422.
- Grill, A. *Cold Plasma in Materials Fabrication: From fundamentals to applications*; IEEE Press: New York, 1994.
- Imai, H.; Tagawa, T. Oxidative Coupling of Methane over Lanthanum Aluminum Trioxide. *J. Chem. Soc., Chem. Commun.* **1986**, 52.
- Lee, J.; Grabowski, J. J. Reactions of the Atomic oxygen Radical Anion and the Synthesis of Organic Reactive Intermediates. *Chem. Rev.* **1992**, 92, 1611.
- Lee, J.S.; Oyama, S.T. Oxidative Coupling of Methane to Higher Hydrocarbons. *Catal. Rev., Sci. Eng.* **1988**, 30, 249.

- Lobban, L.; Changjun, L.; Marafee, A.; Hill, B.; Genhui, X.; Mallinson, R. Oxidative Coupling of Methane with AC and dc Corona Discharges. *Ind. Eng. Chem. Res.* **1996**, *35*, 3295.
- Marston, G. The Excited State in Atmospheric Chemistry. *Chemical Society Review*. **1996**, *25*, 33.
- Orient, O.J.; Srivastava, S.K. Production of  $O^-$  from  $CO_2$  by Dissociative Electron Attachment. *Chem. Phys. Lett.* **1983**, *96*, 681.
- Oumghar, A.; Legrand, J.C.; Diamy, A.M.; Turillon, N. Methane Conversion by an Air Microwave Plasma. *Plasma Chemistry and Plasma Processing*. **1995**, *15*, 87.
- Otsuka, K.; Shimizu, Y.; Komatsu, T. Ba Doped Cerium Oxides Active for Oxidative Coupling of Methane. *Chem. Lett.* **1987**, 1835.
- Yamagata, N.; Igarashi, K.; Saitoh, H.; Okazake, S. Preparation of a Voluminous Composite Barium-Lanthanum Oxide of  $BaLa_2O_4$  and its Catalytic Performance for the Oxidative Coupling of Methane. *Bull. Chem. Soc. Jpn.* **1993**, *66*, 1799.



**PRELIMINARY EXPERIMENTS WITH HELIUM**

**(NONADIABATIC & ADIABATIC)**

**4.1 NONADIABATIC EXPERIMENTS**

Appendix D contains data for preliminary experiments with 75 % volume helium. The effects of voltage, frequency, and gap width were investigated. These experiments are very similar to the experiments in chapter 3. Some of the same trends were observed. Methane and oxygen conversions increase with increases in voltage, and gap width. Likewise, the conversions decrease with increasing frequency. The C<sub>2</sub> yields are generally higher (above 12 %) due to higher C<sub>2</sub> selectivities. Experiments in chapter three were conducted without helium to view the effects over a wider range of operating conditions. In addition, the energy analysis of chapter three shows that the AC electric gas discharge reactor operates more efficiently without helium diluent.

**4.1.1 Nonadiabatic vs. Adiabatic**

Operation of the AC electric gas discharge reactor under near adiabatic conditions was conducted in an attempt to improve the C<sub>2</sub> yields. The highest C<sub>2</sub> yields achieved for

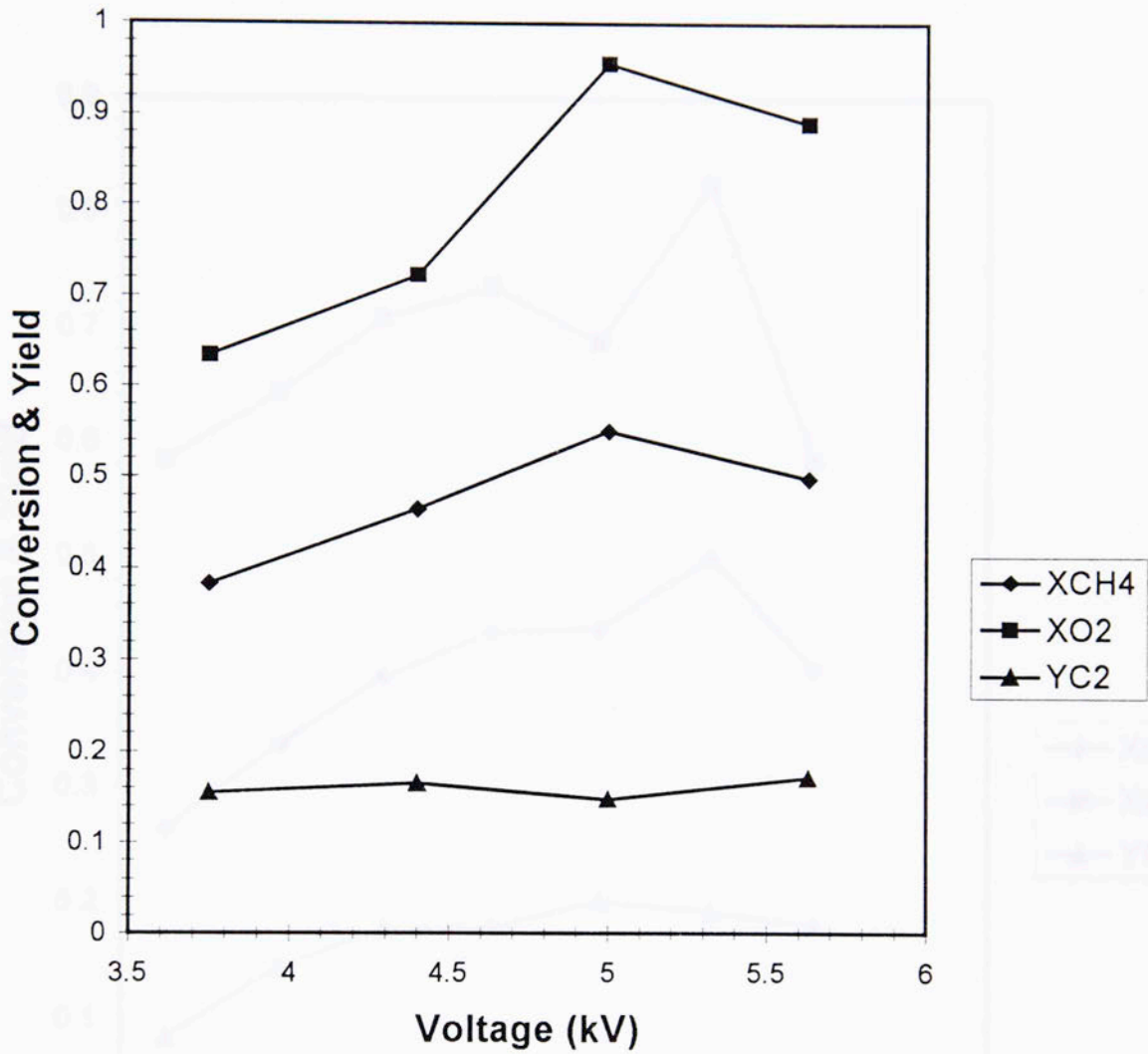
the adiabatic reactor was at a flowrate of 50 cm<sup>3</sup>/min and 75 % volume helium. At 60 Hz the maximum C<sub>2</sub> yield of the adiabatic reactor was 0.17 with a voltage of 5.6 kV. Under the same conditions at 100 Hz the highest C<sub>2</sub> yield was 0.19 at a voltage of 6.9 kV. The frequency of 100 Hz extended the normal operating voltage range (from 3.75 - 5.63 kV to 3.75 – 7.5kV) which allowed an increase in the C<sub>2</sub> yield. The maximum operating voltage is determined by the beginning stages of carbon formation.

However, the nonadiabatic reactor at 50 cm<sup>3</sup>/min produced a higher C<sub>2</sub> yield of 0.20 at a voltage of 5 kV and a frequency of 60 Hz. The operating voltage range for the nonadiabatic reactor was 3.75 – 5.63 kV. Figures 4.1 – 4.3 show the conversions and C<sub>2</sub> yields for the nonadiabatic and adiabatic conditions. The decrease in conversions of Figure 4.1 and 4.2 are due to carbon formation, which occurs at adiabatic temperatures over 500° C. Appendix D contains the data for the adiabatic and nonadiabatic experiments at 50 cm<sup>3</sup>/min.

Voltage (kV)

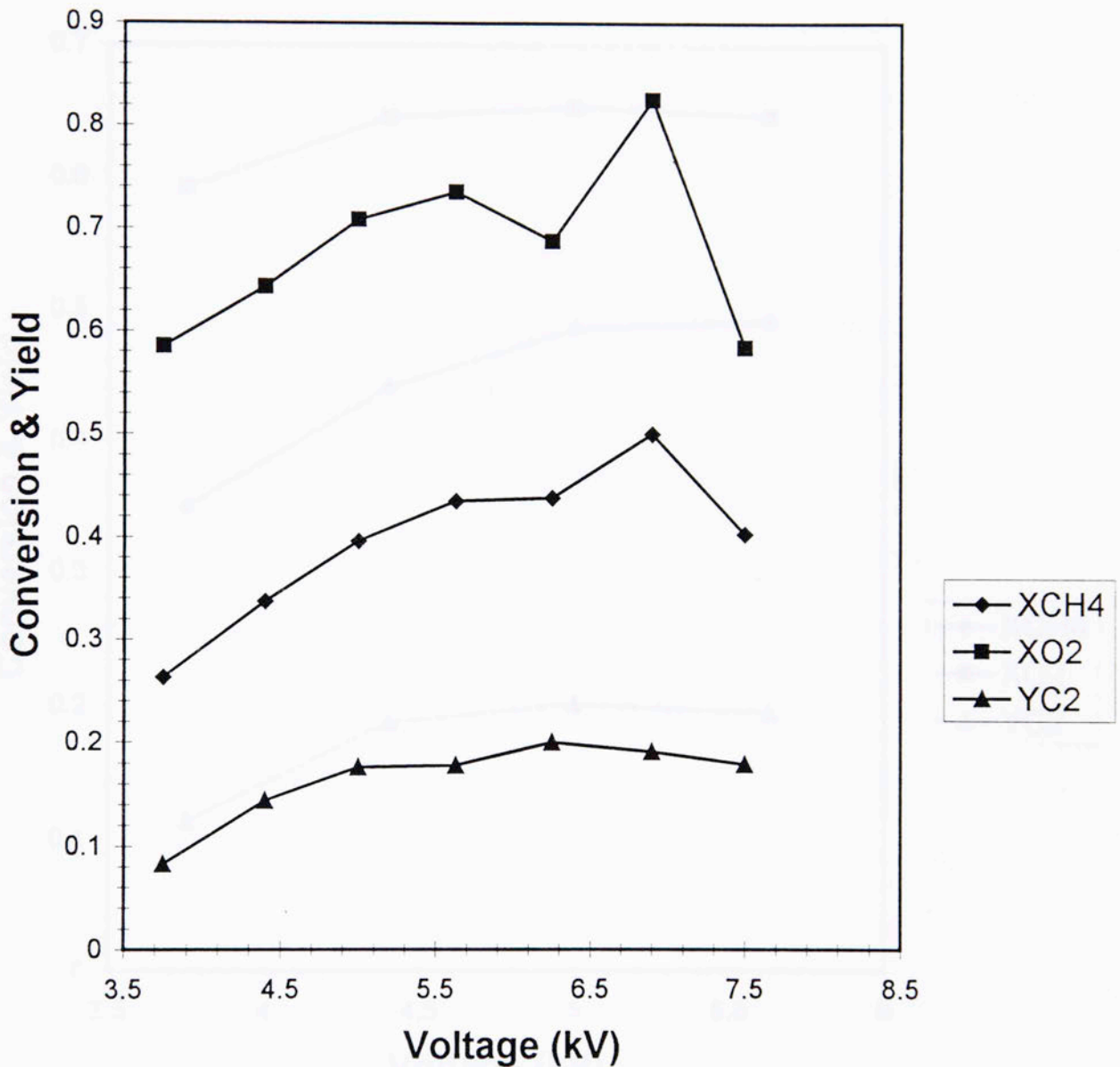
Conditions: 50 SCCM, 60 Hz, 4/1  
methane/oxygen, 75 % vol. He, & 1/2  
inch gap

Figure 4.1: Adiabatic 60 Hz: Conversions & Yield vs. Voltage



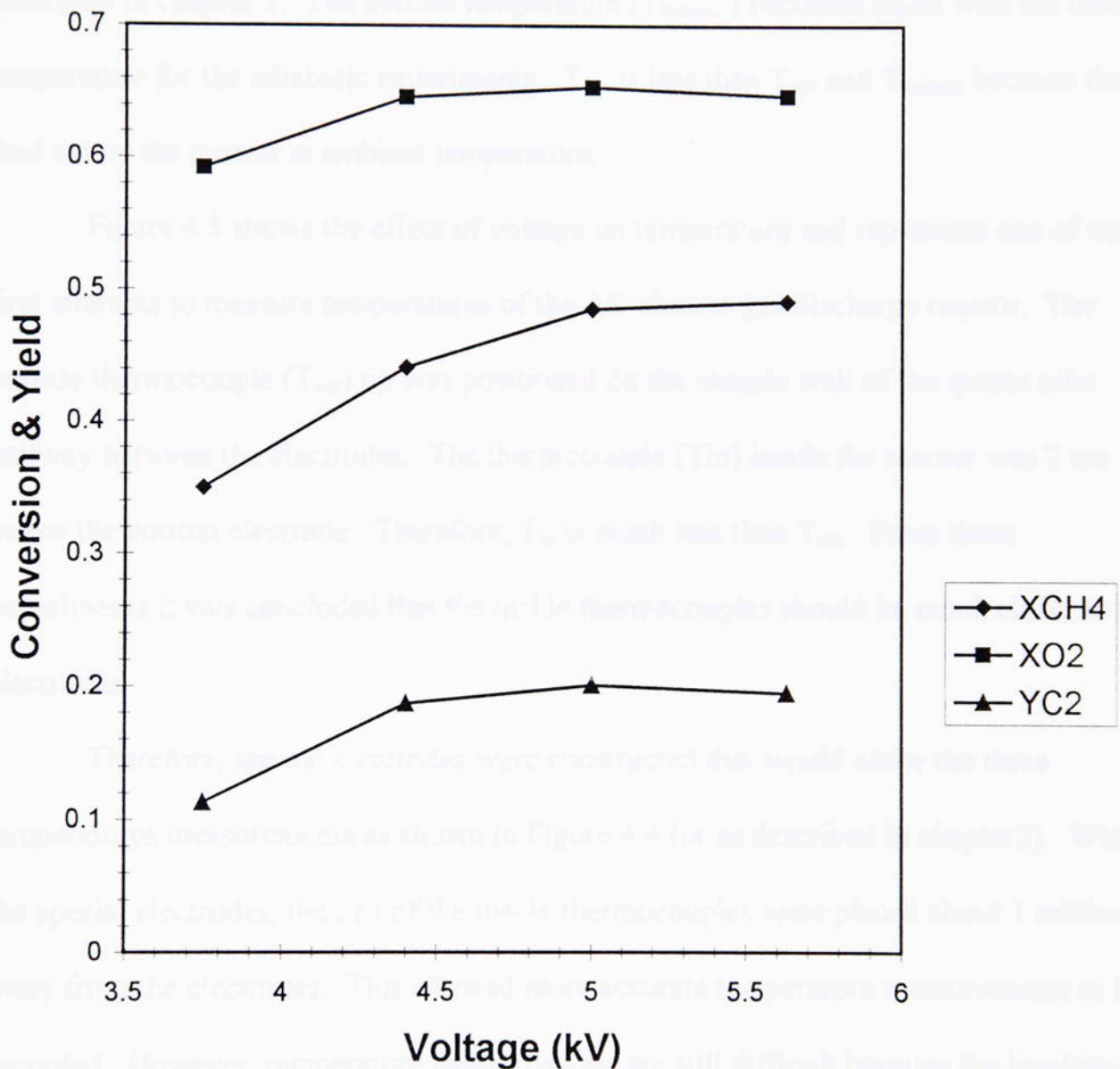
Conditions: 50 SCCM, 60 Hz, 4/1 methane/oxygen, 75 % vol. He, & 1/2 inch gap

Figure 4.2: Adiabatic 100 Hz: Conversions & Yield vs. Voltage



Conditions: 50 SCCM, 100 Hz, 4/1 methane/oxygen, 75 % vol. He, & 1/2 inch gap

Figure 4.3: Nonadiabatic 60 Hz:  
Conversions & Yield vs. Voltage



Conditions: 50 SCCM, 60 Hz, 4/1  
methane/oxygen, 75 % vol. He, & 1/2  
inch gap

#### 4.1.2 Adiabatic Temperature Measurements

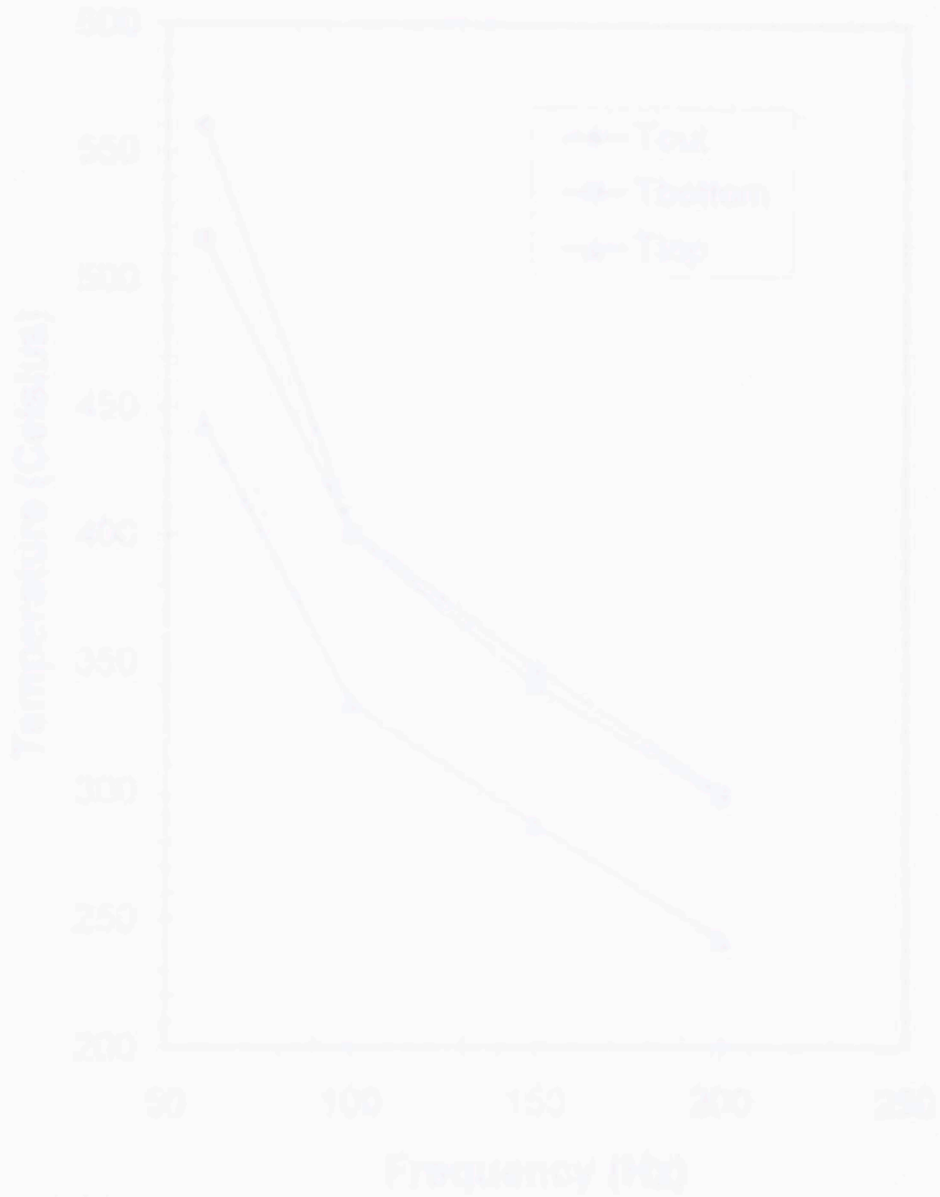
Temperatures in the adiabatic discharges exceed 500°C. Figure 4.4 shows the effect of increasing frequency on temperature. The thermocouples were positioned as described in chapter 2. The bottom temperature ( $T_{\text{bottom}}$ ) becomes equal with the outside temperature for the adiabatic experiments.  $T_{\text{top}}$  is less than  $T_{\text{out}}$  and  $T_{\text{bottom}}$  because the feed enters the reactor at ambient temperature.

Figure 4.5 shows the effect of voltage on temperature and represents one of our first attempts to measure temperatures of the AC electric gas discharge reactor. The outside thermocouple ( $T_{\text{out}}$ ) tip was positioned on the outside wall of the quartz tube halfway between the electrodes. The thermocouple ( $T_{\text{in}}$ ) inside the reactor was 2 cm below the bottom electrode. Therefore,  $T_{\text{in}}$  is much less than  $T_{\text{out}}$ . From these experiments it was concluded that the inside thermocouples should be much closer to the electrodes.

Therefore, special electrodes were constructed that would allow the three temperatures measurements as shown in Figure 4.4 (or as described in chapter 2). With the special electrodes, the tips of the inside thermocouples were placed about 1 millimeter away from the electrodes. This allowed more accurate temperature measurements to be recorded. However, temperature measurements are still difficult because the insulated thermocouples affect the behavior of the discharge by conducting electricity from the discharge. This affects the temperature readout devices by causing the temperatures to continuously fluctuate over a range of about 10 to 15°C. The highest temperatures viewed on the temperature readout devices were recorded to obtain temperature

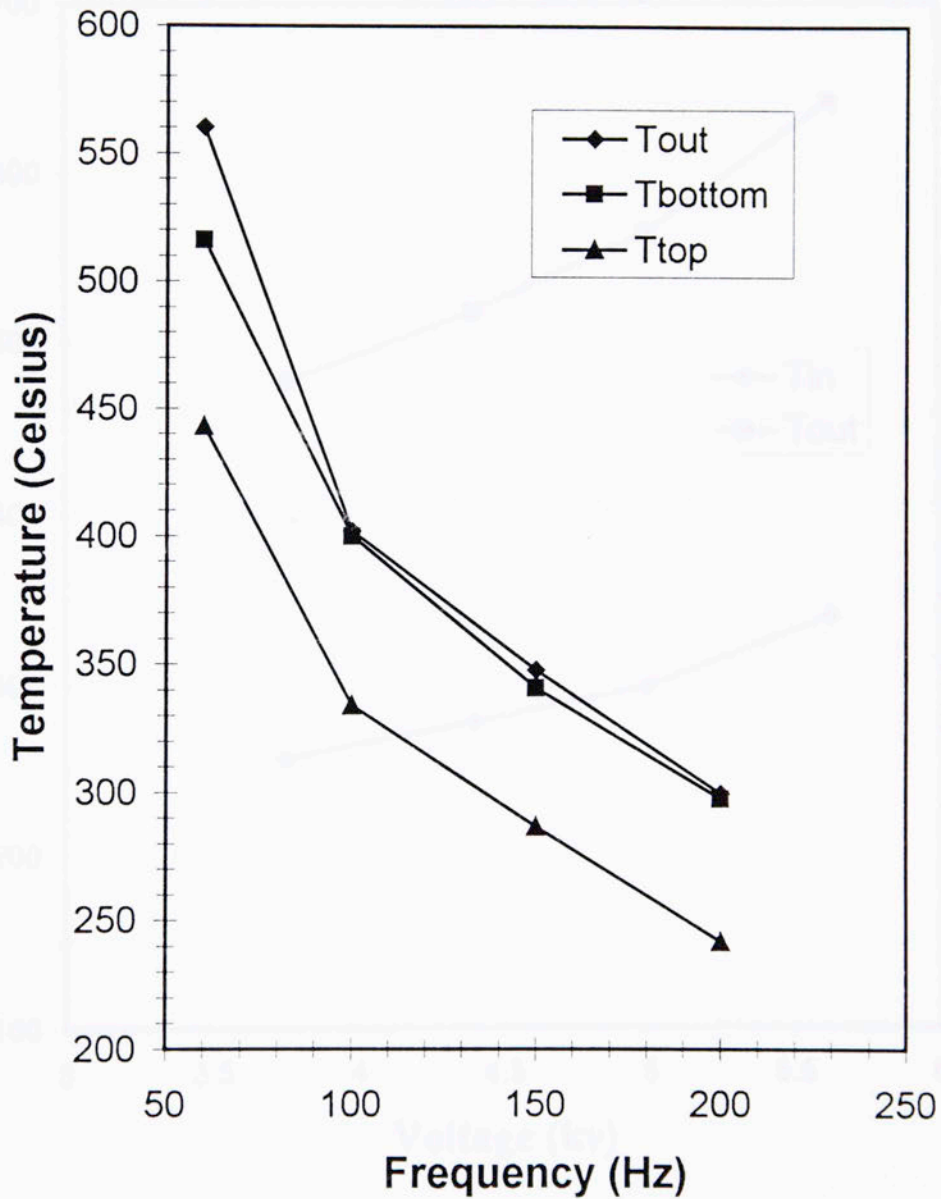
measurement data. Improved techniques that do not include thermocouples such as an infrared technique should be developed to improve temperature measurements for the AC electric gas discharge reactor.

Figure 4.4: Adiabatic Temperature Measurements vs. Frequency



Conditions: 100 SCCM,  $Y_{He}=0.78$ ,  $CH_4/O_2 = 4/1$ , &  $V=4.4$  kV

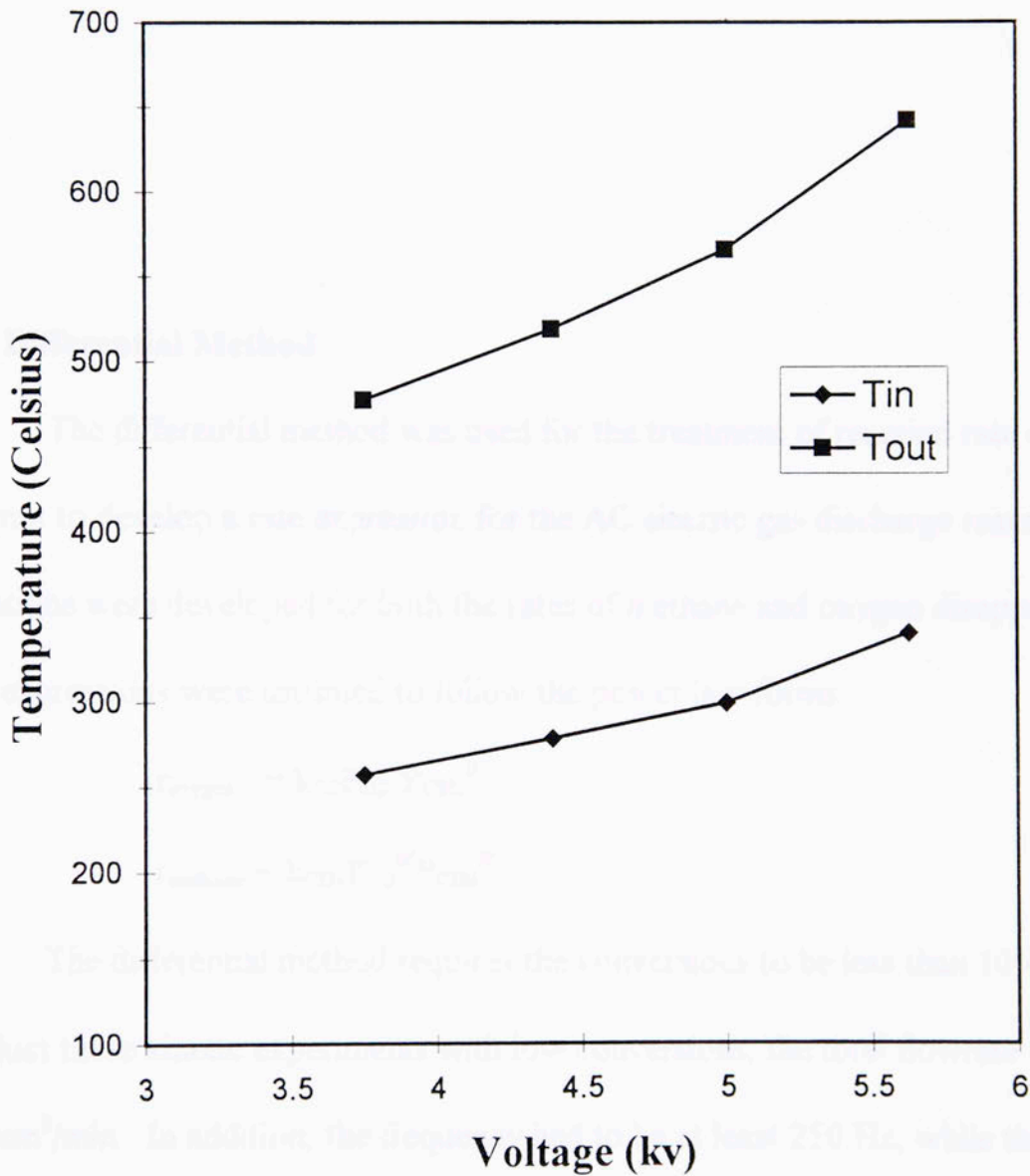
**Figure 4.4: Adiabatic Temperature Measurements vs. Frequency**



**Conditions: 100 SCCM, YHe=0.75, CH4/O2 = 4/1,  
& V=4.4 kV**



**Figure 4.5: Near Adiabatic Conditions:  
Temperature vs. Voltage**



**Conditions: 100 SCCM, XHe=0.75, CH<sub>4</sub>/O<sub>2</sub>=4/1, &  
f=60 Hz**

### Rate Expressions

#### 5.1 Differential Method

The differential method was used for the treatment of reaction rate data in an attempt to develop a rate expression for the AC electric gas discharge reactor. Rate equations were developed for both the rates of methane and oxygen disappearance. The rate expressions were assumed to follow the power law forms:

$$r_{\text{oxygen}} = k_{\text{O}_2} P_{\text{O}_2}^{\alpha} P_{\text{CH}_4}^{\beta}$$

$$r_{\text{methane}} = k_{\text{CH}_4} P_{\text{O}_2}^{\alpha'} P_{\text{CH}_4}^{\beta'}$$

The differential method requires the conversions to be less than 10%. In order to conduct these kinetic experiments with low conversions, the total flowrate required was 500 cm<sup>3</sup>/min. In addition, the frequency had to be at least 250 Hz, while the voltage was maintained at 6.25 kV. Experiments were conducted for frequencies of 250 and 300 Hz. Methane to oxygen ratios varied from 3/1 to 8/1. Operation of the reactor only occurs at atmospheric pressure, which limits the range of partial pressures for methane and oxygen.

Average partial pressures (of inlet and outlet) were used for treatment of the reaction rate data. Experimental reaction rates were obtained from the BASIC computer program calculations. The method of least squares (linear multiple regression) in Excel 5.0 was used to calculate the constants  $\alpha$ ,  $\alpha'$ ,  $\beta$ ,  $\beta'$ ,  $k_{\text{CH}_4}$ , and  $k_{\text{O}_2}$  from the experimental data.

Kinetic experiments were conducted with a feed of methane and oxygen only where the methane/oxygen ratios were varied from 3/1 to 8/1 at a flowrate of 500  $\text{cm}^3/\text{min}$ . In addition, experiments were conducted with the same ratios where either methane or oxygen was held constant, and helium was used to maintain the flowrate at 500  $\text{cm}^3/\text{min}$ . Appendix C contains charts of experimental and calculated rates versus the average partial pressure of methane or oxygen.

Tables 5.1 and 5.2 show the concentration dependencies for methane ( $\beta$  or  $\beta'$ ) and oxygen ( $\alpha$  or  $\alpha'$ ) changing with each experiment. The rate equations developed for oxygen show similar behavior except for the negative  $\alpha$  and  $\beta$  as well as a much smaller rate constant at 300 Hz. The rate constants for the rest of the experiments are on the same order of magnitude. The rate expressions developed for methane show positive  $\alpha'$  and either positive or negative  $\beta'$ .

In the experiments where either methane or oxygen is held constant the  $\alpha'$  or  $\beta'$  values have to be positive for the rate to increase. The rate constants also include the constant partial pressure value and concentration dependence from either methane or oxygen. The rate expressions for these experiments:

$$r_{\text{oxygen}} = k_{\text{O}_2} P_{\text{O}_2}^{\alpha}$$

$$r_{\text{methane}} = k_{\text{CH}_4} P_{\text{CH}_4}^{\beta'}$$

When the methane partial pressure was held constant, the rate of oxygen disappearance increases with increasing oxygen partial pressure. However, when oxygen was held constant the rate of methane disappearance increased then subsequently decreased beyond a methane partial pressure of 0.72 atm (5.5/1 methane/oxygen ratio). As shown in Table 5.2, this limited the data fit to only methane/oxygen ratios from 3.5/1 to 5.5/1. Beyond the 5.5/1 ratio the determinate coefficient rapidly decreases because of the decrease in the rate of methane disappearance. The addition of helium in these experiments is probably responsible for the increase and decrease in the rate of methane disappearance.

This kinetic data shows that a simple power law rate equation cannot predict the reaction rates for the AC electric gas discharge reactor over a wide range of operating conditions. A rate equation for the reactor should account for the distribution of electron energies in the discharge, since nonequilibrium discharge reactions depend on the electron energy. This would require a computer simulation (i.e., Monte Carlo simulation) describing all the possible reactions that may occur in the discharge. Various researchers have simulated nonequilibrium discharges with varying degrees of success (Jing, L. et al., 1995; Eliasson, B., 1994; Dahiya, R.P. et al., 1993), but such a simulation was not attempted for this work.

**Table 5.1: Treatment of Reaction Rate Data by Method of Least Squares on the Rate of Oxygen Disappearance**

**Conditions:** 500 SCCM, 6.25 kV, & 1/2 inch gap

**Rate Equations:**  $r_{\text{oxygen}} = k_{\text{O}_2} P_{\text{O}_2}^\alpha P_{\text{CH}_4}^\beta$  or  $r_{\text{oxygen}} = k_{\text{O}_2} P_{\text{O}_2}^\alpha$

Frequency (Hz)	$k_{\text{O}_2}$	$\alpha$	$\beta$	CH <sub>4</sub> /O <sub>2</sub> %Volume	Average P <sub>O<sub>2</sub></sub> or range (atm)	Average P <sub>CH<sub>4</sub></sub> or range (atm)	P <sub>He</sub> in Feed (atm)	Determinate Coefficient r <sup>2</sup>
250	3.33E-5	0.918	0.0655	3.5/1-8/1	0.11-0.22	0.80-0.92	0	0.980
300	7.27E-7	-0.552	-6.24	3.0/1-8/1	0.11-0.25	0.77-0.92	0	0.979
250	2.61E-5	0.762		3.5/1-8/1	0.090-0.21	0.774	0.036-0.15	0.992
300	3.12E-5	0.851		3.5/1-8/1	0.091-0.21	0.774	0.036-0.15	0.981

**Table 5.2: Treatment of Reaction Rate Data by Method of Least Squares on the Rate of Methane Disappearance**

**Conditions:** 500 SCCM, 6.25 kV, & 1/2 inch gap

**Rate Equations:**  $r_{\text{methane}} = k_{\text{CH}_4} P_{\text{O}_2}^\alpha P_{\text{CH}_4}^\beta$  or  $r_{\text{methane}} = k_{\text{CH}_4} P_{\text{CH}_4}^\beta$

Frequency (Hz)	$k_{\text{CH}_4}$	$\alpha'$	$\beta'$	CH <sub>4</sub> /O <sub>2</sub> %Volume	Average P <sub>O<sub>2</sub></sub> or range (atm)	Average P <sub>CH<sub>4</sub></sub> or range (atm)	P <sub>He</sub> in Feed (atm)	Determinate Coefficient r <sup>2</sup>
250	4.54E-6	0.500	-4.75	3.5/1-8/1	0.11-0.22	0.80-0.92	0	0.985
300	3.63E-6	0.431	-3.75	3/1-8/1	0.11-0.25	0.77-0.92	0	0.968
250	3.04E-6		0.487	3.5/1-5.5/1	0.096	0.36-0.72	0.2-0.55	0.832
300	3.26E-6		0.764	3.5/1-5.5/1	0.096	0.36-0.72	0.2-0.55	0.955

Works Cited

Dahiya, R.P.; Mishra, K.; Veefkind, A. Plasma Chemical Investigations for NO<sub>x</sub> and SO<sub>2</sub> Removal from Flue Gas. *IEEE TRANS. on PLASMA SCI.* **1993**, 21, 346.

Eliasson, B.; Egli, W.; Kogelschatz, U. Modeling of a Dielectric Barrier Discharge Chemistry. *Pure & Appl. Chem.* **1994**, 66, 1275.

Jing, L.; Sun, W.; Pashaie, B; Dhali, S.K. Streamer Discharge Simulation in Flue Gas. *IEEE TRANS. on PLASMA SCI.* **1995**, 23, 672.

6.1 Conclusions

The investigation into the catalytic coupling of methane using an AC electric gas discharge device, under the dielectric and catalytic methane conversion may eventually lead to significant advances for methane conversion to higher valued hydrocarbons (liquids). The experimental results of the AC electric gas discharge demonstrate:

1. Under corona discharge conditions, the energy of the AC electric gas discharge sufficiently promotes the conversion of methane with low power (10 - 20 watts).
2. Methane conversion increases with increasing oxygen partial pressure, voltage and gap width. Oxygen conversions increase along with methane conversion. Methane conversion decreases with increasing flowrate and frequency.

## CONCLUSIONS AND RECOMMENDATIONS

### CHAPTER 6

#### 6.1 Conclusions

The investigation into the oxidative coupling of methane using an AC electric gas discharge demonstrates that alternative and innovative methane conversions may eventually lead to significant advances for methane conversion to higher valued hydrocarbons (liquids). The experimental results of the AC electric gas discharge demonstrate:

1. Under corona discharge conditions, the energy of the AC electric gas discharge sufficiently promotes the conversion of methane with low power (10 - 20 watts).
2. Methane conversion increases with increasing oxygen partial pressure, voltage, and gap width. Oxygen conversions increase along with methane conversion. Methane conversion decreases with increasing flowrate and frequency.

3. The  $C_2$  selectivity generally decreases with increasing methane conversion, but secondary reactions and CO formation increase.
4. The  $C_2$  yield either increases slowly or remains almost constant due to a tradeoff between  $C_2$  selectivity and methane conversion. Experiments with helium diluent provide the highest  $C_2$  yields. However, experiments with pure methane and oxygen produce effluent gas streams with much higher  $C_2$  composition (up to 5 %).
5. The formation of  $CO_2$  is usually constant and very low compared to CO.
6. Power requirements remain constant with increasing flowrate.
7. Electron multiplication increases with increasing gap width and promotes higher reaction rates.
8. Current and power increase with increasing voltage producing higher energy discharges.
9. Current and power decrease with increasing frequency producing lower energy discharges.
10. Temperatures increase with increasing voltage due to higher energy discharges and increasing exothermic reactions.
11. Temperatures decrease with increasing frequency due to lower energy discharges and decreasing exothermic reactions.
12. Significant improvements in the  $C_2$  yields were not achieved under adiabatic operation.
13. A power law rate equation cannot predict reaction rates of the AC electric gas discharge reactor over a wide range of conditions.



## 6.2 Recommendations

### Appendix A

1. Measurements in the secondary power will further develop the understanding of the discharge characteristics, such as current, voltage, and frequency waveforms.

Measurements of secondary and primary power will also allow the calculation of the power efficiency.

2. The current gas analysis cannot quantify hydrogen, which is probably produced in the discharge. Therefore, attempts should be made to determine the amount of hydrogen in the effluent gases. Significant amounts of synthesis gas may possibly be obtained from the discharge reactions, which is utilized in ammonia synthesis. In addition, the gas analysis only quantifies  $C_2$  hydrocarbons. The analysis should quantify higher hydrocarbons since they may be produced in the discharge reactions.

3. The liquid analysis requires a volatile liquid analysis, because some of the liquids evaporate at atmospheric pressure and room temperature.

4. Other corona type discharges such as the coaxial or wire duct may improve the OCM reactions and should be investigated.

5. An initial economic analysis should be conducted and compared with an economic analysis for catalytic OCM. This would determine if improvements have been made for the OCM to higher hydrocarbons.

6. Reactor modeling by computer simulation is required to develop the kinetics and test new reactor designs.

## Appendix A

### Electron Molecule Reactions

Excitation	$e^- + A_2 \rightarrow A_2^* + e^-$
Dissociation	$e^- + A_2 \rightarrow 2A + e^-$
Attachment	$e^- + A_2 \rightarrow A_2^-$
Dissociative Attachment	$e^- + A_2 \rightarrow A^- + A$
Ionization	$e^- + A_2 \rightarrow A_2^+ + 2e^-$
Dissociative Ionization	$e^- + A_2 \rightarrow A^+ + A^- + e^-$
Recombination	$e^- + A_2^+ \rightarrow A_2$
Detachment	$e^- + A_2^- \rightarrow A_2 + 2e^-$

## Appendix B

### Mass Flow Controller and GC Calibrations

#### B.1 Mass Flow Controller Calibrations

Gas	Porter Mass Flow Controller Flowrate (SCCM)	Calibration Equation R(%), F(SCCM)
CH <sub>4</sub>	CH <sub>4</sub> (500)	$R = 0.1889 * F$
O <sub>2</sub>	O <sub>2</sub> (30)	$R = 3.284 * F$
CO <sub>2</sub>	O <sub>2</sub> (30)	$R = 4.32 * F$
CO	O <sub>2</sub> (30)	$R = 3.21 * F$
C <sub>2</sub> H <sub>6</sub>	CO <sub>2</sub> (5)	$R = 26.442 * F$
C <sub>2</sub> H <sub>4</sub>	CO <sub>2</sub> (5)	$R = 25.743 * F$
He	He(200)	$R = 0.4530 * F$

#### B.2 GC Calibration Factors

Gas	Factor
CH <sub>4</sub>	1.0
O <sub>2</sub>	0.797
CO <sub>2</sub>	0.770
CO	0.935
C <sub>2</sub> H <sub>6</sub>	0.889
C <sub>2</sub> H <sub>4</sub>	0.74

```

9998 REM THIS PROGRAM IS FOR ELECTRIC FIELD ENHANCED CATALYTIC CONVERSION
OF METHANE
10 INPUT "E="; E
20 INPUT "T="; T
30 INPUT "N="; N
40 IF E = 0 GOTO 70
50 LPRINT "EFEC DATA V="; E; "~~~~~"
60 GOTO 80
70 LPRINT "NO EFEC DATA-----"
80 PRINT "THIS PROGRAM HAS BEEN MODIFIED TO ADD CALCULATING CO SELECTIVITY"
81 PRINT "-----SCO IS SELECTIVITY FOR CO"
82 INPUT "MT0="; MT0
90 INPUT "O20="; O20
100 O20 = O20 * .799
110 INPUT "XHE="; XHE
120 FA0 = (MT0 + O20) * XHE / (1 - XHE)
150 FOR I = 1 TO N
160 MT0(I) = MT0
200 INPUT "CO="; CO(I)
210 INPUT "C4="; C4(I)
220 INPUT "C6="; C6(I)
230 INPUT "MT="; MT(I)
240 INPUT "O2="; O2(I)
242 INPUT "MO="; MO(I)
245 MO(I) = MO(I) * .935
250 CO(I) = CO(I) * .77
260 C4(I) = C4(I) * .74
270 C6(I) = C6(I) * .889
280 O2(I) = O2(I) * .797
282 MC(I) = MO(I) - O2(I)
283 ERC(I) = (MT0(I) - (MT(I) + MC(I) + CO(I) + 2 * (C4(I) + C6(I)))) / MT0(I)
284 PRINT "ERC="; ERC(I)
285 IF ERC(I) < .05 THEN 440
290 SUMM = MT(I) + O2(I) + MC(I) + CO(I) + C4(I) + C6(I) + FA0 + (ERC(I) - .05) * MT0(I)
300 YCO(I) = CO(I) / SUMM
310 YMT(I) = MT(I) / SUMM
320 YC4(I) = C4(I) / SUMM
330 YC6(I) = C6(I) / SUMM
340 YO2(I) = O2(I) / SUMM
342 YMC(I) = MC(I) / SUMM
350
360 YC3(I) = (ERC(I) - .05) * MT0(I) / SUMM
370 SCO(I) = (YCO(I) + YMC(I)) / (YCO(I) + YMC(I) + 2 * (YC4(I) + YC6(I)) + YC3(I))
380 SC4(I) = 2 * (YC4(I)) / (YCO(I) + YMC(I) + 2 * (YC4(I) + YC6(I)) + YC3(I))
390 SC6(I) = 2 * (YC6(I)) / (YCO(I) + YMC(I) + 2 * (YC4(I) + YC6(I)) + YC3(I))
400 SC3(I) = 1 - SCO(I) - SC4(I) - SC6(I)
410 SMC(I) = YMC(I) / (YCO(I) + YMC(I) + YC3(I) + 2 * (YC4(I) + YC6(I)))
420 SC2(I) = SC4(I) + SC6(I)
430 GOTO 560
440 SUMM = MT(I) + O2(I) + MC(I) + CO(I) + C4(I) + C6(I) + FA0
441 YCO(I) = CO(I) / SUMM
442 YMT(I) = MT(I) / SUMM
443 YC4(I) = C4(I) / SUMM

```

```

444 YC6(I) = C6(I) / SUMM
445 YO2(I) = O2(I) / SUMM
446 YMC(I) = MC(I) / SUMM
490 YC3(I) = 0
491 SCO(I) = (YCO(I) + YMC(I)) / (YCO(I) + YMC(I) + 2 * (YC4(I) + YC6(I)) + YC3(I))
492 SC4(I) = 2 * (YC4(I)) / (YCO(I) + YMC(I) + 2 * (YC4(I) + YC6(I)) + YC3(I))
493 SC6(I) = 2 * (YC6(I)) / (YCO(I) + YMC(I) + 2 * (YC4(I) + YC6(I)) + YC3(I))
494 SMC(I) = YMC(I) / (YCO(I) + YMC(I) + YC3(I) + 2 * (YC4(I) + YC6(I)))
495 SC2(I) = SC4(I) + SC6(I)
540 SC3(I) = 0
560 XMT(I) = (ABS(MT0(I) - MT(I))) / MT0(I)
570 YC2(I) = SC2(I) * XMT(I)
580 Y3(I) = SC3(I) * XMT(I)
590 XO2(I) = (ABS(O20 - O2(I))) / O20
600 LPRINT "T="; T, "ERC="; ERC(I)
610 LPRINT "SCOX="; SCO(I); "SMC="; SMC(I); " SC2="; SC2(I); " XMT="; XMT(I); " YC2=";
YC2(I); "XO2="; XO2(I)
620 LPRINT "Y3="; Y3(I); "SC3="; SC3(I); "YC3="; YC3(I); "YMC="; YMC(I)
630 LPRINT
640 S2 = S2 + SC2(I)
641 SCO = SCO + SMC(I)
650 Y2 = Y2 + YC2(I)
660 XM = XM + XMT(I)
670 XO = XO + XO2(I)
680 ZCO = ZCO + YCO(I)
685 ZMC = ZMC + YMC(I)
690 ZMT = ZMT + YMT(I)
700 ZC4 = ZC4 + YC4(I)
710 ZC6 = ZC6 + YC6(I)
720 ZO2 = ZO2 + YO2(I)
730 ZC3 = ZC3 + YC3(I)
740 S3 = S3 + SC3(I)
750 Y3 = Y3 + Y3(I)
760 S4 = S4 + SC4(I)
770 S6 = S6 + SC6(I)
780 NEXT I
790 S4 = S4 / N
800 S6 = S6 / N
802 SCO = SCO / N
810 S2 = S2 / N
820 Y2 = Y2 / N
830 XM = XM / N
840 XO = XO / N
850 S3 = S3 / N
860 Y3 = Y3 / N
870 ZC3 = ZC3 / N
890 ZCO = ZCO / N
895 ZMC = ZMC / N
900 INPUT "V="; V1
930 ZMT = ZMT / N
940 ZC4 = ZC4 / N
950 ZC6 = ZC6 / N
960 ZO2 = ZO2 / N

```

```

970 RC2 = (ZC4 + ZC6) * V1 / (60 * .082 * 298)
980 RCO = ZCO * V1 / (60 * .082 * 298)
990 RCH4 = 2 * RC2 + RCO
1000 LPRINT "RC2="; RC2, "RCO="; RCO, "RCH4="; RCH4, "S4="; S4, "S6="; S6
1200 IF ZC6 = 0 THEN 1990
1980 ZZ = ZC4 / ZC6
1990 LPRINT "C2H4/C2H6="; ZZ; " ZC3="; ZC3; "S3="; S3; "Y3="; Y3; "ZMC="; ZMC
2000 LPRINT "ZCO="; ZCO; "ZMT="; ZMT; "SCO="; SCO; "ZC4="; ZC4; "ZC6="; ZC6; "ZO2=";
ZO2
2920 LPRINT "S2="; S2; " Y2="; Y2; " XM="; XM; " XO="; XO; "V1="; V1
2930 S3 = 0
2940 Y3 = 0
2990 S2 = 0
2992 SCO = 0
3000 Y2 = 0
3100 XM = 0
4000 XO = 0
4005 ZMC = 0
4100 ZCO = 0
4110 S4 = 0
4260 S6 = 0
4200 ZMT = 0
4300 ZC4 = 0
4350 ZC6 = 0
4360 ZC3 = 0
4400 ZO2 = 0
5000 GOTO 10
10000 END

```

Composition	Z <sub>CO</sub>	Z <sub>CH<sub>4</sub></sub>	Z <sub>C<sub>2</sub>H<sub>6</sub></sub>	Z <sub>O<sub>2</sub></sub>	Z <sub>N<sub>2</sub></sub>	Z <sub>H<sub>2</sub>O</sub>	Z <sub>SO<sub>2</sub></sub>
0.17	0.0724	0.0272	0.0000	0.0223	0.6567	0.0594	0.0000
0.123	0.0522	0.0278	0.0000	0.0221	0.6572	0.0578	0.0000
0.087	0.0379	0.0242	0.0000	0.01835	0.6510	0.0578	0
0.067	0.0279	0.0205	0.0000	0.01394	0.6456	0.0578	0
0.05	0.0181	0.0169	0.0000	0.00997	0.6403	0.0578	0

## Appendix C

### Experimental Data for Chapter 3

#### C.1 Experimental Data for Oxygen Partial Pressure Effect

<b>PO<sub>2</sub></b> <b>atm</b>	<b>Selectivity</b> <b>C<sub>2</sub></b>	<b>Selectivity</b> <b>CO</b>	<b>Selectivity</b> <b>S<sub>liq</sub></b>	<b>Selectivity</b> <b>CO<sub>2</sub></b>	<b>Yield</b> <b>C<sub>2</sub></b>
0.17	0.28	0.467	0.219	0.034	0.16
0.125	0.378	0.386	0.211	0.025	0.132
0.083	0.595	0.348	0.036	0.021	0.126
0.062	0.664	0.315	0	0.021	0.0998
0.05	0.673	0.303	0	0.024	0.0906

<b>PO<sub>2</sub></b> <b>atm</b>	<b>Conversion</b> <b>methane</b>	<b>Conversion</b> <b>oxygen</b>	<b>Selectivity</b> <b>C<sub>2</sub>H<sub>4</sub></b>	<b>Selectivity</b> <b>C<sub>2</sub>H<sub>6</sub></b>	<b>C<sub>2</sub>H<sub>4</sub>/C<sub>2</sub>H<sub>6</sub></b>
0.17	0.571	0.785	0.234	0.0459	5.09
0.125	0.35	0.547	0.226	0.152	1.49
0.083	0.212	0.399	0.259	0.335	0.773
0.062	0.15	0.355	0.207	0.457	0.454
0.05	0.135	0.343	0.161	0.512	0.314

#### Compositions

<b>PO<sub>2</sub></b> <b>atm</b>	<b>ZCO</b>	<b>ZCO<sub>2</sub></b>	<b>ZCH<sub>4</sub></b>	<b>ZC<sub>2</sub>H<sub>4</sub></b>	<b>ZC<sub>2</sub>H<sub>6</sub></b>	<b>ZO<sub>2</sub></b>	<b>Z<sub>liq</sub></b>
0.17	0.0726	0.00654	0.359	0.0228	0.00907	0.0966	0.0508
0.125	0.0422	0.00336	0.408	0.0123	0.0102	0.0838	0.0283
0.083	0.0229	0.00142	0.455	0.00825	0.0110	0.0638	0
0.062	0.0130	0.00094	0.469	0.00334	0.00969	0.0486	0
0.05	0.0141	0.00075	0.467	0.00297	0.0103	0.0388	0

## C.2 Experimental Data for the Effect of Helium Diluent

$P_{\text{he}}$ atm	Selectivity $\text{C}_2$	Selectivity $\text{CO}$	Selectivity $\text{S}_{\text{liq}}$	Selectivity $\text{CO}_2$	Yield $\text{C}_2$
0.87	0.273	0.444	0.238	0.045	0.0994
0.733	0.408	0.4308	0.124	0.0372	0.121
0.6	0.507	0.4272	0.0347	0.0305	0.147
0.4	0.355	0.401	0.212	0.0326	0.136
0.2	0.276	0.418	0.271	0.0352	0.126
0	0.234	0.419	0.307	0.0398	0.117

$P_{\text{he}}$ atm	Conversion methane	Conversion oxygen	Selectivity $\text{C}_2\text{H}_4$	Selectivity $\text{C}_2\text{H}_6$	$\text{C}_2\text{H}_4/\text{C}_2\text{H}_6$
0.87	0.364	0.549	0.0405	0.233	0.174
0.733	0.297	0.395	0.135	0.274	0.493
0.6	0.289	0.341	0.245	0.262	0.936
0.4	0.383	0.472	0.253	0.102	2.48
0.2	0.456	0.629	0.211	0.0557	3.95
0	0.498	0.692	0.193	0.0418	4.63

**Compositions**

$P_{\text{he}}$ atm	$Z_{\text{CO}}$	$Z_{\text{CO}_2}$	$Z_{\text{CH}_4}$	$Z_{\text{C}_2\text{H}_4}$	$Z_{\text{C}_2\text{H}_6}$	$Z_{\text{O}_2}$	$Z_{\text{liq}}$
0.87	0.0147	0.00147	0.0669	0.0669	0.00384	0.0143	0.00789
0.733	0.0227	0.00196	0.150	0.00356	0.00722	0.040	0.00654
0.6	0.0334	0.00238	0.233	0.00958	0.0102	0.0667	0.00205
0.4	0.0693	0.00564	0.320	0.0219	0.00881	0.0851	0.0366
0.2	0.127	0.0107	0.408	0.0335	0.00848	0.0851	0.0825
0	0.189	0.0179	0.505	0.0434	0.00937	0.0968	0.139



### C.3 Experimental Data for the Effect of Flowrate

Flowrate cm <sup>3</sup> /min	Selectivity C <sub>2</sub>	Selectivity CO	Selectivity S <sub>liq</sub>	Selectivity CO <sub>2</sub>	Yield C <sub>2</sub>
50	0.243	0.37	0.345	0.0416	0.1087
100	0.293	0.415	0.257	0.035	0.102
150	0.349	0.347	0.259	0.045	0.11
200	0.371	0.398	0.192	0.039	0.0666

Flowrate cm <sup>3</sup> /min	Conversion methane	Conversion oxygen	Selectivity C <sub>2</sub> H <sub>4</sub>	Selectivity C <sub>2</sub> H <sub>6</sub>	C <sub>2</sub> H <sub>4</sub> /C <sub>2</sub> H <sub>6</sub>
50	0.447	0.76	0.188	0.0556	3.38
100	0.349	0.593	0.224	0.0696	3.32
150	0.315	0.528	0.28	0.0691	4.05
200	0.179	0.294	0.239	0.132	1.81

#### Compositions

Flowrate cm <sup>3</sup> /min	ZCO	ZCO <sub>2</sub>	ZCH <sub>4</sub>	ZC <sub>2</sub> H <sub>4</sub>	ZC <sub>2</sub> H <sub>6</sub>	ZO <sub>2</sub>	Z <sub>liq</sub>
50	0.153	0.0174	0.579	0.0389	0.0115	0.0573	0.143
100	0.124	0.0104	0.650	0.0333	0.0104	0.0924	0.0770
150	0.0912	0.0119	0.680	0.0368	0.00909	0.103	0.0680
200	0.0477	0.00463	0.761	0.0143	0.00792	0.142	0.0231

#### C.4 Experimental Data for the Effect of Gap Width

Gap Width cm	Selectivity C <sub>2</sub>	Selectivity CO	Selectivity S <sub>liq</sub>	Selectivity CO <sub>2</sub>	Yield C <sub>2</sub>
0.365	0.422	0.338	0.211	0.029	0.0592
1.27	0.334	0.392	0.236	0.038	0.0888
1.91	0.252	0.377	0.338	0.033	0.109
2.54	0.245	0.38	0.347	0.028	0.111

Gap Width cm	Conversion methane	Conversion oxygen	Selectivity C <sub>2</sub> H <sub>4</sub>	Selectivity C <sub>2</sub> H <sub>6</sub>	C <sub>2</sub> H <sub>4</sub> /C <sub>2</sub> H <sub>6</sub>
0.365	0.14	0.171	0.294	0.126	2.3
1.27	0.266	0.429	0.23	0.103	2.23
1.91	0.433	0.726	0.2	0.0524	3.82
2.54	0.452	0.747	0.193	0.0519	3.72

#### Compositions

Gap Width cm	ZCO	ZCO <sub>2</sub>	ZCH <sub>4</sub>	ZC <sub>2</sub> H <sub>4</sub>	ZC <sub>2</sub> H <sub>6</sub>	ZO <sub>2</sub>	Z <sub>liq</sub>
0.365	0.0272	0.00237	0.765	0.0118	0.00514	0.171	0.0170
1.27	0.0810	0.00782	0.702	0.0238	0.0107	0.126	0.0488
1.91	0.150	0.0129	0.587	0.0397	0.0104	0.0659	0.134
2.54	0.159	0.0118	0.571	0.0404	0.0109	0.0613	0.145

### C.5 Experimental Data for the Effect of Voltage

Voltage kV	Selectivity C <sub>2</sub>	Selectivity CO	Selectivity S <sub>liq</sub>	Selectivity CO <sub>2</sub>	Yield C <sub>2</sub>
5.75	0.336	0.331	0.306	0.027	0.0796
6.25	0.326	0.331	0.316	0.027	0.0837
6.9	0.281	0.335	0.346	0.038	0.0888
7.5	0.265	0.364	0.33	0.041	0.094

Voltage kV	Conversion methane	Conversion oxygen	Selectivity C <sub>2</sub> H <sub>4</sub>	Selectivity C <sub>2</sub> H <sub>6</sub>	C <sub>2</sub> H <sub>4</sub> /C <sub>2</sub> H <sub>6</sub>
5.75	0.237	0.34	0.204	0.132	1.55
6.25	0.257	0.382	0.211	0.114	1.84
6.9	0.316	0.502	0.196	0.0845	2.32
7.5	0.353	0.592	0.196	0.0688	2.85

Compositions							
Voltage kV	ZCO	ZCO <sub>2</sub>	ZCH <sub>4</sub>	ZC <sub>2</sub> H <sub>4</sub>	ZC <sub>2</sub> H <sub>6</sub>	ZO <sub>2</sub>	Z <sub>liq</sub>
5.75	0.0578	0.00477	0.709	0.178	0.0114	0.145	0.0532
6.25	0.0575	0.00577	0.721	0.1304	0.0118	0.145	0.0461
6.9	0.0866	0.00988	0.663	0.0253	0.0109	0.115	0.0892
7.5	0.110	0.0123	0.643	0.295	0.0104	0.0961	0.0994

## C.6 Experimental Data for the Effect of Frequency

Frequency Hz	Selectivity C <sub>2</sub>	Selectivity CO	Selectivity S <sub>liq</sub>	Selectivity CO <sub>2</sub>	Yield C <sub>2</sub>
150	0.277	0.360	0.315	0.0483	0.0894
175	0.306	0.375	0.271	0.048	0.0813
200	0.357	0.374	0.224	0.0453	0.0837
225	0.373	0.358	0.228	0.041	0.0804
250	0.404	0.358	0.202	0.0363	0.0771
275	0.391	0.356	0.22	0.033	0.0732
300	0.434	0.362	0.173	0.0311	0.0718

Frequency Hz	Conversion methane	Conversion oxygen	Selectivity C <sub>2</sub> H <sub>4</sub>	Selectivity C <sub>2</sub> H <sub>6</sub>	C <sub>2</sub> H <sub>4</sub> /C <sub>2</sub> H <sub>6</sub>
150	0.323	0.541	0.2	0.0775	2.58
175	0.268	0.442	0.21	0.0986	2.18
200	0.236	0.387	0.2183	0.138	1.59
225	0.222	0.330	0.217	0.156	1.5
250	0.194	0.29	0.2183	0.185	1.25
275	0.189	0.268	0.201	0.190	1.13
300	0.169	0.238	0.217	0.217	1.1

### Compositions

Frequency Hz	ZCO	ZCO <sub>2</sub>	ZCH <sub>4</sub>	ZC <sub>2</sub> H <sub>4</sub>	ZC <sub>2</sub> H <sub>6</sub>	ZO <sub>2</sub>	Z <sub>liq</sub>
150	0.0960	0.00924	0.678	0.286	0.0108	0.101	0.0764
175	0.0678	0.00629	0.720	0.0212	0.0119	0.126	0.0472
200	0.0638	0.0040	0.743	0.0204	0.0128	0.131	0.024
225	0.0568	0.00468	0.742	0.0187	0.0128	0.137	0.0282
250	0.0574	0.00460	0.74	0.0193	0.0129	0.137	0.0283
275	0.0530	0.00410	0.744	0.0186	0.0129	0.141	0.0264
300	0.0467	0.00355	0.743	0.0166	0.0124	0.144	0.0343

### C.7 Energy Yield and Electricity Cost for the Effect of Helium Diluent

$P_{he}$ atm	Power Watts	Current Amps	gram of $C_2$ / min	grams of $C_2$ /Joule	Electricity Cost \$/lb of $C_2$
0.87	10	0.62	0.0005	9.13E-7	13.80
0.733	11	0.61	0.0013	1.96E-6	6.43
0.6	12	0.60	0.0023	3.26E-6	3.86
0.4	13	0.58	0.0036	4.60E-6	2.74
0.2	14	0.56	0.0049	5.80E-6	2.17
0	15	0.53	0.0061	6.80E-6	1.85

### C.8 Energy Yield and Electricity Cost for the Effect of Flowrate

Flowrate $cm^3/min$	Power Watts	Current Amps	gram of $C_2$ / min	grams of $C_2$ /Joule	Electricity Cost \$/lb of $C_2$
50	15	0.45	0.0029	3.26E-6	3.87
100	15	0.45	0.0051	5.65E-6	2.23
150	15	0.45	0.008	8.88E-6	1.42
200	15	0.45	0.0052	5.80E-6	2.17

### C.9 Energy Yield and Electricity Cost for the Effect of Gap Width

Gap Width cm	Power Watts	Current Amps	gram of $C_2$ / min	grams of $C_2$ /Joule	Electricity Cost \$/lb of $C_2$
0.365	10	0.45	0.0020	3.30E-6	3.82
1.27	14	0.44	0.0040	4.81E-6	2.62
1.91	18	0.43	0.0058	5.39E-6	2.34
2.54	20	0.36	0.0060	4.97E-6	2.54

### C.10 Energy Yield and Electricity Cost for the Effect of Voltage

Voltage kV	Power Watts	Current Amps	gram of C <sub>2</sub> / min	grams of C <sub>2</sub> /Joule	Electricity Cost \$/lb of C <sub>2</sub>
5.75	11	0.34	0.0034	5.21E-6	2.42
6.25	12	0.38	0.0039	5.43E-6	2.32
6.9	14	0.46	0.0042	5.04E-6	2.50
7.5	15	0.52	0.0047	5.17E-6	2.44

### C.11 Energy Yield and Electricity Cost for the Effect of Frequency

Frequency Hz	Power Watts	Current Amps	gram of C <sub>2</sub> / min	grams of C <sub>2</sub> /Joule	Electricity Cost \$/lb of C <sub>2</sub>
150	15	0.54	0.0046	5.11E-6	2.47
175	13	0.48	0.0039	4.98E-6	2.53
200	12	0.43	0.0039	5.43E-6	2.32
225	11	0.37	0.0037	5.62E-6	2.24
250	10	0.32	0.0038	6.32E-6	1.99
275	10	0.31	0.0037	6.19E-6	2.04
300	9	0.28	0.0034	6.34E-6	1.99

## Appendix D

### Experimental Data for Chapter 4

#### D.1 Experimental Data for the Effect of Voltage with 75 % Helium

Voltage kV	Selectivity C <sub>2</sub>	Selectivity CO	Selectivity S <sub>liq</sub>	Selectivity CO <sub>2</sub>	Yield C <sub>2</sub>
3.75	0.474	0.415	0.0724	0.0336	0.114
4.4	0.446	0.421	0.0973	0.0357	0.118
5.0	0.437	0.378	0.148	0.0370	0.147
5.63	0.388	0.352	0.223	0.0370	0.154

Voltage kV	Conversion methane	Conversion oxygen	Selectivity C <sub>2</sub> H <sub>4</sub>	Selectivity C <sub>2</sub> H <sub>6</sub>	C <sub>2</sub> H <sub>4</sub> /C <sub>2</sub> H <sub>6</sub>
3.75	0.240	0.408	0.138	0.336	0.412
4.4	0.265	0.422	0.128	0.318	0.403
5.0	0.335	0.474	0.188	0.249	0.753
5.63	0.397	0.521	0.198	0.190	1.01

#### Compositions

Voltage kV	ZCO	ZCO <sub>2</sub>	ZCH <sub>4</sub>	ZC <sub>2</sub> H <sub>4</sub>	ZC <sub>2</sub> H <sub>6</sub>	ZO <sub>2</sub>	Z <sub>liq</sub>
3.75	0.0165	0.00154	0.159	0.00276	0.00669	0.030	0.00289
4.4	0.0190	0.00158	0.154	0.00289	0.00717	0.0293	0.00439
5.0	0.0228	0.00218	0.140	0.00565	0.00751	0.0269	0.00889
5.63	0.0258	0.00271	0.128	0.00727	0.00699	0.0246	0.0164

## D.2 Experimental Data for the Effect of Frequency with 75 % Helium

Frequency Hz	Selectivity C <sub>2</sub>	Selectivity CO	Selectivity S <sub>liq</sub>	Selectivity CO <sub>2</sub>	Yield C <sub>2</sub>
60	0.446	0.421	0.0973	0.0357	0.118
100	0.425	0.533	0	0.0420	0.0827
150	0.362	0.596	0	0.042	0.0529
200	0.343	0.610	0	0.0470	0.0463
250	0.352	0.605	0	0.0430	0.0387

Frequency Hz	Conversion methane	Conversion oxygen	Selectivity C <sub>2</sub> H <sub>4</sub>	Selectivity C <sub>2</sub> H <sub>6</sub>	C <sub>2</sub> H <sub>4</sub> /C <sub>2</sub> H <sub>6</sub>
60	0.265	0.422	0.128	0.318	0.403
100	0.195	0.388	0.0797	0.345	0.232
150	0.146	0.347	0.0532	0.309	0.172
200	0.135	0.320	0.0444	0.299	0.149
250	0.110	0.293	0.0289	0.323	0.0889

### Compositions

Frequency Hz	ZCO	ZCO <sub>2</sub>	ZCH <sub>4</sub>	ZC <sub>2</sub> H <sub>4</sub>	ZC <sub>2</sub> H <sub>6</sub>	ZO <sub>2</sub>	Z <sub>liq</sub>
60	0.0190	0.00158	0.154	0.00289	0.00717	0.0293	0.00439
100	0.0178	0.00142	0.168	0.00133	0.00574	0.0309	0
150	0.0159	0.00111	0.176	0.00071	0.00412	0.0326	0
200	0.0135	0.00103	0.179	0.00049	0.00330	0.0340	0
250	0.0133	0.00092	0.183	0.00031	0.00352	0.0351	0



### D.3 Experimental Data for the Effect of Gap Width with 75 % Helium

Gap Width cm	Selectivity C <sub>2</sub>	Selectivity CO	Selectivity S <sub>liq</sub>	Selectivity CO <sub>2</sub>	Yield C <sub>2</sub>
0.365	0.356	0.367	0.241	0.036	0.0898
1.27	0.483	0.410	0.0688	0.038	0.148
1.91	0.424	0.408	0.134	0.034	0.174
2.54	0.379	0.376	0.218	0.027	0.196

Gap Width cm	Conversion methane	Conversion oxygen	Selectivity C <sub>2</sub> H <sub>4</sub>	Selectivity C <sub>2</sub> H <sub>6</sub>	C <sub>2</sub> H <sub>4</sub> /C <sub>2</sub> H <sub>6</sub>
0.365	0.252	0.256	0.0922	0.264	0.350
1.27	0.306	0.437	0.193	0.290	0.665
1.91	0.411	0.609	0.201	0.223	0.902
2.54	0.518	0.728	0.222	0.157	1.41

Compositions Gap Width cm	ZCO	ZCO <sub>2</sub>	ZCH <sub>4</sub>	ZC <sub>2</sub> H <sub>4</sub>	ZC <sub>2</sub> H <sub>6</sub>	ZO <sub>2</sub>	Z <sub>liq</sub>
0.365	0.0153	0.00147	0.154	0.00192	0.00549	0.0386	0.0100
1.27	0.0220	0.00203	0.145	0.00516	0.00777	0.0296	0.00368
1.91	0.0311	0.00263	0.125	0.00768	0.00852	0.0208	0.0102
2.54	0.0375	0.0275	0.103	0.00111	0.00783	0.0147	0.0218

**D.4 Nonadiabatic 60 Hz & 50 cm<sup>3</sup>/min: Experimental Data for the Effect of Voltage with 75 % Helium**

Voltage kV	Selectivity C <sub>2</sub>	Selectivity CO	Selectivity S <sub>liq</sub>	Selectivity CO <sub>2</sub>	Yield C <sub>2</sub>
3.75	0.324	0.561	0.0742	0.0408	0.113
4.4	0.423	0.438	0.107	0.032	0.187
5.0	0.414	0.468	0.0895	0.0285	0.201
5.63	0.397	0.425	0.145	0.033	0.195

Voltage kV	Conversion methane	Conversion oxygen	Selectivity C <sub>2</sub> H <sub>4</sub>	Selectivity C <sub>2</sub> H <sub>6</sub>	C <sub>2</sub> H <sub>4</sub> /C <sub>2</sub> H <sub>6</sub>
3.75	0.35	0.592	0.0823	0.242	0.341
4.4	0.441	0.646	0.252	0.171	1.47
5.0	0.485	0.653	0.281	0.133	2.11
5.63	0.491	0.647	0.289	0.109	2.66

**Compositions**

Voltage kV	ZCO	ZCO <sub>2</sub>	ZCH <sub>4</sub>	ZC <sub>2</sub> H <sub>4</sub>	ZC <sub>2</sub> H <sub>6</sub>	ZO <sub>2</sub>	Z <sub>liq</sub>
3.75	0.0356	0.00258	0.138	0.00262	0.00768	0.0208	0.00471
4.4	0.0367	0.00264	0.119	0.0106	0.00717	0.0182	0.00897
5.0	0.0436	0.0027	0.11	0.0131	0.0062	0.0179	0.00831
5.63	0.04	0.00307	0.109	0.0136	0.00512	0.0182	0.0137

**D.5 Adiabatic 60 Hz & 50 cm<sup>3</sup>/min: Experimental Data for the Effect of Voltage with 75 % Helium**

Voltage kV	Selectivity C <sub>2</sub>	Selectivity CO	Selectivity S <sub>liq</sub>	Selectivity CO <sub>2</sub>	Yield C <sub>2</sub>
3.75	0.405	0.433	0.0653	0.0967	0.155
4.4	0.357	0.343	0.194	0.106	0.165
5.0	0.269	0.336	0.238	0.157	0.148
5.63	0.343	0.357	0.149	0.151	0.171

Voltage kV	Conversion methane	Conversion oxygen	Selectivity C <sub>2</sub> H <sub>4</sub>	Selectivity C <sub>2</sub> H <sub>6</sub>	C <sub>2</sub> H <sub>4</sub> /C <sub>2</sub> H <sub>6</sub>
3.75	0.383	0.634	0.182	0.223	0.813
4.4	0.464	0.723	0.209	0.148	1.4
5.0	0.55	0.956	0.192	0.0769	2.49
5.63	0.498	0.89	0.26	0.083	3.13

**Compositions**

Voltage kV	ZCO	ZCO <sub>2</sub>	ZCH <sub>4</sub>	ZC <sub>2</sub> H <sub>4</sub>	ZC <sub>2</sub> H <sub>6</sub>	ZO <sub>2</sub>	Z <sub>liq</sub>
3.75	0.0305	0.00681	0.131	0.0064	0.00786	0.0193	0.00459
4.4	0.0303	0.00941	0.115	0.0094	0.00656	0.0146	0.0171
5.0	0.0363	0.017	0.0971	0.0104	0.00415	0.0233	0.0257
5.63	0.0345	0.0146	0.108	0.0125	0.004	0.0586	0.0143

**D.6 Adiabatic 100 Hz & 50 cm<sup>3</sup>/min: Experimental Data for the Effect of Voltage with 75 % Helium**

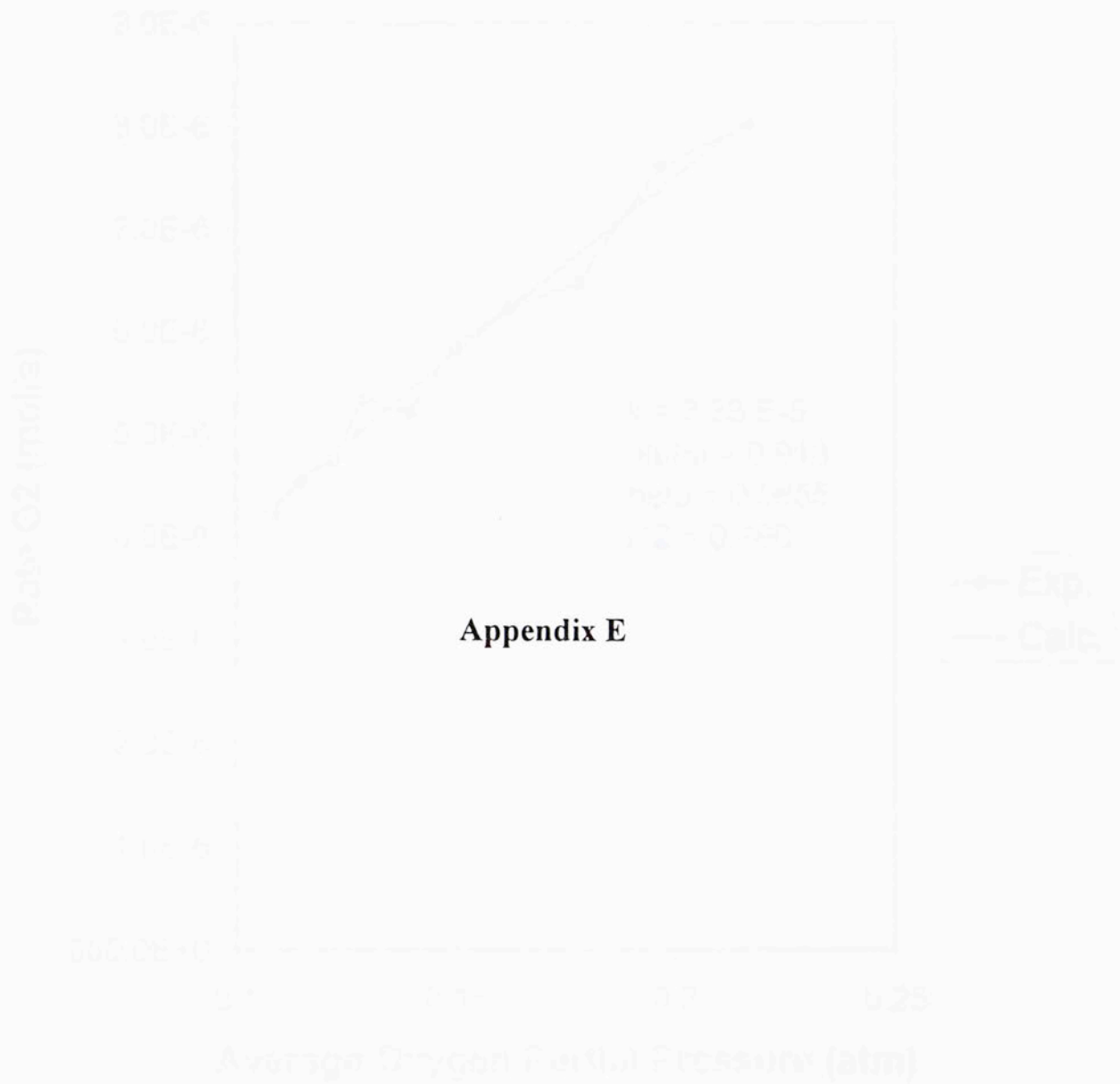
Voltage kV	Selectivity C <sub>2</sub>	Selectivity CO	Selectivity S <sub>liq</sub>	Selectivity CO <sub>2</sub>	Yield C <sub>2</sub>
3.75	0.313	0.563	0.0159	0.1081	0.0823
4.4	0.426	0.435	0.0448	0.0942	0.144
5.0	0.443	0.4	0.065	0.092	0.176
5.63	0.409	0.411	0.0918	0.0882	0.178
6.25	0.457	0.3811	0.0786	0.0833	0.2
6.9	0.382	0.418	0.112	0.088	0.191
7.5	0.446	0.389	0.0852	0.0798	0.179

Voltage kV	Conversion methane	Conversion oxygen	Selectivity C <sub>2</sub> H <sub>4</sub>	Selectivity C <sub>2</sub> H <sub>6</sub>	C <sub>2</sub> H <sub>4</sub> /C <sub>2</sub> H <sub>6</sub>
3.75	0.263	0.585	0.049	0.264	0.187
4.4	0.337	0.643	0.149	0.277	0.537
5.0	0.396	0.708	0.209	0.233	0.896
5.63	0.435	0.735	0.214	0.195	1.09
6.25	0.438	0.687	0.274	0.182	1.5
6.9	0.5	0.825	0.256	0.126	2.05
7.5	0.403	0.584	0.298	0.147	2.05

**Compositions**

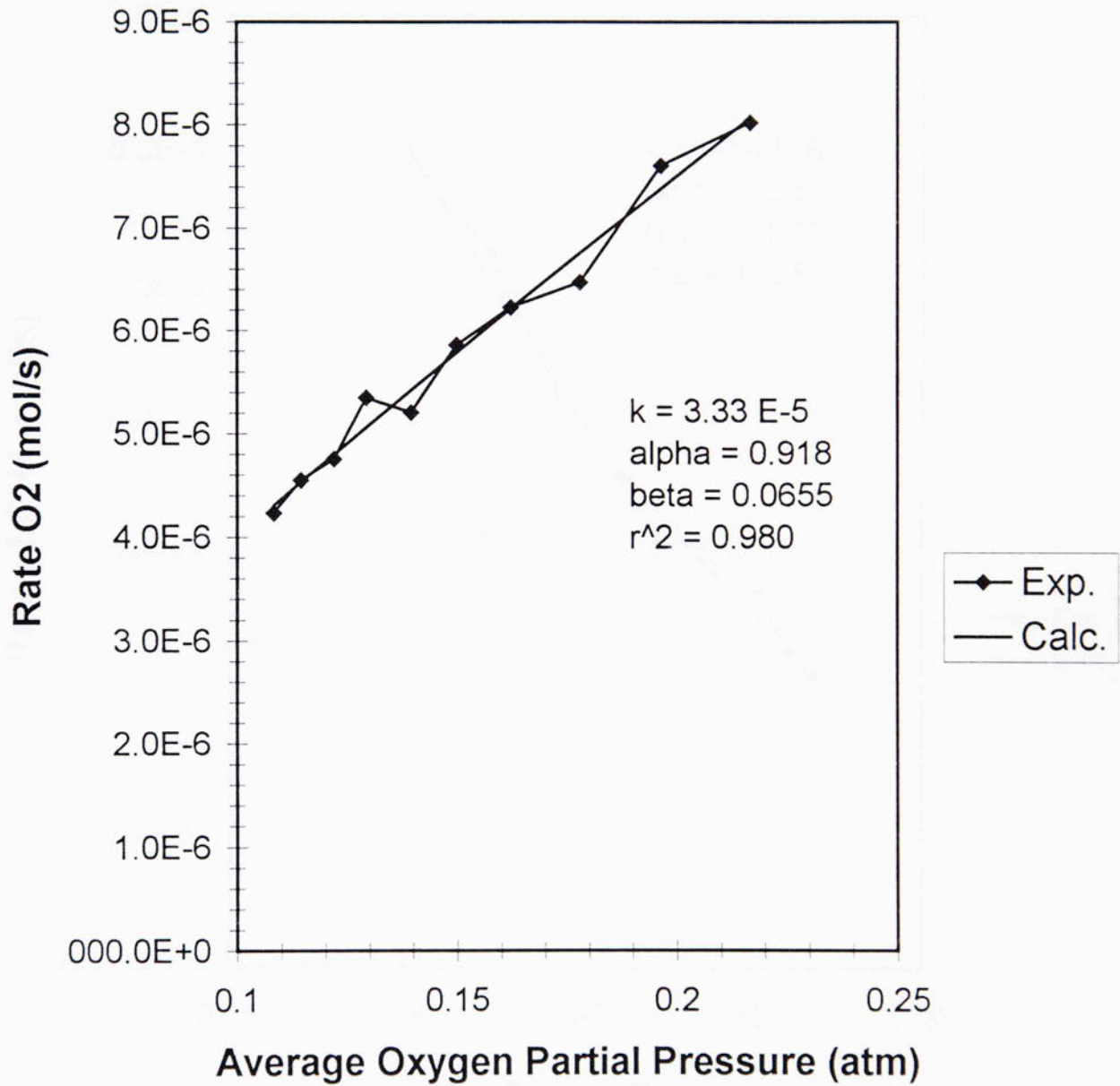
Voltage kV	ZCO	ZCO <sub>2</sub>	ZCH <sub>4</sub>	ZC <sub>2</sub> H <sub>4</sub>	ZC <sub>2</sub> H <sub>6</sub>	ZO <sub>2</sub>	Z <sub>liq</sub>
3.75	0.0257	0.00493	0.155	0.0113	0.00604	0.0215	0.00074
4.4	0.0264	0.00571	0.141	0.00453	0.00843	0.0187	0.00272
5.0	0.0296	0.00674	0.129	0.00773	0.00863	0.0154	0.0048
5.63	0.0338	0.0073	0.121	0.00879	0.00803	0.014	0.00761
6.25	0.0316	0.00692	0.12	0.0114	0.00756	0.0165	0.00652
6.9	0.0403	0.00851	0.108	0.0124	0.00607	0.0093	0.0108
7.5	0.029	0.00607	0.127	0.0112	0.00546	0.0218	0.00658

## Rate of Oxygen Disappearance Experimental & Calculated vs. Average Oxygen Partial Pressure



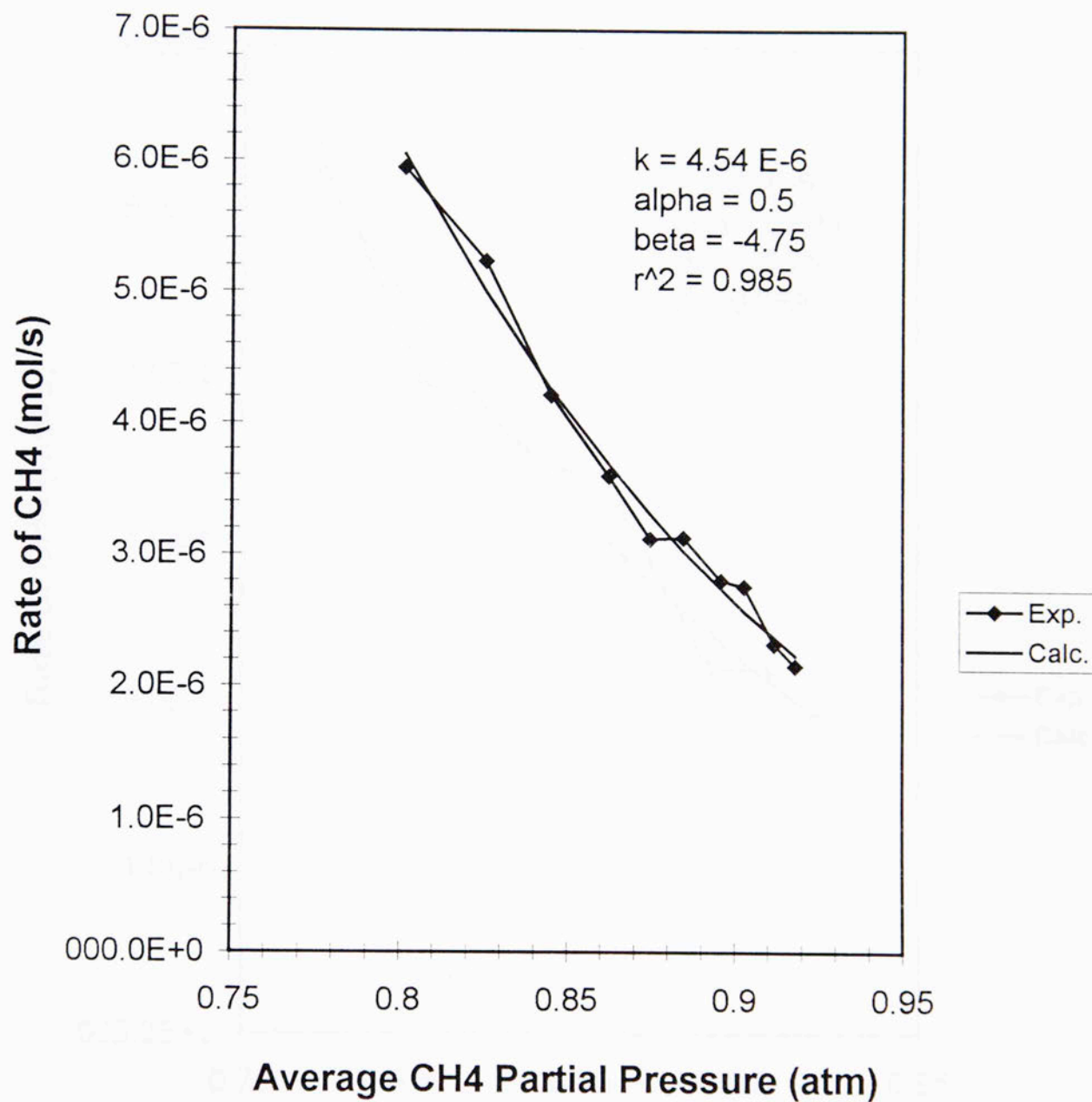
Conditions: 500 SCCM, 6.25 kV, 250 Hz,  
 1/2 inch gap, & 3.5/1-0/1  
 air:1.2/c oxygen

## Rate of Oxygen Disappearance - Experimental & Calculated - vs. Average Oxygen Partial Pressure



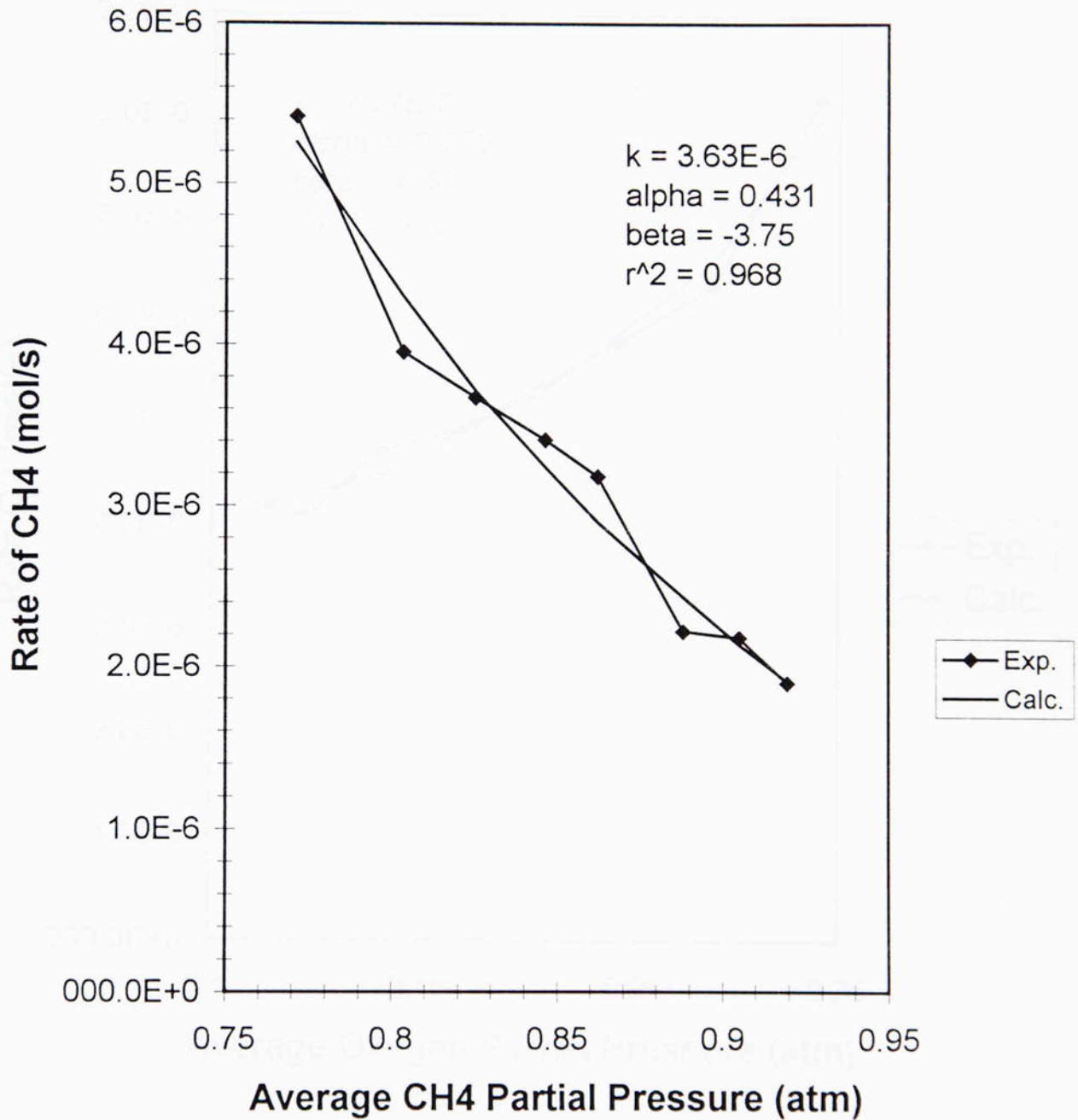
Conditions: 500 SCCM, 6.25 kV, 250 Hz,  
1/2 inch gap, & 3.5/1-8/1  
methane/oxygen

## Rate of Methane Disappearance - Experimental & Calculated - vs. Methane Partial Pressure



Conditions: 500 SCCM, 6.25 kV, 250 Hz,  
1/2 inch gap, & 3.5/1-8/1 methane/oxygen

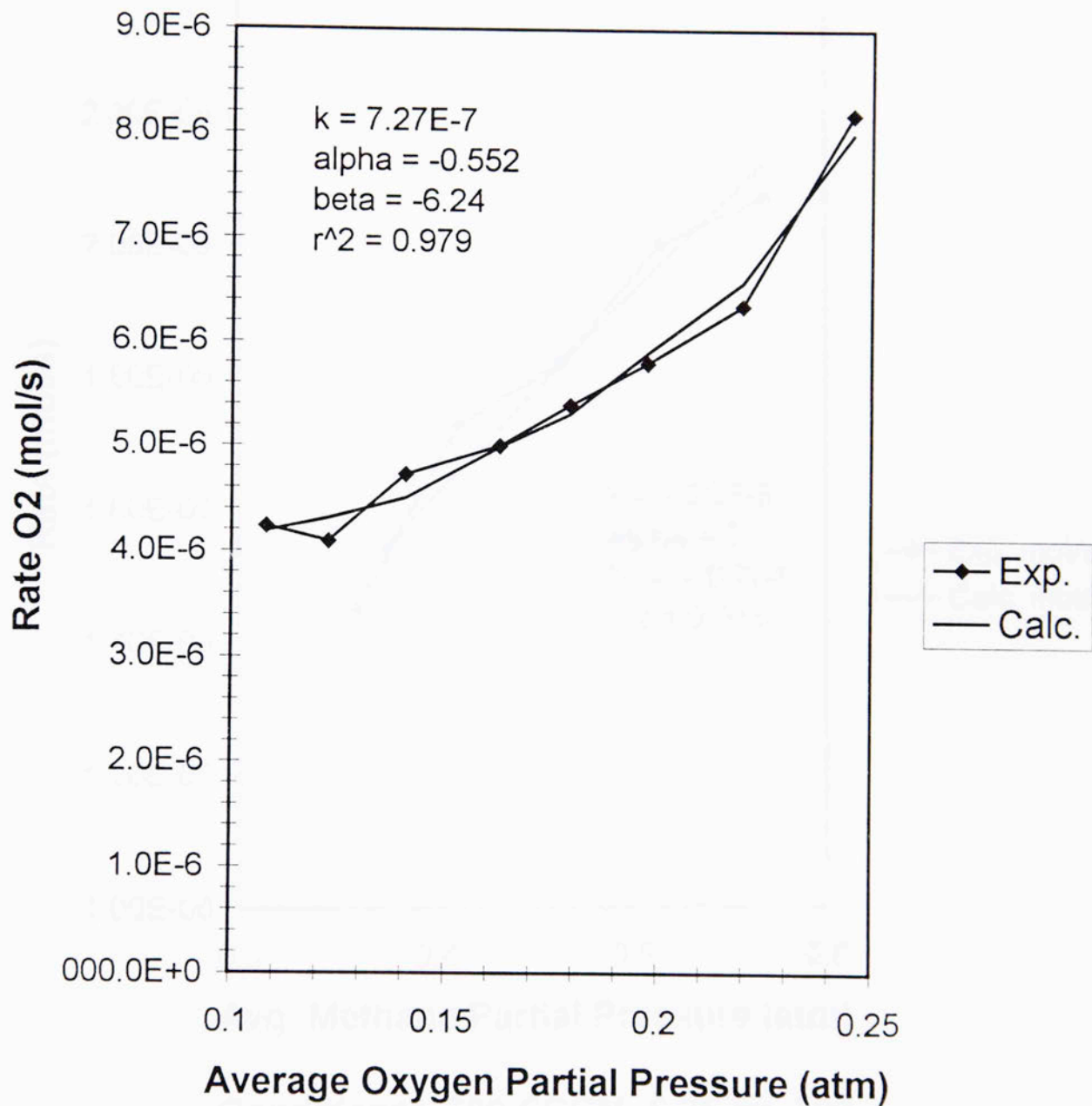
# Rate of Methane Disappearance - Experimental & Calculated - vs. Methane Partial Pressure



Conditions: 500 SCCM, 6.25 kV, 300 Hz,  
1/2 inch gap, & 3/1-8/1 methane/oxygen

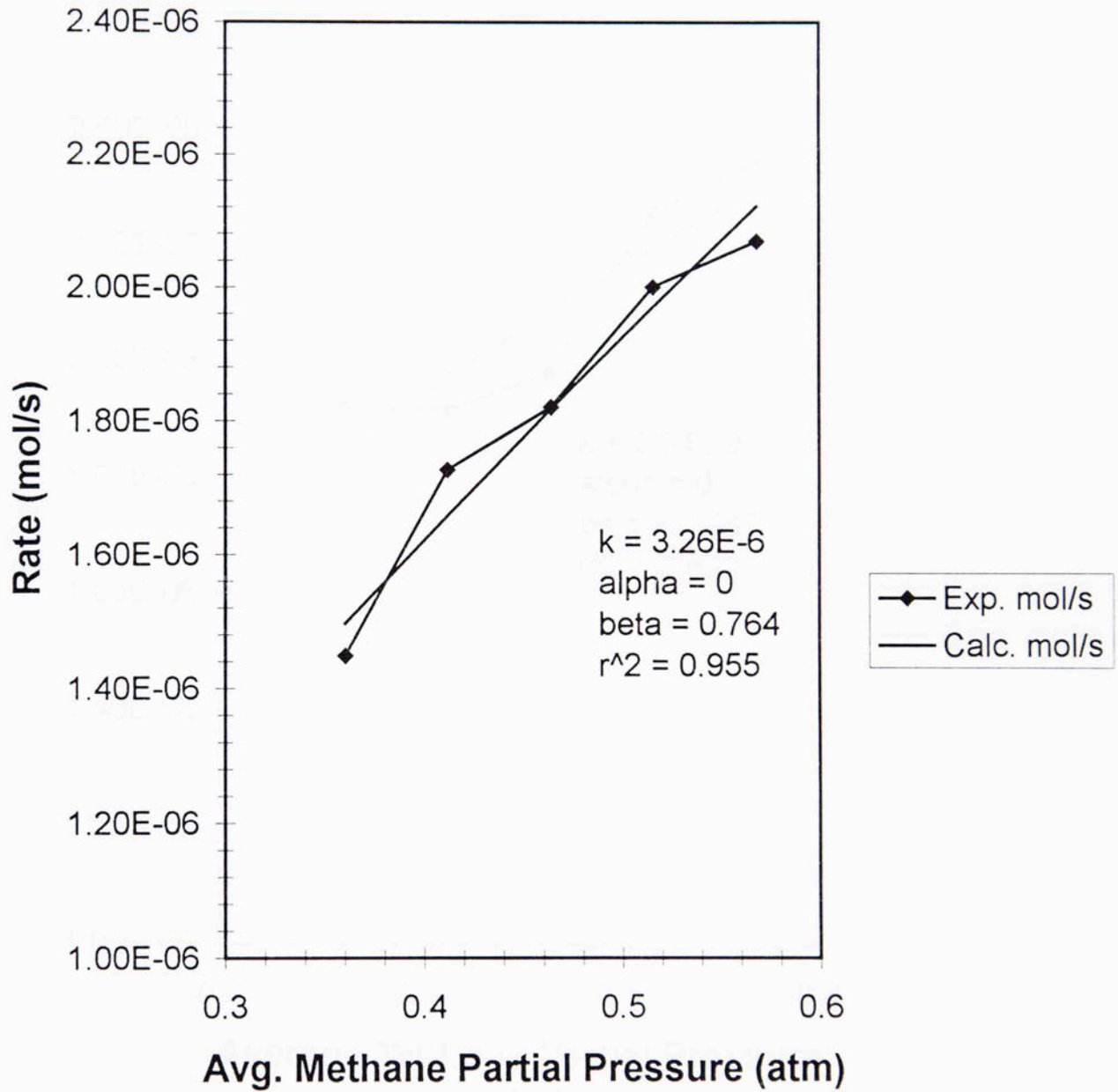


## Rate of Oxygen Disappearance - Experimental & Calculated - vs. Average Oxygen Partial Pressure



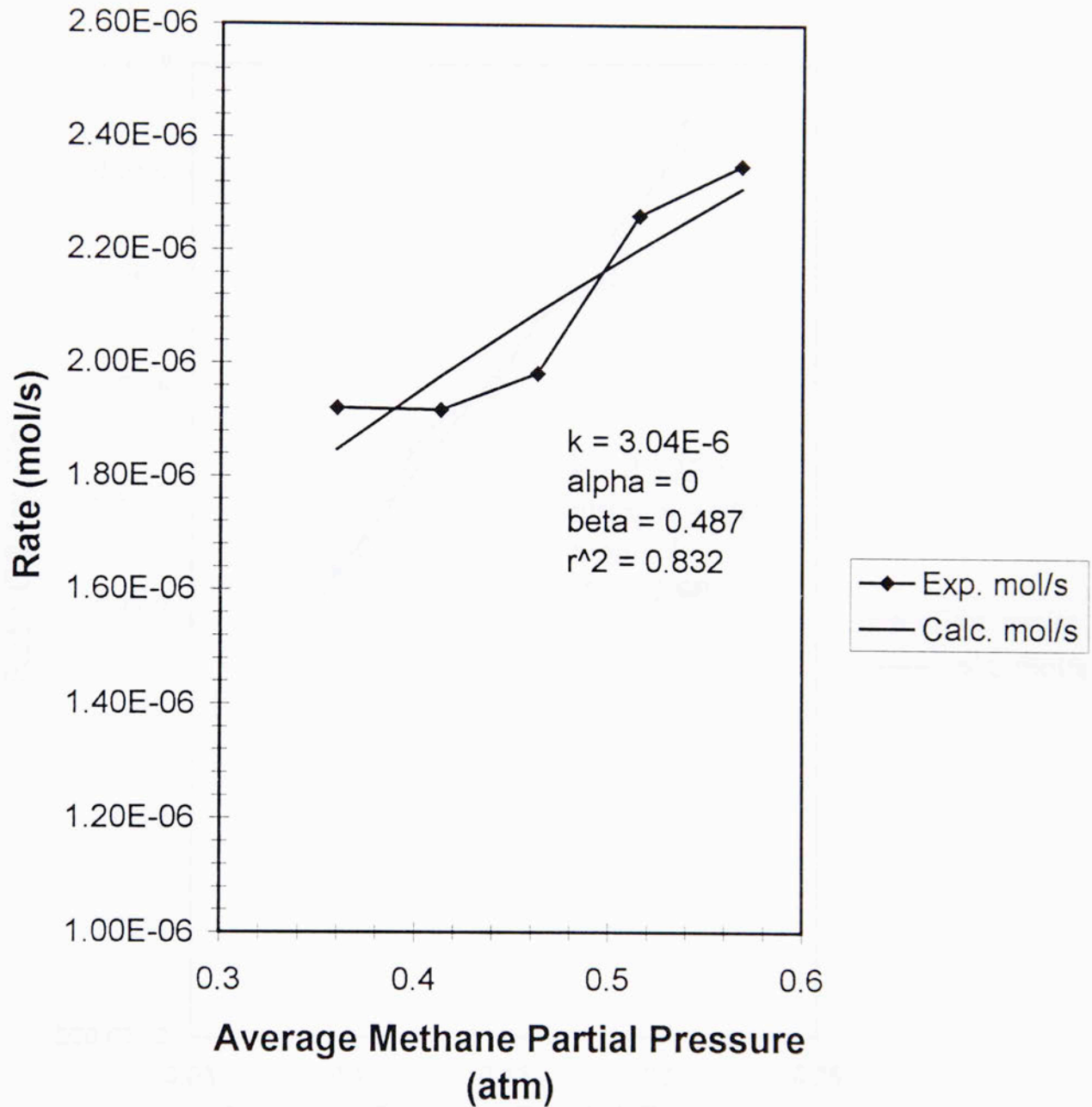
Conditions: 500 SCCM, 6.25 kV, 300 Hz,  
1/2 inch gap, & 3/1-8/1 methane/oxygen

## Rate of Methane Disappearance vs. Average Methane Partial Pressure



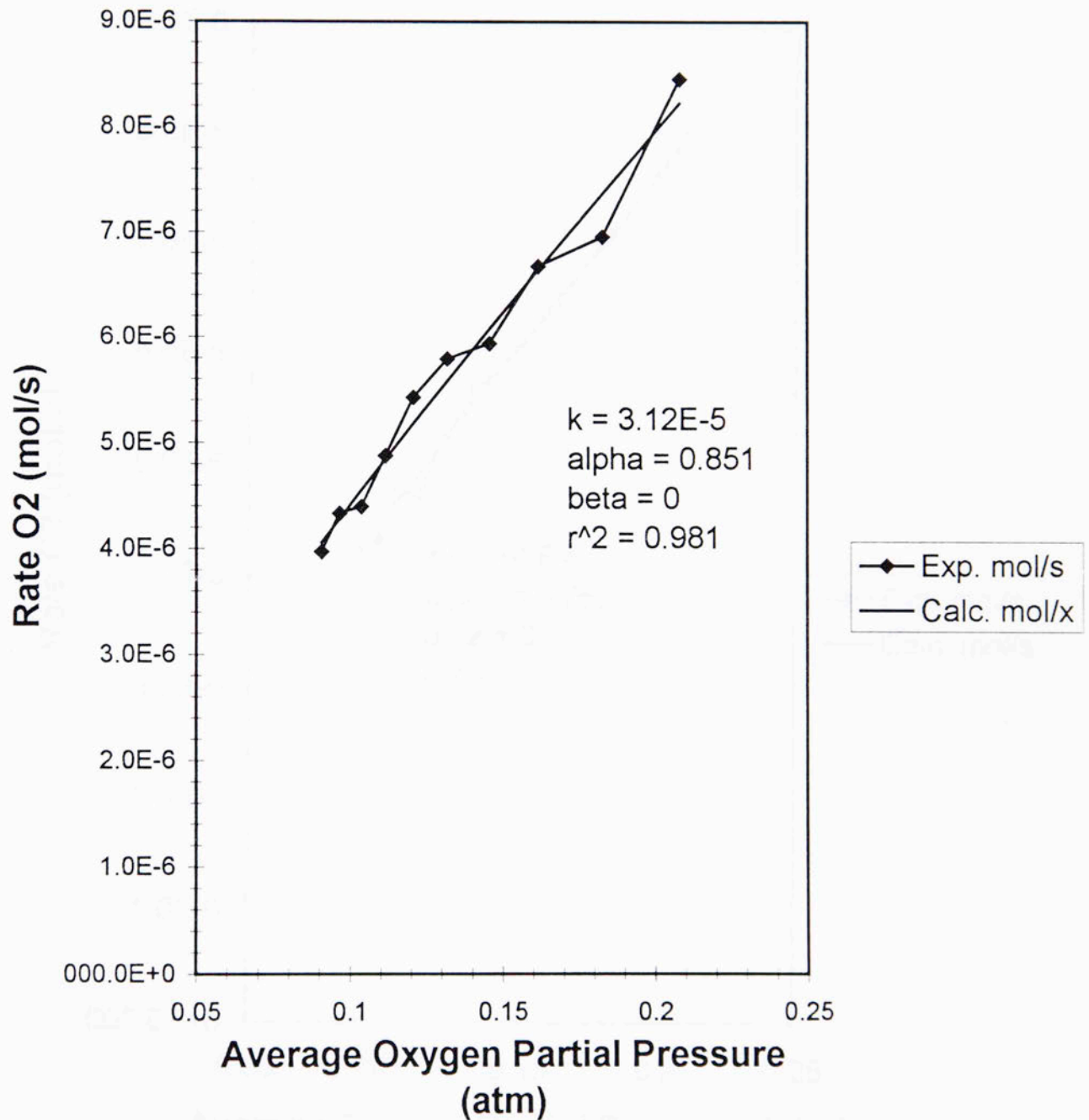
Conditions: 500 SCCM, 6.25 kv, 300 Hz, methane/oxygen 3.5/1 - 7/1, & YHe=0.55-0.2

## Rate of Methane Disappearance - Experimental & Calculated vs. Average Methane Partial Pressure



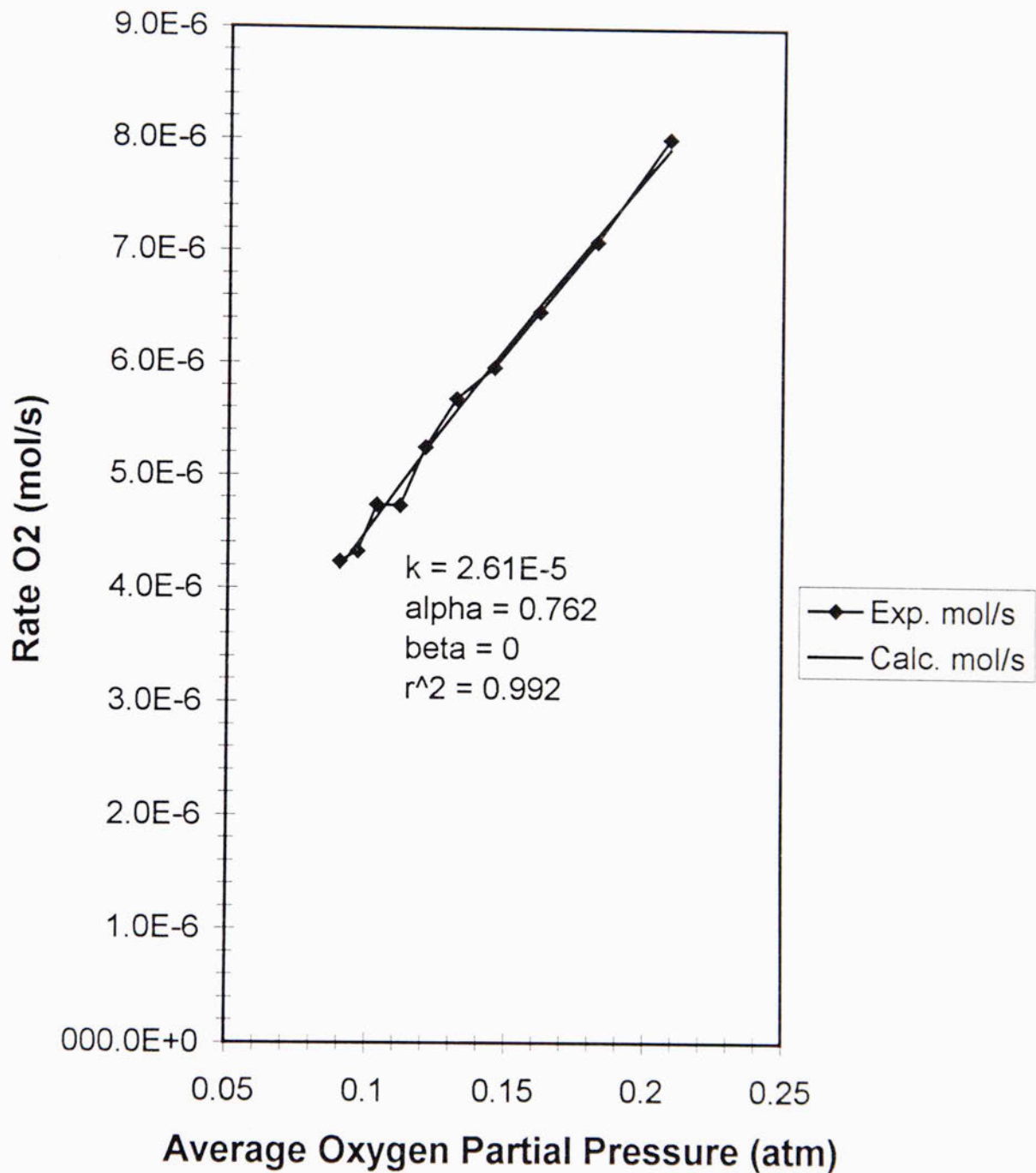
Conditions: 500 SCCM, 6.25 kV, 250  
Hz, 1/2 inch gap, 3.5/1 - 7/1  
methane/oxygen, & YHe = 0.55-0.2

## Rate of Oxygen Disappearance - Experimental & Calculated - vs. Average Oxygen Partial Pressure



Conditions: 500 SCCM, 6.25 kV, 300  
Hz, 1/2 inch gap, & 3.5/1-8/1  
methane/oxygen

## Rate of Oxygen Disappearance - Experimental & Calculated - vs. Average Oxygen Partial Pressure



Conditions: 500 SCCM, 6.25 kV, 250 Hz, 1/2 inch  
gap, & 3.5/1-8/1 methane/oxygen

This volume is the property of the University of Oklahoma, but the literary rights of the author are a separate property and must be respected. Passages must not be copied or closely paraphrased without the previous written consent of the author. If the reader obtains any assistance from this volume, he must give proper credit in his own work.

I grant the University of Oklahoma Libraries permission to make a copy of my thesis upon the request of individuals or libraries. This permission is granted with the understanding that a copy will be provided for research purposes only, and that requestors will be informed of these restrictions.

NAME \_\_\_\_\_  
DATE \_\_\_\_\_

A library which borrows this thesis for use by its patrons is expected to secure the signature of each user.

This thesis by Bobby Joe Hill has been used by the following persons, whose signatures attest their acceptance of the above restrictions.

\_\_\_\_\_

NAME AND ADDRESS

DATE

DISCHARGE

A THESIS

SUBMITTED TO THE GRADUATE FACULTY

in partial fulfillment of the requirements for the

degree of

MASTER OF SCIENCE

(CHEMICAL ENGINEERING)

By

BOBBY JOE HILL

Norman, Oklahoma

1947

UNIVERSITY OF OKLAHOMA  
LIBRARIES